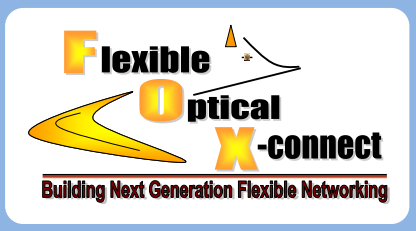

PROJECT: **FOX-C** CONTRACT NO.: **318415**
FLEXIBLE OPTICAL CROSS-CONNECT NODES ENABLING NEXT-GENERATION FLEXIBLE OPTICAL NETWORKING
Specific Targeted Research Project (STREP)

Document Type: Deliverable

Dissemination Level: RE

D2.3

Benefits of FOX-C enabled networking in terms of performance, power consumption and cost savings

Lead beneficiary: Finisar, AIT

Contact person: Shalva Ben-Ezra (Finisar), Pouria S. Khodashenas (AIT), Jose M. Rivas (AIT)

Address: Finisar Corp., Holon 58858, Israel

Athens Information Technology (AIT), Monumental Plaza, 44 Kifisias Ave., Marousi, 15125, Athens, Greece.

e-mail: Shalva.Ben-Ezra@finisar.com; pkhodashenas@ait.gr; jmrivas@ait.gr

Date due of delivery: 31/01/2015

Submission date: 22/05/2015

Contributing institutes: Finisar, AIT, FT

Authors: Pouria S. Khodashenas (AIT), José M. Rivas-Moscoso (AIT), Shalva Ben-Ezra (Finisar), Gilles Thouénon (FT), Christophe Betoule (FT)

This deliverable reports on the benefits of introducing of the FOX-C solutions in a flexible optical network. In this deliverable we provide extensive studies and analysis with the purpose to: a) identify the system performance limitations, b) evaluate the overall energy consumption of the nodes and c) calculate the expected cost benefits from the adoption of the FOX-C solutions in networks. In all cases, comparisons are made with legacy technologies with the main purpose to identify the expected economic benefits and the improvements in power consumption.

Revision History

No.	Version	Author(s)	Date
1	0.1	Pouria S. Khodashenas and José M. Rivas-Moscoso (AIT)	**15/12/14**
	Comments:	**Initial template and ToC**	
2	0.2	Pouria S. Khodashenas and José M. Rivas-Moscoso (AIT)	**21/01/15**
	Comments:	**First draft with inputs in chapters 2, 3 and 4**	
3	0.3	Shalva Ben-Ezra (Finisar)	**28/01/15**
	Comments:	**Inputs in chapter 3**	
4	0.4	G. Thouénon and Ch. Betoule (FT), Pouria S. Khodashenas and José M. Rivas (AIT)	**05/03/15**
	Comments:	**Inputs in chapter 1, 4, 5 and 6**	
5	0.5	Kyriakos Vlachos (OPT)	**11/03/15**
	Comments:	**Internal review**	
6	0.6	José M. Rivas-Moscoso (AIT)	**11/03/15**
	Comments:	**Review of chapter 5 with comments to FT. Corrections to section 2.2. Modification of chapter 6 and new inputs. Overall review to improve readability**	
7	0.7	José M. Rivas-Moscoso (AIT) with inputs from G. Thouénon (FT)	**13/03/15**
	Comments:	**Changes in chapter 5 in response to comments in previous version**	
8	0.8	José M. Rivas-Moscoso (AIT) with inputs from G. Thouénon (FT)	**20/03/15**
	Comments:	**Changes in chapter 5.**	
9	0.9	Dan M. Marom (HUJI)	**03/05/15**
	Comments:	**Internal review**	
10	1.0	Pouria S. Khodashenas and José M. Rivas-Moscoso (AIT), G. Thouénon and Ch. Betoule (FT)	**21/05/15**
	Comments:	**Update of document according to internal review comments**	

Table of Contents

List of Figures

List of Tables

Executive Summary

The FOX-C project aims at enabling the end-to-end network routing of tributary channels with flexible bandwidth down to 10Gb/s carried over super-channels with aggregated capacity of at least 1Tb/s. This is made possible by the adoption of flexible switching nodes with fine switching granularity, together with flexible transmission solutions compatible with the FOX-C switching concept.

According to the FOX-C switching concept, a super-channel can be regarded by the network nodes both as an autonomous high capacity end-to-end channel and as a channel carrying a group of flex-channels with common characteristics. Therefore we can define two switching levels: a coarse switching level that handles the whole super-channel as one high capacity channel and a fine switching level that handles the individual contents of the super-channel.

In this deliverable, drawing on the work carried out in work packages 2, 3 and 4, we focus on the evaluation of the expected benefits from the introduction of the FOX-C transport and node solutions in a flexible optical network. To do so, an extensive study and analysis is carried out with the purpose of

a) identifying the system performance limitations,
b) evaluating the overall energy consumption of network components, and
c) calculating the expected cost benefits of the adoption of the FOX-C solutions in networks.

Regarding the first point, we present in chapter 2 a stand-alone executable software-based program, relying on an analytical Gaussian noise model, which provides a fast and accurate estimation of the signal quality in Nyquist WDM and OFDM transmission systems. Using the experimental back-to-back transmission performance for the different transceiver realisations studied in work package 3 and reported in D3.4 and D3.5, we estimate the transmission reach in a point-to-point and multi-link scenario. In the latter case, we consider the effect of the OSNR penalty due to the amplification and the two-stage filtering through a cascade of intermediate nodes, showing that the coarse filters are mainly responsible for the reach penalty observed.

In chapter 3, we present a cost and power consumption model for the transceiver and ROADM implementations developed in work packages 3 and 4. We perform sensitivity analyses of transceiver cost on the cost of the high-spectral resolution (HSR) filters developed by partner HUJI in work package 3 (HSR filter cost: 0.54 times the cost of a 100G transceiver) and show the viability of Nyquist WDM transceivers based on optical filtering, if the assumed new technology cost of the HSR filter decreases by 26% due to technology maturity and mass production (which is a realistic assumption since currently commercial 1×9 WSSs cost around 0.2 times the cost of a 100G transceiver). It is expected that the HSR filter cost could drop to that of a 1×9 WSS, in which case the optical-filter-based transceiver would prove superior to the one based on digital filtering from a cost perspective.

We use the results presented in chapters 2 and 3 to perform a network-wide techno-economic evaluation in chapters 4 and 5. We consider a national (Orange group national network) and an international (the pan-European GÉANT2 network) reference networks and conduct the studies from two different networking perspectives: 1) single-layer networking perspective (considering only the core DWDM network) and 2) multi-layer networking perspective (core network plus metro/core interfaces).

However, to exploit the network resources in a more efficient way, a study on the impact of the frequency slot size and filter resolution on the performance of flexible Nyquist WDM networks (for both single-carrier and multi-carrier based systems) from a networking perspective needs to be performed. It is significant because it identifies the specifications of the associated sub-systems (transceivers and WSS) and the WDM grid in order to derive the maximum benefits from the flexible Nyquist WDM

networks. We demonstrate that a granularity of 6.25 GHz offers a good compromise between network performance and filter requirements for spectrum assignment to single-carrier and super-channel signals. However, for sub-channel allocation within a super-channel, granularities as fine as 3.125 GHz are required to take advantage of filters with resolutions in the region of 1-1.2 GHz. Finer filter resolutions and frequency slots provide negligible performance improvement.

Furthermore, to maximize the exploitation of FOX-C-enabled all-optical traffic grooming (AOTG), it is necessary to introduce an impairment-aware resource allocation algorithm. Hence, in chapter 4, after reviewing the proposed AOTG network solution, an AOTG-capable routing, modulation level and spectrum allocation (AOTG-RMLSA) algorithm is presented. Relying on it, the performance of the AOTG solution is compared with legacy technologies. In the single-layer optical network study, the full FOX-C solution (with all-optical sub-channel add/drop capable nodes) is compared to the conventional (single/multi- line rate over fixed grid, and multi-line rate over flex-grid) and the quasi-FOX-C (with all-optical sub-channel drop-only capable nodes) solutions. The reported results show that the full FOX-C solution outperforms all conventional solutions in the range of study when it comes to spectrum utilization, and leads to 20% improvement in total cost of ownership compared to the second best performing scenario (multi-line rate over flex-grid).

The global multi-layer network analysis –the second approach– demonstrates the CAPEX benefits provided by AOTG vs. the more conventional OTN-based aggregation solution. Comparisons are carried out thanks to an Orange-Labs in-house multi-layer network architecture tool, which optimizes the routing of traffic demands, and the location and dimensioning of the aggregation functions. The results show that, depending on the load volume, AOTG offers from 36% to 56% CAPEX gain over the electrical grooming solution, thereby justifying the migration to the FOX-C solution in the short term and reinforcing the development of the ultra-narrow and ultra-selective optical filters.

The outcomes of this deliverable are meant to help network operators and potential consumers assess both direct and indirect costs and benefits related to the deployment of the FOX-C solution.

1 Introduction

Triggered by emerging services such as high-definition video distribution, cloud computing, and social networking, the IP traffic volume has been exponentially increasing. It is expected that the global IP traffic volume surpasses the zettabyte threshold by the end of 2017 [1]. Furthermore, new hardware advances, such as multi-core processing, virtualization and network storage, are envisaged to support innovative e-Science and grid applications with data flows of 10 Gb/s up to terabit level, making traffic profile extremely diverse and time varying. The predictable consequence is that the network operators will require a new generation of optical transport networks in the near future to efficiently serve this colossal and heterogeneous volume of traffic in a cost-effective and scalable manner.

In response to these large capacity and disparate traffic granularity needs of the future Internet, flexible optical network architectures have been proposed [2]. Such networks rely on the capability to assign a spectrum portion, data rate and modulation format to bandwidth adaptable (i.e. flexible) connections, with the aim of optimizing the use of the network resources. Although the main concept is widely accepted, the specific characteristics that define its operation and capabilities depend on the utilized technology. The FOX-C project proposes a novel flexi-grid optical solution capable to drop and add low-rate tributaries (defined as sub-channels) directly from/to ultra-high capacity super-channels at the intermediate nodes. FOX-C creates a great opportunity for the operators to enjoy the benefits of all-optical traffic grooming over flexible optical network architecture.

To this end, the FOX-C project targets the development of a flexible switching node based on an advanced two-tier ROADM able to add, drop and pass-through low-granularity sub-channels extracted from and added to super-channels. This is addressed in a hierarchical topology (for the modulation formats and multiplexing schemes shown in Figure 1.1), providing the following functionality:

- At the **fibre link level**, a WSS can select one super-channel that contains the sub-channels to be dropped locally. The rest of the super-channels continue directly to the output port. Up to this point the function of the node is similar to a typical WDM ROADM but with a finer adaptation to a variable spectral range and not to a fixed grid (e.g. 100GHz or 50GHz band) as in WDM systems.
- At the **super-channel level**, a distinction has to be made between the drop and the add sections of the FOX-C node:
    - At the **drop section**, the extracted super-channel is subdivided into sub-channels for either drop or express pass-through. This differs from the conventional spectral filtering used for WDM channel processing on account of the overlapping properties of the orthogonal subcarriers in the frequency domain for the case of OFDM or the inability to provide sharp edge filtering for the case of Nyquist FDM.
    - At the **add section**, the newly inserted sub-channels are either coupled and then processed by a phase synchronization and regeneration stage in the case of optical OFDM or first spectrally pre-shaped and then coupled with the through sub-channels for the case of Nyquist WDM.
- At the **sub-channel level**, the dropped sub-channels destined to the metro/access network segment are either expressed transparently to the lower segment of the system for processing at the access terminal nodes or coherently detected with the appropriate Nyquist FDM or OFDM receivers and processed with common low rate switching elements (e.g. DXCs). Similarly, at the add interface the Nyquist FDM or OFDM encoded tributaries are fed to the FOX-C node either directly from the metro/access segments or from the edge switches.

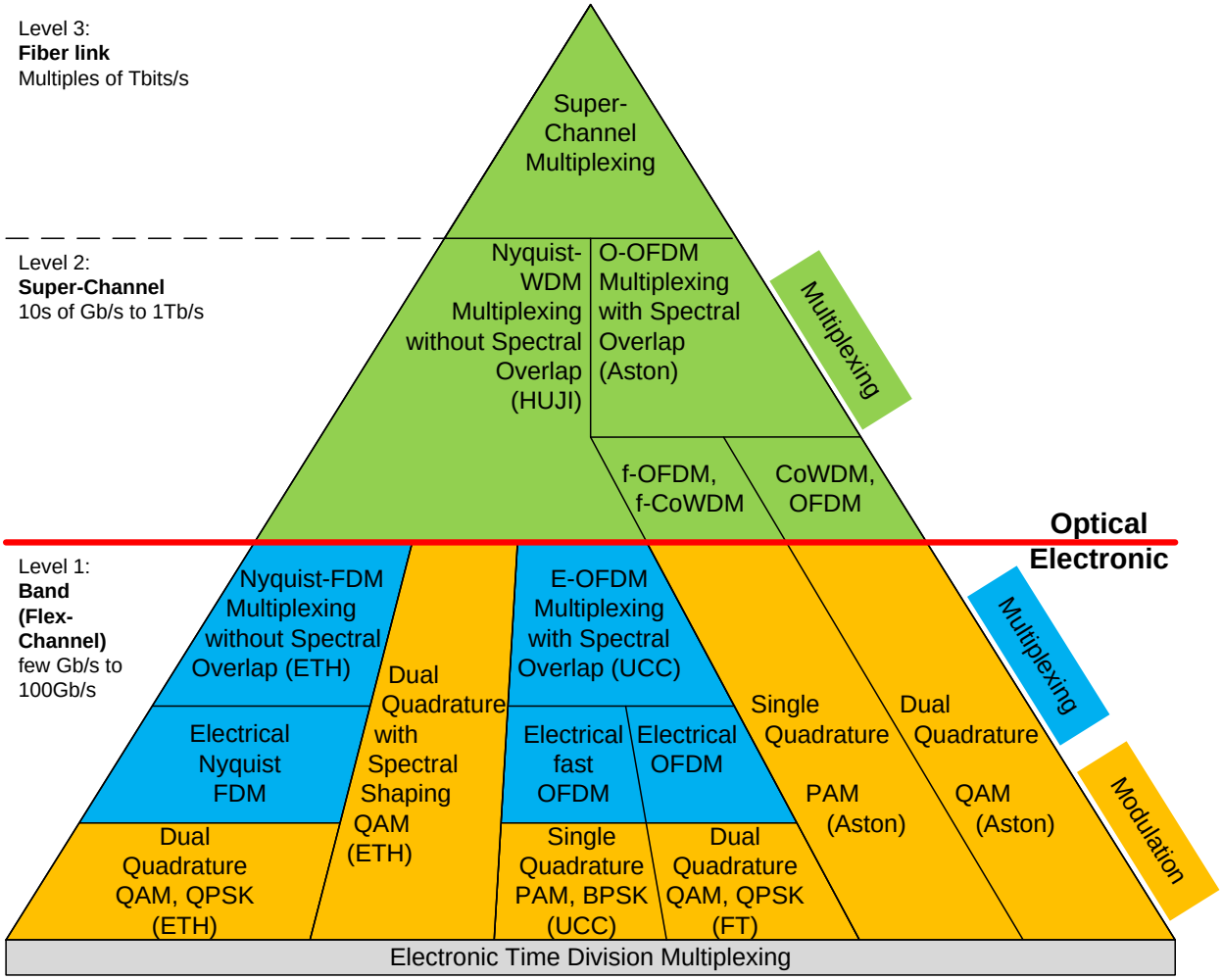

Figure 1.1 – Overview of optical multiplexing schemes investigated in FOX-C (in green), electrical multiplexing schemes (in blue) and the targeted modulation formats (in orange).

To study the benefits introduced by FOX-C, a cost-benefit analysis is performed in this deliverable. To do so, after the development of the cost and power consumption model for the network elements such as transceivers and optical cross connects, and the selection of the benchmarking scenarios, the total cost of ownership for benchmarks and FOX-C solution is calculated and a comparison between them is drawn. To provide a wider outlook the network level studies have been carried out with both single- and multi-layer approaches, the outcome of this deliverable being a good measure for determining the total economic value of FOX-C development investment.

After the introduction, the document is organized as follows: in section 2, the transmission performance estimation is detailed, i.e. the point-to-point transmission reach estimation as well as the transmission through the FOX-C nodes. Section 3 is devoted to the cost and power consumption models for the transceivers and optical cross connects. The network level performance evaluations using the single-layer approach is presented in Section 4 for two reference network topologies (a large national-scale network and a continental network). In contract, in section 5, the multi-layer networking study is detailed. Finally, section 6 concludes the document.

2 Transmission performance estimation

This chapter introduces the QoT Tool, whose algorithm is based on the Gaussian noise model developed in [3], [4] and [5], to estimate the maximum transmission reach of a connection according to the transmission technology. To do that, it is important to measure the OSNR penalty incurred by the signal when it goes through a node. This penalty will be estimated with the help of a Matlab®-VPI® co-simulation platform which will also allow us to study the impact of filter cascading on the transmission performance.

2.1 The QoT Tool algorithm

The QoT Tool is a stand-alone executable software-based program created in Matlab® that provides a fast and accurate estimation of the signal quality in heterogeneous transmission systems by implementing advanced physical layer modelling algorithms. The tool contains three different algorithms for the transmission performance estimation of DWDM, Nyquist-WDM and optical OFDM signal formats, providing results for any type of coherent phase modulated format over different types of fibres. Additionally, it can calculate the end-to-end performance of optical paths composed of several optical links carrying a different number of co-propagating optical channels. The purpose of this algorithm is to assess the impact of the physical layer impairments on the optical paths under different transmission conditions and feed the network level performance evaluation.

The QoT Tool algorithm is described in detail in this section. Initially, the adopted methodology and theoretical background are presented with an emphasis on the closed form relationships that are extracted and used in the QoT Tool models. Next, the QoT Tool functions and the overall structure are described. Finally, this section comments on the use of the QoT Tool functions and its parameters, especially for the case of a multi-hop system that emulates the optical network connections.

2.1.1 Theoretical background

The QoT Tool is based on an analytical model which calculates the transmission impairments according to closed form expressions derived for different types of signal multiplexing formats and by taking into consideration the link and lightpath characteristics. These analytical models have been derived from recent works in which it is shown that the non-linear interference (NLI) in a single optical link without dispersion compensation can be accurately estimated as additive Gaussian noise and therefore included in the final OSNR expression of the optical link [4][6][7]. This is true for both spectrally efficient Nyquist WDM and OFDM formats, while a correction to the Nyquist WDM analytical expression has been provided in [5] to also cover the case of fixed-grid WDM signals far from the Nyquist limit.

The performance degradation factors that affect the signal quality in a long-haul point-to-point transmission system are: a) the ASE noise due to the in-line optical amplifiers, b) the NLI stemming from the fibre Kerr effect and c) the transceiver characteristics. If all three signal quality degradation factors are assumed to be noise terms with Gaussian distribution then the total noise power is the sum of the individual noise power terms and the estimated OSNR at the receiver is

$$OSNR = \frac{P_{ch}}{P_{ASE} + P_{NLI} + P_{B2B}} \tag{2.1}$$

where P_{ch} is the optical channel power at the receiver, P_{ASE} is the noise power contribution due to the ASE noise, P_{NLI} is the noise power contribution to the non-linear interference over the examined optical channel and P_{B2B} is an additional noise power term that refers to the transmitter-receiver performance

limits and other signal-related interference effects (such as, for example, signal cross-talk). Therefore, by extracting the analytical expressions for the ASE and NLI noise power and also knowing the back-to-back performance in terms of the OSNR, the total link OSNR can be extracted from Equation (*2.1*). Then the SNR can be calculated based on [8]

$$OSNR = 2\frac{B_{Rx}}{B_N}SNR \tag{2.2}$$

where B_{Rx} is the receiver bandwidth (limited by the matched filter at the receiver) and B_N is the reference noise bandwidth for the calculations (typically 12.5 GHz). The factor 2 is inserted to take into consideration the two polarization states. In turn, based on the SNR values in Equation (*2.2*), the BER can be calculated for the different modulation formats according to [8]

$$BER = \frac{1}{2}erfc(\sqrt{SNR}) \quad \text{for PM-BPSK} \tag{2.3}$$

$$BER = \frac{1}{2}erfc\left(\sqrt{\frac{SNR}{2}}\right) \quad \text{for PM-QPSK} \tag{2.4}$$

$$BER = \frac{2}{3}erfc\left(\sqrt{\frac{3}{14}SNR}\right) \quad \text{for PM-8QAM} \tag{2.5}$$

$$BER = \frac{3}{8}erfc\left(\sqrt{\frac{1}{10}SNR}\right) \quad \text{for PM-16QAM} \tag{2.6}$$

In all cases except PM-8QAM, it is assumed that Gray coding is applied. For PM-8QAM Gray coding is not possible and the BER formula is a very tight best-fit of the actual BER curve. For the case of PM-16QAM the BER formula is derived from a tight approximation of the exact SER formula, which is then converted into BER as BER=SER/4. The accuracy of the approximations for both PM-8QAM and PM-16QAM is better than ±0.05 dB of SNR over a range around the FEC limit (i.e. at BER = 10^{-3}).

From the BER formulas the Q factor is also derived according to

$$Q = \sqrt{2}\,\mathrm{erfc}^{-1}(2BER) \tag{2.7}$$

$$Q^2[dB] = 20\log_{10}\left(\sqrt{2}\,\mathrm{erfc}^{-1}(2BER)\right) \tag{2.8}$$

where $\mathrm{erfc}^{-1}(x)$ is the inverse of the complementary error function.

Finally, the QoT provides the EVM measure which is derived directly from the signal OSNR value and is calculated based on the methodology and formulae presented in [9].

From the above formulae it is evident that an accurate estimation of the noise power terms in Equation (*2.1*) is required in order to extract the rest of the performance evaluation terms. The next paragraphs will be devoted to the derivation of the formulae for the calculation of the noise power terms for the ASE and NLI noise.

The effect of the ASE noise can be easily studied through the accumulated noise power P_{ASE} at the receiver. Optical amplifiers are considered at the end of each fibre span to boost the power of the signal channels, compensating for fibre attenuation in the span. However, amplification generates ASE noise, which is among the most severe impairments affecting reach and capacity. Each amplifier contributes ASE noise and each contribution is added cumulatively throughout the amplifier chain. This accumulated ASE gives rise to signal-spontaneous beat noise at the receiver, which is the fundamental noise limit in an optically amplified transmission system. Under these assumptions, the accumulated ASE power for a cascade of *N* amplifiers is given by the well-known formula [8]

$$P_{ASE} = 2h\nu B_N n_{sp} N(G-1) \tag{2.9}$$

where P_{ASE} is the power over the reference optical bandwidth B_N, h is Planck's constant, ν is the optical frequency, n_{sp} is the spontaneous emission factor, and G is the optical amplifier gain. The spontaneous

emission factor n_{sp} is determined by the inversion of the amplifier's Er^{3+} ions. The contribution of each amplifier's ASE to the accumulated ASE is characterised by the amplifier's noise figure (NF), which at high gain can be approximated by $N_F \cong 2n_{sp}$. The coefficient 2 in the formula of the accumulated ASE power accounts for the two orthogonal polarizations, one parallel to the signal polarization and one orthogonal to it.

An accurate approximation of the NLI in coherent and uncompensated systems is given by the analytical models presented in [3], [5] and [6] for the case of N-WDM signals and in [4] and [10] for OFDM signals. In both cases it is shown that coherent systems perform better in the presence of high chromatic dispersion and without dispersion management and it is assumed that NLI can be described by a statistically independent, zero-mean Gaussian distribution. Further analysis resulted in the extraction of closed-form expressions for the P_{NLI} term, enabling a fast and accurate estimation of the NLI impact.

For the case of WDM signal formats, the closed-form expression for the P_{NLI} term is given by

$$P_{NLI}^{WDM} = \frac{8}{27}\gamma^2 \frac{P_{ch}^3}{\Delta F^3} L_{eff}^2 \frac{\operatorname{asinh}(\frac{\pi^2}{2}\beta_2 L_{eff,a} BW^2)}{\pi\beta_2 L_{eff,a}} N_s^{1+\varepsilon} B_N \tag{2.10}$$

This is the general formula extracted from [5], and it can be further simplified for specific cases like the N-WDM case, without significant loss in accuracy. However, this formula has been considered in the latest version of the QoT Tool since this is the most general one and it includes all the examined cases.

In the expression shown in Equation (*2.10*), γ is the non-linear coefficient, L_{eff} is the fibre effective length and $L_{eff,a}$ is the asymptotic effective length. The parameter $L_{eff,a}$ can be approximated as $L_{eff,a} = 1/a$, where a is the fibre attenuation, if the span length is longer than 40-50 km so that the overall attenuation is significant. ΔF is the channel spectral difference, which is equal to the symbol rate R_s for the case of N-WDM (sub-channels placed exactly at the Nyquist limit). The term BW denotes the overall effective bandwidth over which the NLI is calculated and depends on the channel bandwidth B_{ch}, the total number of channels N_{ch} and the channel spectral difference ΔF, as $BW = B_{ch} N_{ch}^{B_{ch}/\Delta F}$. For the N-WDM case, where $B_{ch} = R_s = \Delta F$, the BW parameter becomes equal to the overall bandwidth $N_{ch}R_s$, since in this case a continuous spectrum is occupied by the channels with no gaps between them. For quasi-Nyquist sub-channels, B_{ch} equals R_s multiplied by a roll-off factor whose value depends on the spectral shape and is typically 1.3. Finally, Equation (*2.10*) contains a correction factor ε which describes the accumulation of the NLI noise over the N_s spans. This correction factor was calculated in [5] as

$$\varepsilon = \frac{3}{10}\log\left(1 + \frac{6}{L_s}\frac{L_{eff,a}}{\operatorname{asinh}(\frac{\pi^2}{2}\beta_2 L_{eff,a} BW^2)}\right) \tag{2.11}$$

where L_s is the span length.

Equation (*2.10*) and Equation (*2.11*) are used in the QoT Tool for the performance estimation of both (q)N-WDM and fixed-grid WDM coherent transmission systems.

For the case of optical OFDM, the orthogonal channels (verifying $R_s = \Delta F$) have a sinc-shaped spectrum. The P_{NLI} formula in this case is different from that for the WDM channels. The analytical expression of the NLI power for coherent optical OFDM systems has been provided in [4] and can be written as

$$P_{NLI}^{OFDM} = \frac{8}{27}\frac{N_s\gamma^2 h_e}{\pi\beta_2 a}\left(1 - \frac{\Delta G}{\Delta F}\right)\left[\log\left(\frac{2\,\pi^2\beta_2 BW^2}{a}\right) - \frac{\Delta G}{\Delta F}\log(2N-1)\right]B_N \tag{2.12}$$

This expression resembles the one for N-WDM signals at the Nyquist limit (i.e. with $\Delta F = R_s$) if Equation (*2.10*) is simplified accordingly. One may find the simplified expression of Equation (*2.10*) in [3]. The two main differences between Equation (*2.12*) and the equation for the N-WDM case are: a) the insertion of the factor ΔG that denotes the spectral guard-band width between the optical OFDM sub-channels (if considered) and, most importantly, b) the correction factor h_e, which is defined as

$$h_e = 1 + \frac{2\left(N_s - 1 + e^{-a\zeta L_s N_s} - N_s e^{-a\zeta L_s}\right)e^{-a\zeta L_s}}{N_s(e^{-a\zeta L_s} - 1)^2} \tag{2.13}$$

The h_e parameter is inserted, similarly to parameter ε, in Equation (*2.11*) to describe the accumulated NLI over multiple spans. In Equation (*2.13*), ζ is the residual dispersion ratio (e.g. ζ = 1 means uncompensated transmission, ζ = 0.05 means 95% dispersion compensation per span, etc.).

2.1.2 Transmission performance estimation over multi-link lightpaths

The analytical expressions described in the previous section are able to accurately estimate the performance of coherent optical super-channels when they propagate over a multi-span optical link. In order to apply the same expressions to network scenarios, the characteristics of the lightpaths established over multiple links across the end-to-end optical path must be considered. A lightpath consists of multiple links with different lengths, number of spans (and therefore span lengths) and number of co-propagating super/sub-channels. As a matter of fact, the optical links could also have different types of fibre or amplifiers with different noise figure parameters.

The methodology used in the QoT Tool addresses the performance estimation of coherent signals over a lightpath based on the calculation of the total lightpath OSNR value as the sum of the individual OSNR values for each optical link (composed of N_S amplifier spans). This assumption is conditioned on the fact that the estimated P_{NLI} per optical link has Gaussian noise properties and therefore the overall $P_{NLI,T}$ of the lightpath can be obtained as the sum of the NLI noise generated over a single link. Thus, the overall OSNR value, $OSNR_T$, of a lightpath composed of N optical links can be expressed as

$$\frac{1}{OSNR_T} = \frac{1}{OSNR_{B2B}} + \sum_{i=1}^{N} \frac{1}{OSNR_i} \tag{2.14}$$

where $OSNR_i$ is the OSNR value of the ith optical link due to the P_{ASE} and P_{NLI} noise terms. The back-to-back OSNR performance, $OSNR_{B2B}$, is obviously not included in the calculation of the OSNR values of each link and is, on the contrary, added once the multi-link OSNR value is calculated from the ASE and NLI terms. From $OSNR_T$, the BER, Q factor and EVM performance metrics can be obtained as explained in the previous section.

2.1.3 Use of the QoT Tool in a multi-path network environment

An optical network consists of a number of nodes connected typically in a partially meshed topology. In a realistic model, any node can request the establishment of an end-to-end connection to any other node in the optical network according to the traffic demand matrix. These end-to-end connections combine multiple optical links from the ingress to the egress node, constituting the network lightpaths (or optical paths). Since, in a dynamic scenario, the traffic demands can vary in time, the establishment and duration of the lightpaths may also vary. The dynamic optimization of the lightpaths' establishment, according to the generated traffic demands and their duration, is an essential network function in order to (a) optimise the network resources, including the utilised spectrum bandwidth and switching ports and (b) maximise the number of traffic demands, i.e. lightpaths that can be established over an existing bandwidth (e.g. the C-band). This dynamic optimisation procedure is handled by a lightpath establishment mechanism, which must take into consideration the network status and available resources along with the characteristics of the requested lightpath, in order to calculate the optimum path and bandwidth allocation.

Based on the QoT Tool estimation models supporting multiple consecutive links, the QoT Tool can perfectly handle single lightpath systems. However, in a network system the established lightpaths may have common optical links (see Figure 2.1). In this case the main issue is that the allocated channels over a certain link may not be placed continuously over the fibre spectrum and therefore gaps will appear between them. Furthermore, the spectral width of these gaps will not necessary have the same value and may vary (typically in multiples of a minimum frequency slot width) depending on the wavelength allocation procedure. The QoT Tool model does not take into consideration spectral gaps and assumes that all channels are allocated continuously in spectrum, since in analytical models it is not feasible to include the option of spectral gaps between the allocated channels given that the width and location of these gaps cannot be described according to a fix pattern.

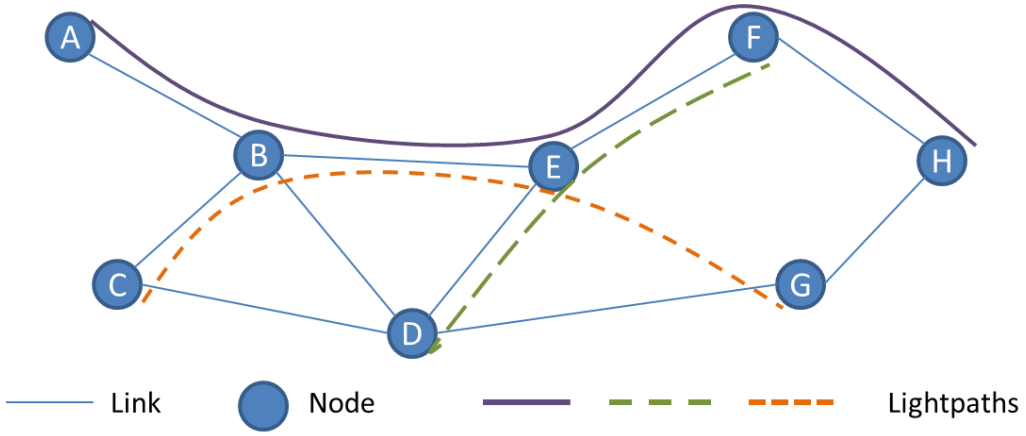

Figure 2.1 – Example of lightpath set-up in an optical network.

Therefore, the QoT Tool must be used to obtain an estimate of the expected performance limits rather than an accurate value. This estimation can be based on the provision of an upper and lower expected performance value or, more simply, on the provision of the worst expected transmission performance. It is the role of the control plane mechanism invoking the QoT Tool to make the appropriate decisions with respect to the input data sent to the QoT Tool according to the expected allocation of the channels over the available spectrum.

One useful yet empirical rule that has been observed in various experimental works is that the non-linear interference between neighbouring bands of multi-carrier signals can be neglected if their spectral difference is wider than 50 GHz. More specifically, this rule implies that when channels are allocated in a spectrally efficient manner (i.e. close to the Nyquist limit), as is the case of the OFDM and (q)N-WDM formats, then the dominant NLI noise stems from the closest neighbouring channels rather than any other channel that is further away than 50 GHz. By applying this rule to the performance estimation of lightpaths given by the QoT Tool, one can assume that any bands of channels that are positioned 50 GHz away from the band under examination will not be considered in the QoT Tool calculations.

This is illustrated in the following example. Assume the simple network topology shown in Figure 2.2. It depicts the transmission of seven flexible multi-carrier super-channels with different number of sub-channels per super-channel, as indicated in the table on the top right-hand side, over a network topology with several nodes (of which four are shown). At the bottom of the figure the spectral allocation of the super-channels is presented over the three links connecting the four nodes shown.

Now assume that super-channel SCh1 is to be established between A and D over links AC and CD while the rest of the super-channels are already established. To estimate the performance of SCh1, we need to know what the total number of co-propagating sub-channels over links AC and CD is. The total number of sub-channels to be taken into account is given by the SCh1 channels plus the channels that affect the SCh1 performance. In this example, it is shown that over link AC, SCh4 is one spectral slot away from SCh1 and that SCh5 is 2 slots away from SCh4. Also SCh6 is 5 slots away from SCh5. If the super-channels consist of N-WDM channels, then the slot width is determined by the symbol rate of the

individual channels. Assuming that the N-WDM sub-channels are transmitted at 28 GBaud and placed close to the Nyquist limit at 30 GHz then a two-slot spectral gap is 60 GHz (i.e. larger than the limit of 50 GHz). In this case, SCh5, SCh6 and SCh7 can be neglected from the calculation of the transmission performance of SCh1, but SCh4, which is only one-slot away, will be considered. Therefore, the QoT Tool will be called up with the parameter 'number of channels' equal to 15 (5 sub-channels from SCh1 and 10 from SCh4) over link AC. Similarly, over link CD, both SCh3 and SCh2 are neglected since they are allocated two or more slots away from SCh1 (and the parameter 'number of channels' over link CD will be 5). Finally, note that if the symbol rate is 20 Gbaud, instead of 28 Gbaud, then a two-slot spectral band occupies less than 50 GHz, and SCh2 sub-channels as well as SCh3 sub-channels should be added the total 'number of channels' over link CD.

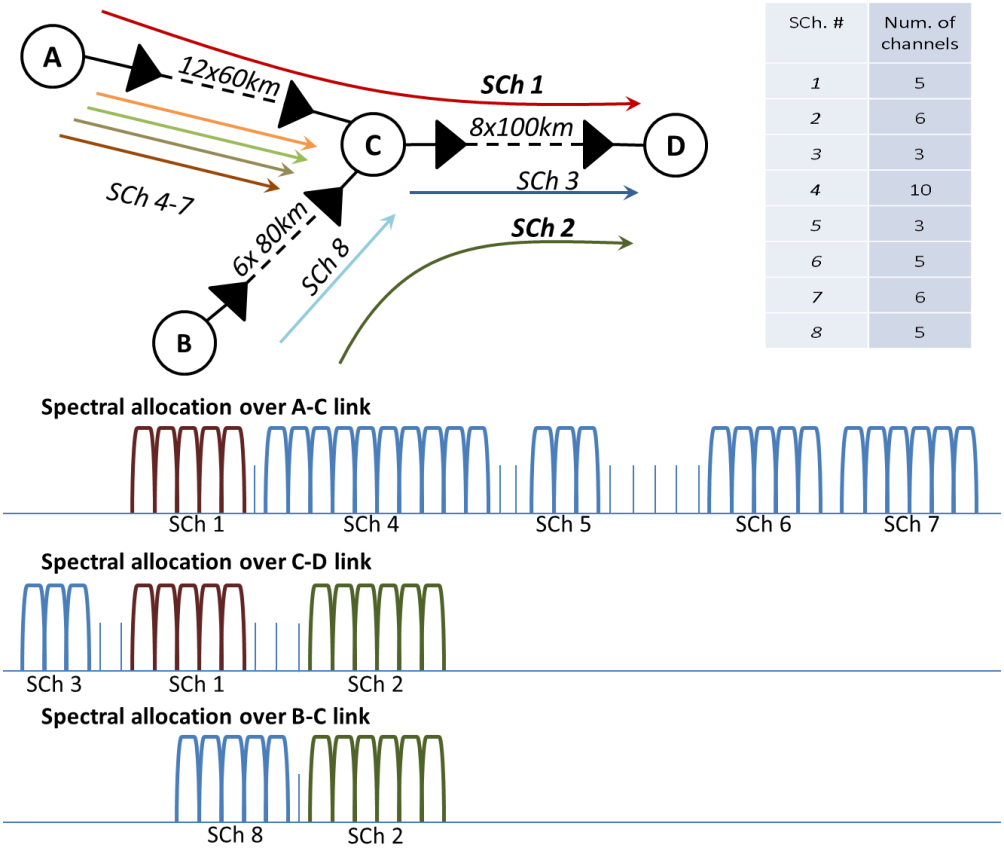

SCh. #	Num. of channels
1	5
2	6
3	3
4	10
5	3
6	5
7	6
8	5

Figure 2.2 – Example of the use of the QoT Tool in a multi-path network environment.

2.2 Maximum point-to-point transmission reach estimation

In this section we are going to use the QoT Tool to estimate the maximum reach of several multiplexing schemes based on the experimental back-to-back results reported in D3.4. In all cases, the transmission medium is a standard SMF, the noise figure (NF) of the amplifiers is assumed to be 5 dB and the span length is 80 km. Furthermore, we always consider polarisation-multiplexed signals in our studies.

2.2.1 Nyquist WDM

Assuming an electrical bandwidth equal to half the symbol rate, the SNR for which a BER of 10^{-3} is achieved corresponds to an OSNR of ~14.5 dB for QPSK and 24.5-26.5 dB for 16QAM (let us take a value of 25 dB for our calculations) with the 28-Gbaud signal, and to an OSNR of ~16 dB for QPSK with the 40-Gbaud signal.

The spectral occupancy is (1+ROF)·Baudrate, i.e. 31.5 GHz (for ROF = 0.125 and Baud rate = 28 Gbaud) and 45 GHz (for ROF = 0.125 and Baud rate = 40 Gbaud).

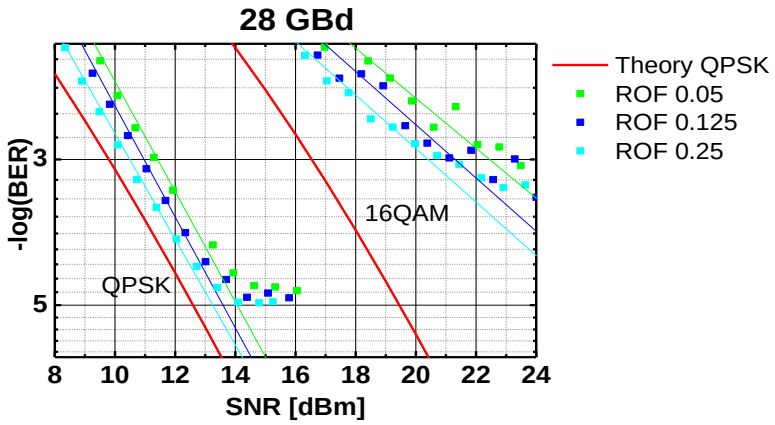

Figure 2.3 – Measured back-to-back BER vs signal-to-noise ratio (SNR) for a root raised cosine shaped signal with different roll-off factors (ROF) at a symbol rate of 28 GBd. The performance is characterized for QPSK and 16QAM.

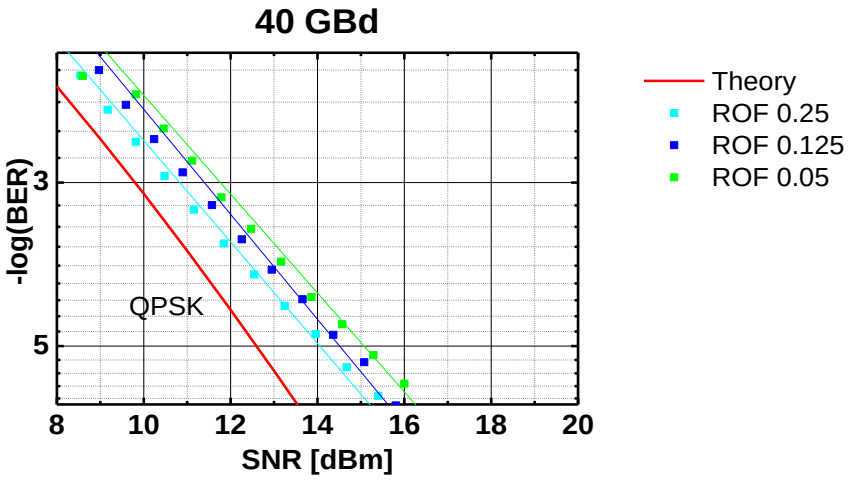

Figure 2.4 – Measured back-to-back BER vs signal-to-noise ratio (SNR) for a root raised cosine shaped signal with different roll-off factors (ROF) at a symbol rate of 40 GBd. The performance is characterized for QPSK.

In Figure 2.5 we show the maximum reach for a point-to-point configuration as a function of the launch power estimated with the QoT Tool for the three cases presented in Figure 2.3 and Figure 2.4 with ROF = 0.125. We have assumed that, instead of single-carrier transmission, we have a qN-WDM super-channel made up of 8 sub-channels (this is one of the specifications considered for the super-channel transceivers in the cost and power consumption reference mode described in chapter 3). We observe that the maximum reach is practically the same for the two QPSK-modulation scenarios (~7000 km), but it reduces dramatically for 16QAM, with a maximum reach in this case of no more than 570 km.

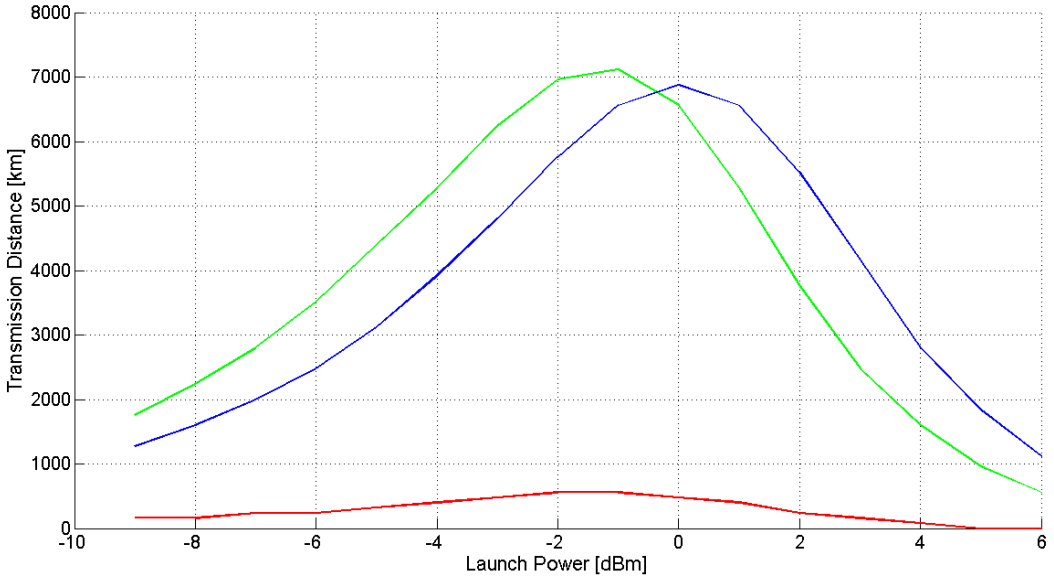

Figure 2.5 – Maximum transmission reach vs launch power estimated with the QoT Tool using the OSNR values for BER = 10^{-3} from Figure 2.3 and Figure 2.4 for qN-WDM transmission of a super-channel composed of 8 sub-channels with a Baud rate of 28 GBaud and modulation format QPSK (green) and16QAM (red), as well as with a Baud rate of 40 GBaud and modulation format QPSK (blue). In all cases, ROF = 0.125.

2.2.2 e-OFDM

The Baud rate of the e-OFDM signal is 10 GBaud, with a spectral occupancy of 12.5 GHz. From Figure 2.6, the back-to-back OSNR is ~14.5 dB for QPSK and ~22.5 dB for 16QAM.

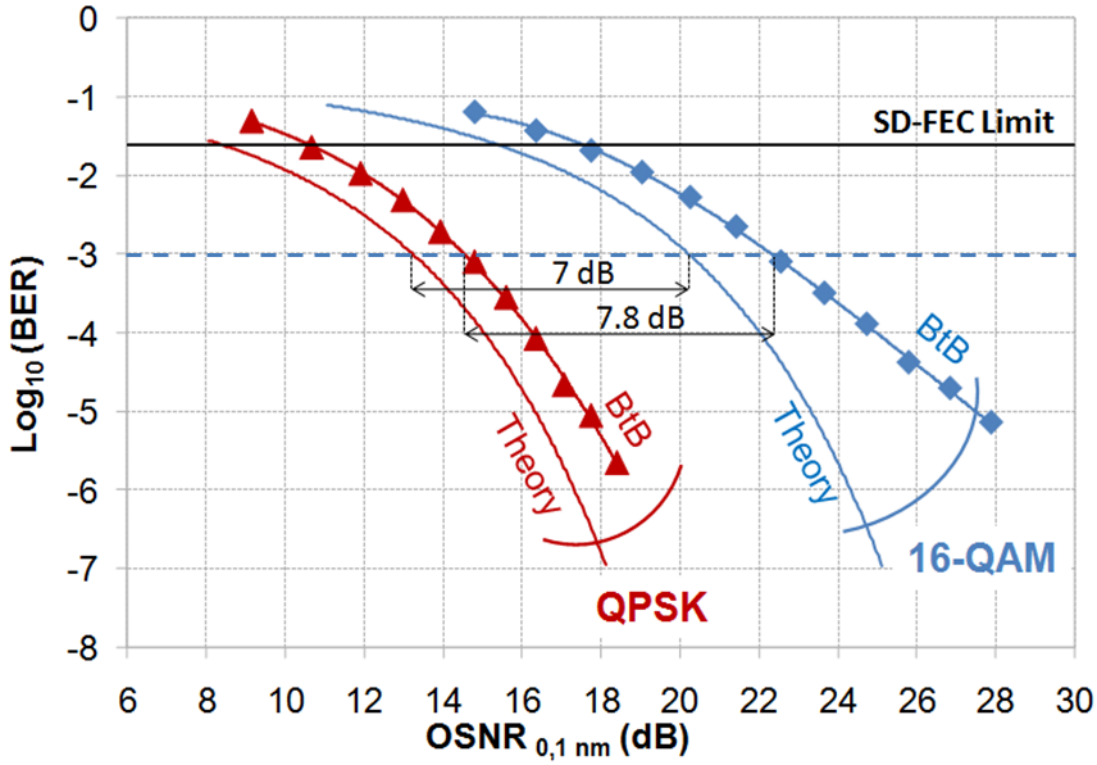

Figure 2.6 – Back-to-back BER vs OSNR for 10-Gbaud, QPSK and 16QAM electrical OFDM (one sub-channel).

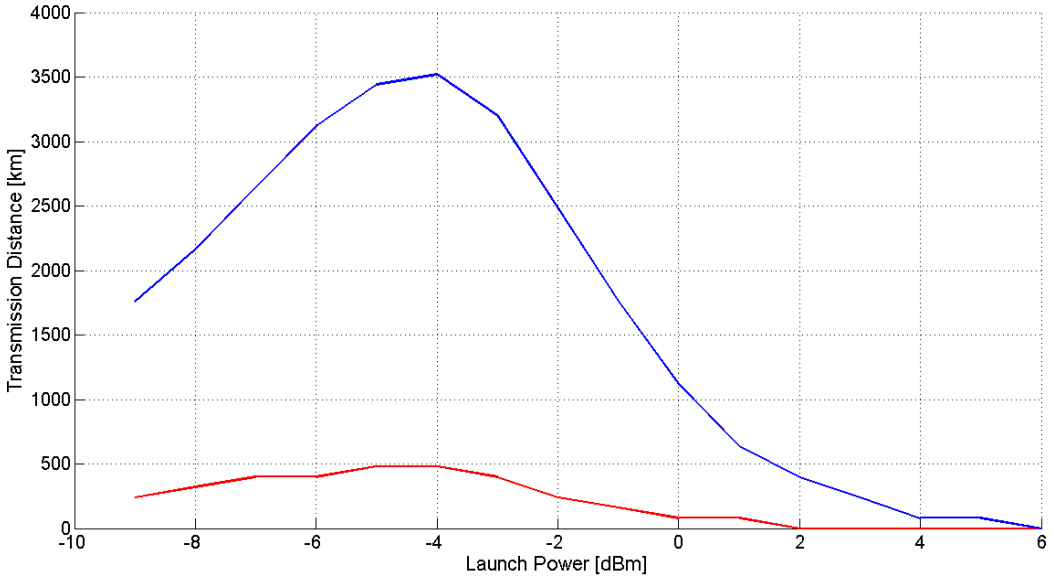

Figure 2.7 – Maximum transmission reach vs launch power estimated with the QoT Tool using the OSNR values for BER = 10^{-3} from Figure 2.6 for eOFDM transmission of a super-channel composed of 8 sub-channels with a Baud rate of 10 GBaud and modulation format QPSK (blue) and16QAM (red).

The maximum reach, as Figure 2.7 shows, is around 3500 km for QPSK and 500 km for 16QAM.

2.2.3 e-fOFDM

The Baud rate of the e-fOFDM signal is 10 GBaud, with a spectral occupancy of 12.5 GHz. From Figure 2.8, the back-to-back OSNR is ~14 dB for 16QAM (single polarisation).

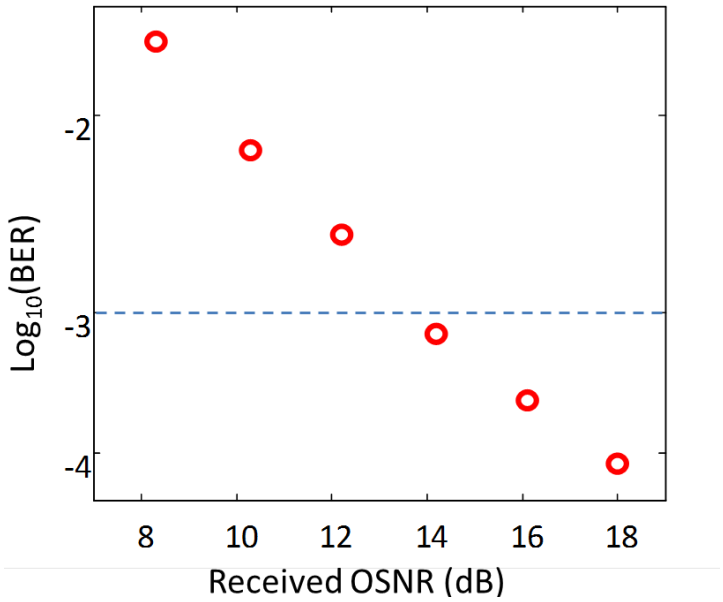

Figure 2.8 – Back-to-back BER versus OSNR for 10-Gbaud, 16QAM electrical fast OFDM (1 sub-channel) with 7-tap equalisers. The signal launch power is optimised as -8 dBm.

Because the results were obtained for a single-polarisation e-fOFDM signal, the QoT Tool is not valid to estimate the transmission performance of the system.

2.2.4 All-optical OFDM

According to Equation (*2.8*) the Q^2 factor corresponding to BER = 10^{-3} is Q^2 = 9.8 dB. The Baud rate of the O-OFDM signal is 10 GBaud, with a spectral occupancy of 12.5 GHz. From Figure 2.9, the back-to-back OSNR is ~5 dB for BPSK and ~7 dB for 16QAM.

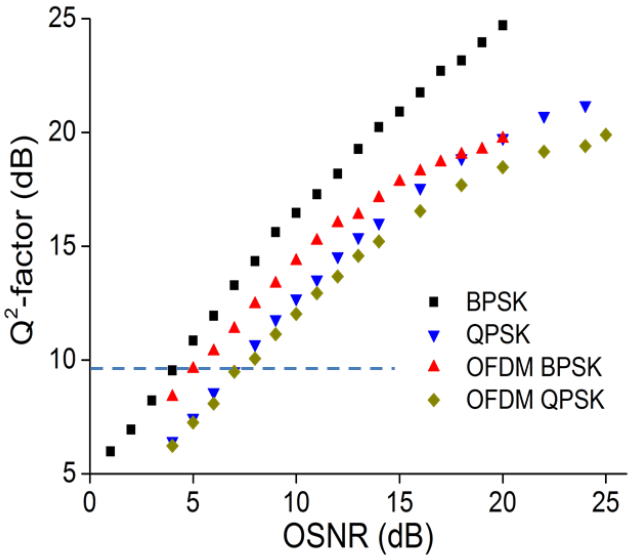

Figure 2.9 – Measured Q^2 factor vs OSNR for 10-GBaud single channel and OFDM BPSK and QPSK modulation formats.

The experimentally measured back-to-back OSNR is smaller than the value of OSNR for BER = 10^{-3} (Q^2 = 9.8 dB) calculated through Equation (*2.3*) when the launch power is smaller than -1 dBm. When that happens, the QoT Tool forces the back-to-back OSNR to be equal to the result obtained with Equation (*2.3*), which explains the constant value observed for low powers. These reach values should not be considered.

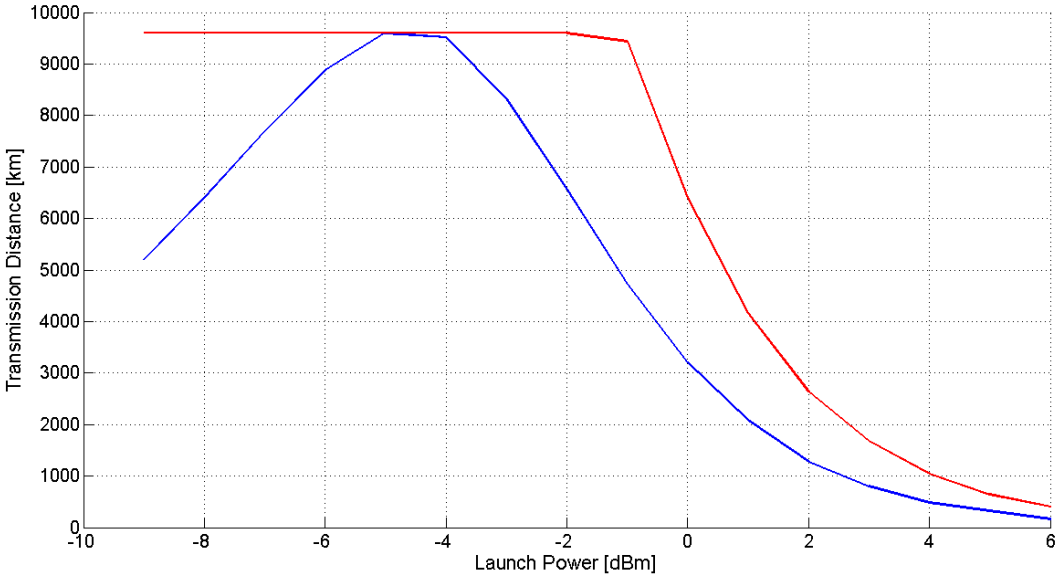

Figure 2.10 – Maximum transmission reach vs launch power estimated with the QoT Tool using the OSNR values for BER = 10^{-3} (Q^2 = 9.8 dB) from Figure 2.9 for O-OFDM transmission of a super-channel composed of 8 sub-channels with a Baud rate of 10 GBaud and modulation format QPSK (blue) and BPSK (red).

2.3 Transmission through a FOX-C node

Several sub-channels can be closely packed together to form a super-channel by employing any of the multiplexing schemes illustrated in Figure 1.1. This super-channel can be optically routed in an elastic optical network (EON) by ROADMs employing flex-grid WSS. In FOX-C, it is also possible to separate out the super-channel constituents through a hierarchical approach [11], with a typical commercially-available coarse-granularity flex-grid WSS operating at the fibre link level, followed by a high spectral resolution (HSR) switching processor [13] with ultra-fine granularity to "break up" the super-channel, allowing sub-channels to be added/dropped. A fundamental component of the HSR processor is an arrayed waveguide grating (AWG), shown in Figure 2.11(a), with optical resolution of 800 MHz. The HSR processor allows generating high-resolution notch and passband filters (Figure 2.11(b) and (c)) with pixel addressability of 400 MHz and an FSR of 200 GHz.

The purpose of this section is to analyze the OSNR penalty and filter cascading degradation undergone by a (quasi) Nyquist WDM [(q)N-WDM] signal when it goes through a two-stage flexible WSS ROADM with coarse and fine switching granularity.

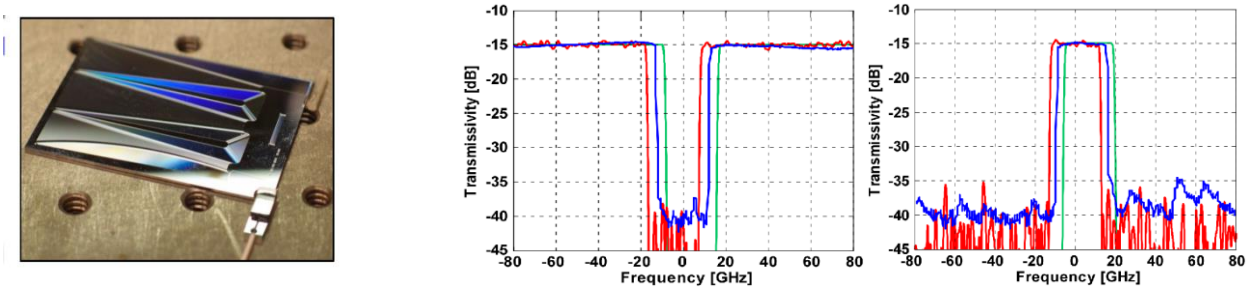

(a) (b) (c)

Figure 2.11 – AWG with sub-1GHz optical resolution. (a) AWG with I/O fibre attached and cylindrical lens to collimate output radiating light in the guided (vertical) direction. (b) & (c) Experimentally measured (blue) and simulated (green: noise free, red: with SNR set to 11) transmissivity of the <1GHz notch (b) and passband (c) filter with 25-GHz width.

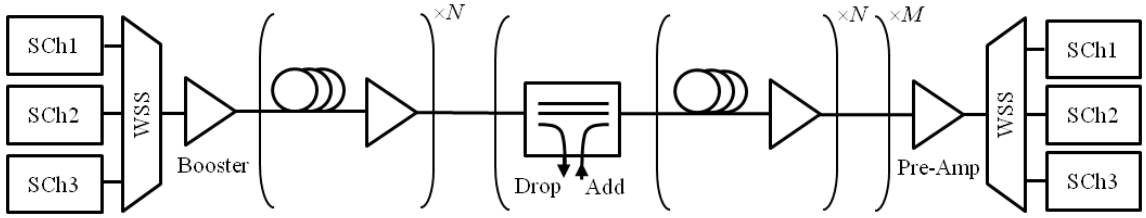

Figure 2.12 – Setup for the MATLAB™/VPI-TransmissionMaker™ co-simulation platform with M ROADMs and N 80-km fibre spans between ROADMs.

The setup for the ROADM emulation and the filter cascading studies, implemented on a MATLAB™/ VPI-TransmissionMaker™ co-simulation platform, is shown in Figure 2.12. Three transmitters generated three contiguous 700-Gbps SChs made up of seven 100-Gb/s DP-QPSK sub-channels, each modulated by two IQ modulators (one per polarization) and Nyquist-shaped by a 4th-order inverse super-Gaussian filter, as shown in Figure 2.13. Even though in this implementation the transmitter uses an optical filter, the shaping can also be performed in the digital domain by pre-processing and complex value modulation, the result being, in both cases, equivalent. The symbol rate of each DP-QPSK signal was 25 GBaud and the sub-channel spacing was chosen to be 25 GHz for the N-WDM case, 25.89 GHz (1.0357·Rs) for the tight qN-WDM case, and 26.79 GHz (= 1.07143·Rs) for the relaxed qN-WDM case. The BW of each SCh was 7× Δf plus a 12.5-GHz BW, forming a 187.5-GHz wide SCh in the N-WDM case and a 200-GHz and 193.7-GHz wide SCh in the qN-WDM cases. The spectra of a sub-channel before and after the Nyquist-shaping filter and of the resulting SCh are shown in Figure 2.14 and Figure 2.15, respectively.

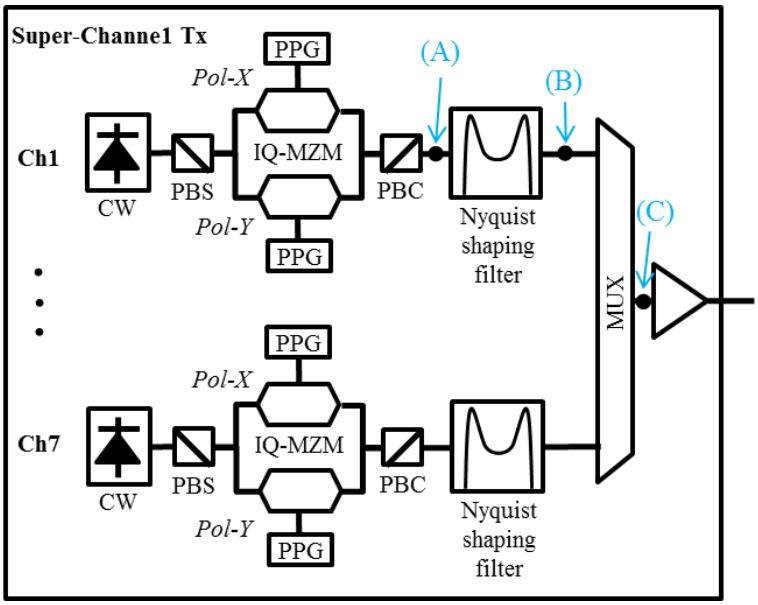

Figure 2.13 – SCh transmitter made up of 7 N-/qN-WDM sub-channel transmitters. PPG: pulse pattern generator, PBC/PBS: polarization beam combiner/splitter.

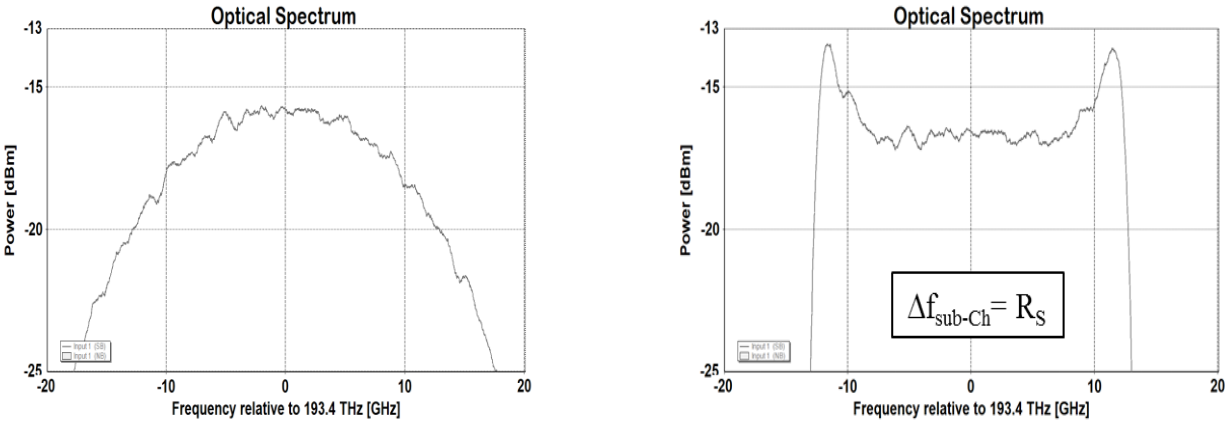

(a) (b)

Figure 2.14 – (a) and (b) Spectrum of a sub-channel at points A and B, respectively, in Figure 2.13.

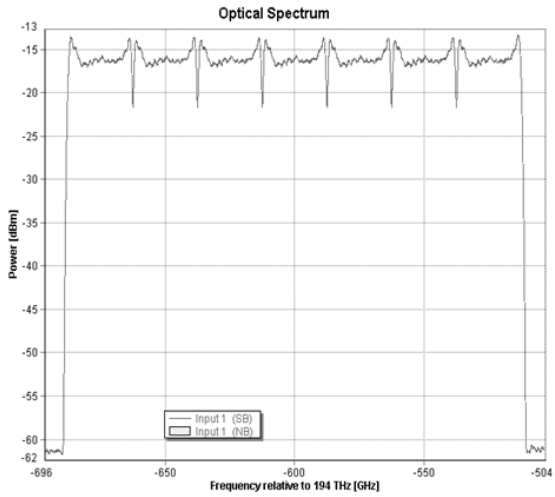

Figure 2.15 – Spectrum of the N-WDM super-channel at the output of the transmitter(point C in Figure 2.13).

Table 2.1 – Fibre parameters for the filter cascading simulation

Attenuation [dB/m]	2.00E-4
Dispersion [s/m^2]	17
Dispersion Slope [s/m^3]	60
γ coeff [1/(W·km)]	1.2
PMD [s/m$^{1/2}$]	3.16E-15

The 100-Gbit/s DP-QPSK signals were generated from a 2^{13} PRBS. The central frequency of the middle SCh was 193.4 THz and an independent laser source was used for each sub-channel, with a 100-kHz linewidth and uncorrelated phase noise. A MATLAB™ code was employed to accurately simulate an optical Nyquist-shaping filter with 3-dB BW equal to Δf (i.e. R_S for the Nyquist case). The seven Nyquist DP-QPSK signals were then multiplexed using an ideal flat-top multiplexer with an insertion loss (IL) of 3.5 dB (this can be substituted by a coupler –with much higher loss– or by two AWGs for combining the even and odd sub-channels separately, followed by a coupler to combine together these two sets of sub-channels. For more information about transceiver implementations, see section 3.1) and the three SChs thus formed were multiplexed in a WSS with 7.5-GHz resolution, 6.25-GHz pixel addressability and 5-dB loss. Before being launched into the fibre, a boost amplifier adjusts the output power to be -2dBm/sub-channel, which was verified to be optimal, according to the results obtained with the QoT Tool described in section 2.1 (see Figure 2.17), for point-to-point transmission when the back-to-back OSNR assumes the values shown in Figure 2.16 (calculated in the middle of the SCh through VPI simulations).

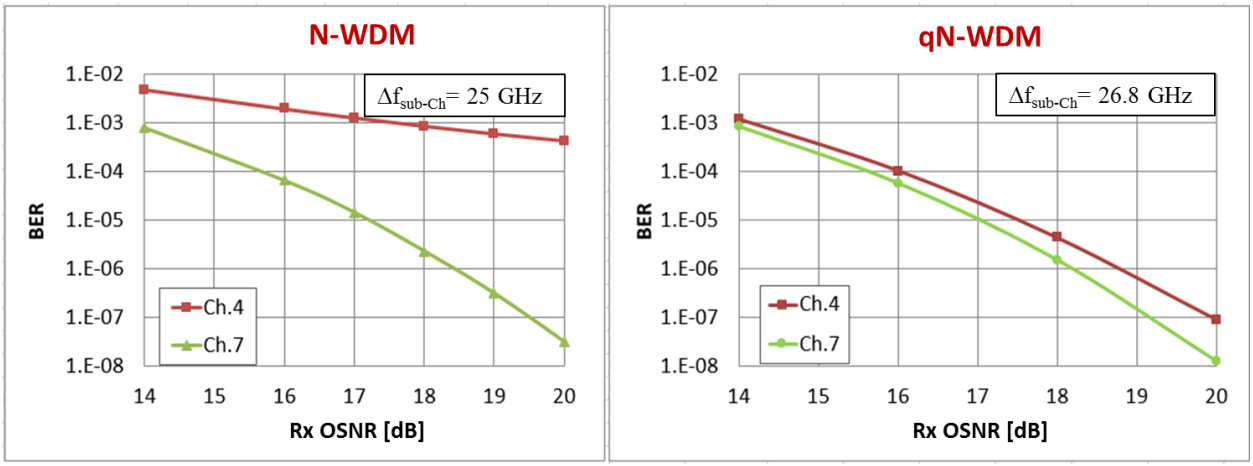

Figure 2.16 – OSNR vs back-to-back BER (X- and Y-polarisation average) for the two extreme cases of N- and relaxed qN-WDM transmission. The calculated OSNR value to achieve BER = 10^{-3} with tight qN-WDM (not shown) was also ~14 dB.

For the transmission part, uncompensated spans of 80 km of standard SMF were considered, followed by in-line amplifiers that exactly compensated for the losses of the previous span. The SMF was simulated using the split-step Fourier method at a sampling rate of 32 samples per symbol (SpS). Its physical parameters are summarized in Table I. All amplifiers used in the system were EDFAs with 5-dB noise figure. To ensure that the sub-channel power at the output of the amplifiers remained as constant as possible, optical band-pass filters (BPF) with an ideal rectangular profile with BW equal to 3× SCh BW were used to remove out-of-band ASE noise

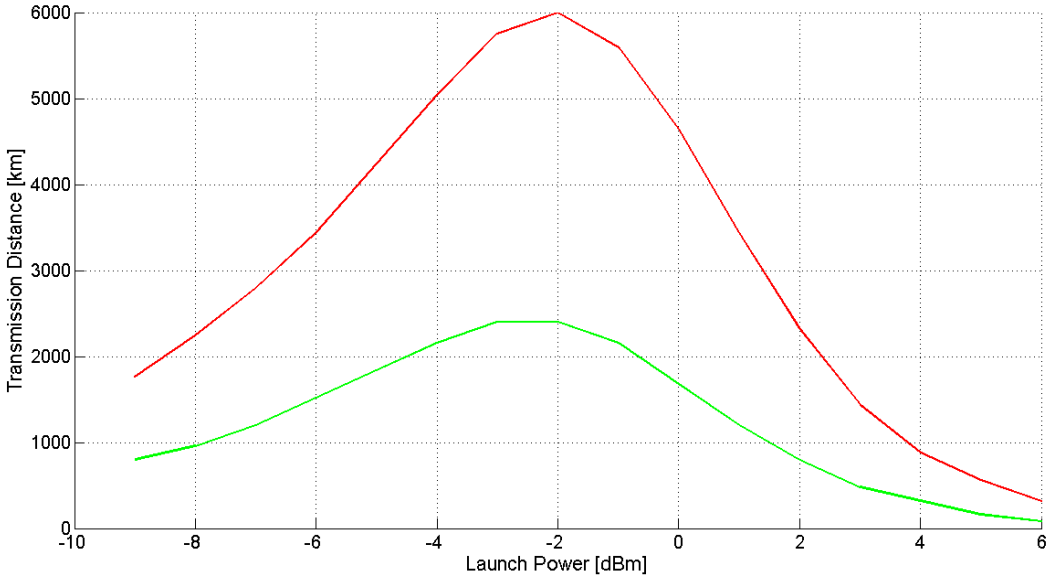

Figure 2.17 – Maximum transmission reach vs launch power in the case of N-WDM (green) and relaxed qN-WDM(red) transmission obtained with the QoT Tool using the OSNR values for BER = 10^{-3} (for the middle sub-channel) shown in Figure 2.16.

.

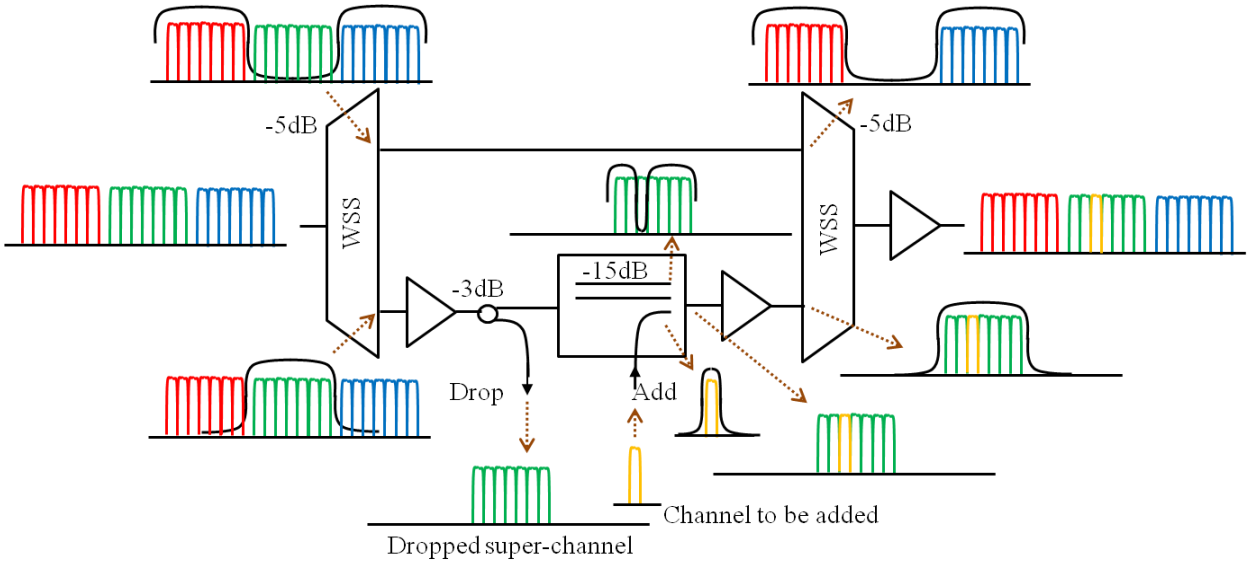

Figure 2.18 – Design and operation of a two-stage flexible ROADM. Shown are the 1st-level coarse-granularity WSS in a route-and-select architecture and the 2nd-level HSR switching processor.

After every 400 km (5 spans) a ROADM was placed over a total transmission distance of 6000 km (14 ROADMs in total) and the sub-channels were detected at the receiver after a last stretch of 400 km of SMF, as depicted in the line system diagram presented in Figure 2.12, where *N* = 5 spans and *M* had a maximum value of 14. The ROADM utilized the route-and-select architecture and was composed of two coarse-granularity WSS as well as an HSR switching processor for the added sub-channels, as shown in Figure 2.18. The ROADM functionality was therefore split into the SCh and the sub-channel levels. In order to drop a sub-channel, at the SCh level, the first WSS dropped the SCh containing the sub-channel to be extracted, while the rest of the SChs were expressed through to the second WSS, which multiplexed the signals added to each of its input ports and launched them back into the fibre. To simulate the worst-case scenario, we extracted the same sub-channel (Ch4 or Ch7) from the middle SCh

and added a newly generated sub-channel (in the dropped Ch4 or Ch7 position) to the existing SCh at every node. This guarantees that the adjacent sub-channels (Ch3 or Ch6) suffer the highest possible penalty due to sub-channel filtering (in the first case) or a combination of sub-channel and SCh filtering in the second case. Both WSS exhibited a spectral roll-off modelled as an error function (as explained in D4.1) with an optical resolution of 7.5 GHz, a pixel addressability of 6.25 GHz and an IL of 5 dB, with 3-dB BW equal to the SCh BW. For simulating the operation at the sub-channel level, the dropped SCh at the first WSS was split, with one of the replicas being sent to a coherent receiver that detected the sub-channel that needed to be dropped and the other replica being sent to the HSR switching processor, where a bandstop filter erased the sub-channel previously dropped and a bandpass filter shaped the new sub-channel to be added.

Both bandstop and bandpass filters had an optical resolution of 800 MHz, a pixel addressability of 400 MHz, an IL of 15 dB, and an FSR of 200 GHz. Several amplifiers were used in the ROADM architecture, as indicated in Figure 2.18, to ensure that the output power remained equal to -2dBm.

On the receiver side, as shown in Figure 2.19, the signal was initially pre-amplified and then detected by seven coherent detectors with local oscillators of 100-kHz linewidth and 5th-order Bessel electrical filters with 3dB bandwidth equal to 1/2 of the baud rate. The single-carrier signal was then interpolated and sampled at 2 SpS by an ADC of 6-bit resolution. In the DSP, an 11-tap MIMO CMA algorithm [14] followed by a frequency domain equalizer [15] of FFT size of 1024 were used for compensating the PMD and CD impairments. Finally, a carrier phase estimator (CPE) based on the Viterbi-Viterbi algorithm [16] with 10 symbols was used for the phase correction. The system performance is expressed in terms of the BER and calculated from the EVM for more precision [17].

The total capacity of the system was 700 Gb/s, with a spectral efficiency (SE) of 3.73 b/s/Hz for the Nyquist case, and 3.61 b/s/Hz and 3.5 b/s/Hz for the tight and relaxed qN-WDM cases, respectively.

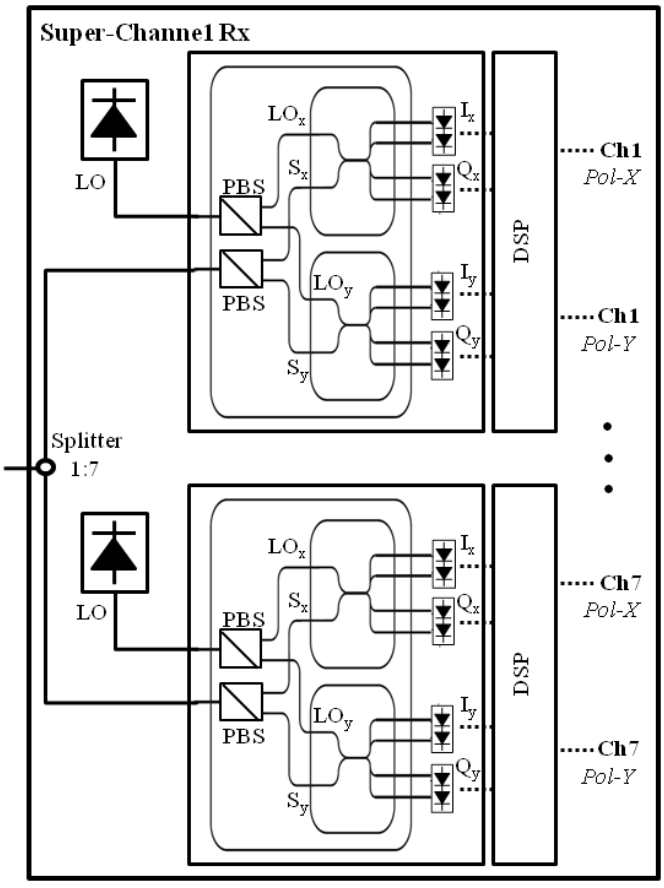

Figure 2.19 – SCh receiver made up of seven N-/qN-WDM sub-channel receivers.

2.3.1 OSNR penalty due to transmission through a FOX-C node

When a super-channel goes through the node depicted in Figure 2.18, the ASE noise arising from the amplification stages for compensating for the losses due to the filtering and switching stages degrades its transmission performance. If we call the noise at the input of the node n_{in} and the noise at the output n_{out}, we can write that $n_{out} - n_{in} = \Delta n_{node}$ or, equivalently,

$$\frac{n_{out} - n_{in}}{n_{in}} = \frac{\Delta n_{node}}{n_{in}} \tag{2.15}$$

If we assume that the input and output powers $P_{in} = P_{out} \gg n_{in}, n_{out}$ we can express the previous equation as

$$\frac{OSNR_{in}}{OSNR_{out}} - 1 = \frac{\Delta n_{node}}{n_{in}} \tag{2.16}$$

which can be finally written in a more convenient form as

$$OSNR \text{ penalty} = \frac{OSNR_{in}}{OSNR_{out}} = \Delta n_{node} \frac{OSNR_{in}}{P_{in}} + 1 \tag{2.17}$$

This is a linear curve, $y = ax + b$, where $a = \Delta n_{node}$ and $b = 1$. With the setup shown in Figure 2.12 we ran several VPI simulations to test the validity of this equation for a transmission system with six nodes and for several launch powers and back-to-back OSNR values. The results are presented in Figure 2.20.

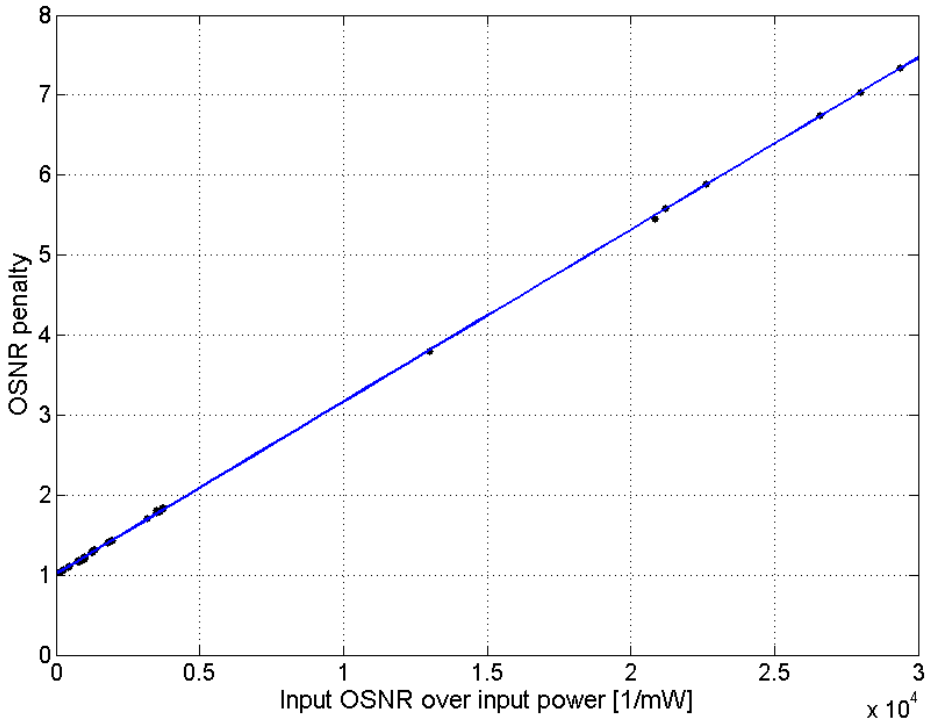

Figure 2.20 – OSNR penalty (OSNRin-OSNRout) when a (q)N-WDM super-channel goes through the FOX-C node depicted in Figure 2.18 as a function of the inverse of the input noise (or OSNRin/Pin).

After a linear curve fit, we obtained the following coefficients (with 95% confidence bounds):

$$a = \Delta n_{node} = 0.0002152 \ (0.0002147, 0.0002157)$$

$$b = 1.011 \ (1.006, 1.015)$$

The output signal from a node will have an OSNR given by

$$OSNR_{out} = \frac{OSNR_{in}}{\Delta n_{node}\frac{OSNR_{in}}{P_{in}} + b} \tag{2.18}$$

or, in dB,

$$OSNR_{out}[dB] = OSNR_{in}[dB] - 10log_{10}\left(\Delta n_{node}\frac{10^{\left(\frac{OSNR_{in}[dB]}{10}\right)}}{P_{in}} + b\right) \tag{2.19}$$

What Figure 2.20 and Equation (*2.17*) tell us is that the OSNR penalty incurred by the input signal to a node increases with the OSNR of the signal. Therefore, the signal will be more impacted at the first node than at subsequent nodes. This also explains some results that will be presented in subsection 2.3.2. For instance, in Figure 2.21 (left) and Figure 2.22 (left) we observe that for sub-channel 4 (of a NWDM super-channel), which has a rather poor back-to-back OSNR, the performance remains quite stable, whereas sub-channel 7, which has a good back-to-back OSNR, experiences a sharp degradation after the first node (and slightly less at the second), but from the third node on its BER-vs-OSNR curve runs parallel to the point-to-point transmission curve. This is also observed in the case of qN-WDM, even though the degradation with respect to the point-to-point transmission scenario is greatly reduced due to the broader separation between the sub-channels. This demonstrates that not only does the ASE noise have an effect on the OSNR penalty incurred by the signal when it goes through a node, but also that the filtering effect plays an important role in the transmission of a super-channel in a multi-link scenario. The next subsection will be devoted to studying this effect.

2.3.2 Impact of cascaded filters on transmission

To evaluate the performance degradation due to the filter cascade, we simulated the back-to-back performance of the N- and qN-WDM transmission (Figure 2.16), followed by the point-to-point transmission with uncompensated spans of 80 km of SMF and the transmission through a number of two-stage ROADMs separated by 400 km of SMF. For the back-to-back configuration the OSNR necessary to achieve a pre-FEC BER of 10^{-3} was ~18 dB and 14 dB for the Nyquist and quasi-Nyquist cases, respectively, as previously shown in Figure 2.16.

This OSNR difference of ~4 dB stems from the higher crosstalk undergone by the Nyquist signal on account of the compactness of the sub-channels within the SCh and explains the far worse performance of the central sub-channels in the Nyquist case, with a BER (average of X and Y polarizations) of ~10^{-4} for distances as short as 400 km (see Figure 2.21 and Figure 2.22). Even though this back-to-back penalty exists, which hinders Nyquist-WDM-based optical SCh transmission for high performance applications, it can be seen that the BER variation is rather stable for more than 1500 km.

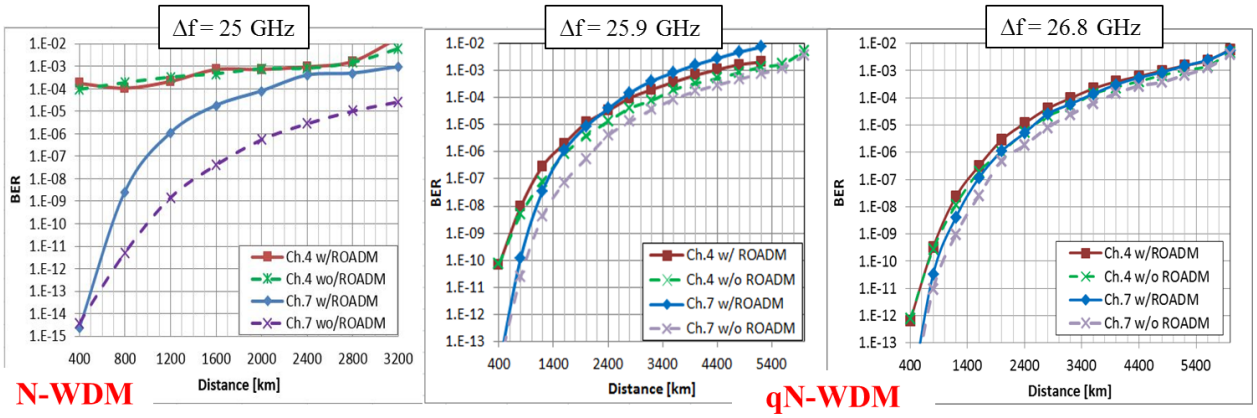

Figure 2.21 – BER vs distance of Ch4 and Ch7 when Ch3 is dropped and a new Ch3 is added at each ROADM with N- and tight and relaxed qN-WDM transmission, respectively. In all cases, the evaluated sub-channels belong to the middle SCh.

For the transmission performance evaluation of a SCh, typical measurements consider only the effects on the middle sub-channel as the worst case scenario [12],[19]. This was proved to be so in the case of point-to-point transmission, especially for the Nyquist case (Ch4/5 limit transmission after ~2500 km for NWDM, and 5000 and 5200 km for the tight and relaxed quasi-Nyquist cases, respectively, in the best-case scenario of a system without ROADMs). However, in the presence of WSS coarse filtering, the middle sub-channel is expected not to be much affected, which is clearly confirmed by the results in Figure 2.21 and Figure 2.22 for N-WDM in the worst-case scenario of SChs going through the two filtering stages at every ROADM, where we observe how the BER of the central sub-channel remains nearly stable whereas the BER of the edge sub-channel degrades rapidly until it reaches the performance of the central sub-channel after ~2400 km transmission.

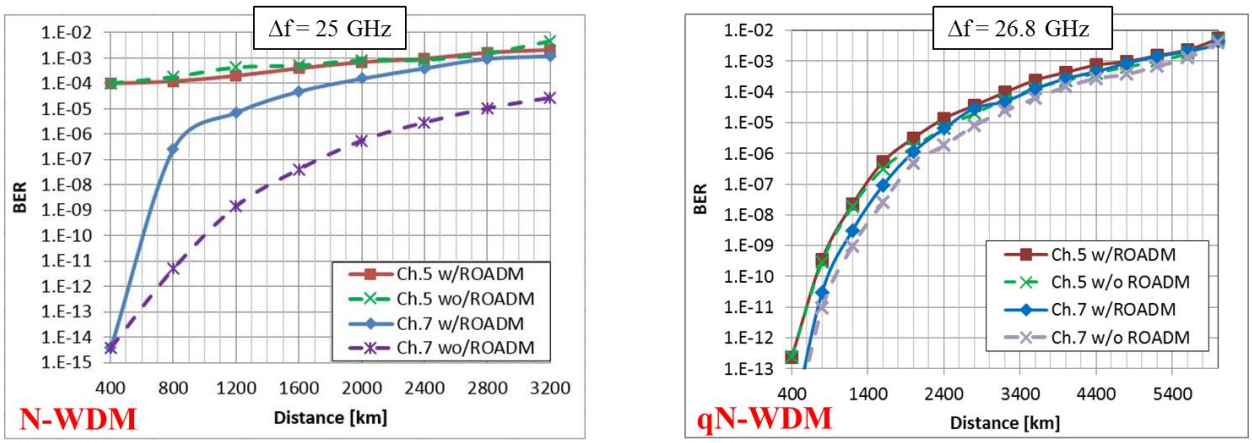

Figure 2.22 – BER vs distance of Ch5 and Ch7 when Ch6 is dropped and a new Ch6 is added at each ROADM with N- and relaxed qN-WDM transmission. In all cases, the evaluated sub-channels belong to the middle SCh.

In the quasi-Nyquist scenarios plotted in Figure 2.21 and Figure 2.22, the central sub-channel also exhibits a worse performance but all sub-channels experience a similar degradation with distance. Despite this, the difference between the BER values for the edge sub-channels in the two extreme cases under examination (with and without ROADMs) rises with the distance, getting increasingly close to the performance of Ch4. Therefore, the edge sub-channels would constitute the worst-case scenario in the case of narrower filtering (NWDM) since they are most prominently affected by the non-ideal roll-off of the WSS filters. However, due to the back-to-back penalty of the N-WDM SCh that limits their reach in the absence of ROADMs, the WSS filtering effects are unfelt, the limiting sub-channels are the central sub-channels (both when the dropped sub-channel is Ch3 and Ch6), and the transmission distance remains roughly the same (~2300-2400km), which allows the signal to go through 3-4 ROADMs. Regarding the HSR filters, they have such sharp edges and the cascade is so small (3-4 HSR filters) that their influence is almost negligible. However, note how Ch7's BER degrades more quickly for dropped sub-channel Ch6 (Figure 2.22) than dropped Ch3 (Figure 2.21) in the NWDM case.

In the case of tight qN-WDM (see Figure 2.21 (centre)), we observe that the worst-performing sub-channel in the scenario with ROADMs is Ch7 after 2400 km and it limits the transmission reach to 3600 km. On the other hand, in the case of relaxed qN-WDM, the BER degradation experienced by Ch7 in Figure 2.21 (right) and Figure 2.22 (right) is very similar, which appears to suggest that the HSR has little effect, with a reduction of the maximum reach to ~4400 km, i.e. 88% of distance attained in the point-to-point configuration.

In Figure 2.23 we show the results of a study to measure the influence of the first and second filtering stages of the FOX-C node on the BER performance of the edge sub-channels. In the graphs, the first stage only refers to WSS coarse filtering and the 2-stage filtering considers both WSS coarse and HSR fine filtering. We observe that in all three plotted scenarios the HSR fine filtering stage is responsible for the BER degradation, and this degradation diminishes as the sub-channel spacing

increases. Indeed, in a cascade of *N* identical WSS, the overall 3-dB BW is given by the 3/N-dB BW of the individual WSS [18]. In the case of relaxed qN-WDM transmission, the SChs traverse 10 ROADMs, equivalent to 20 WSS and 10 HSR filters. The 1.8-GHz and 12.5-GHz spectral gap between sub-channels and SChs, respectively, as well as the flat center section and sharp edges of the filters used in this work explain the little drop in performance observed.

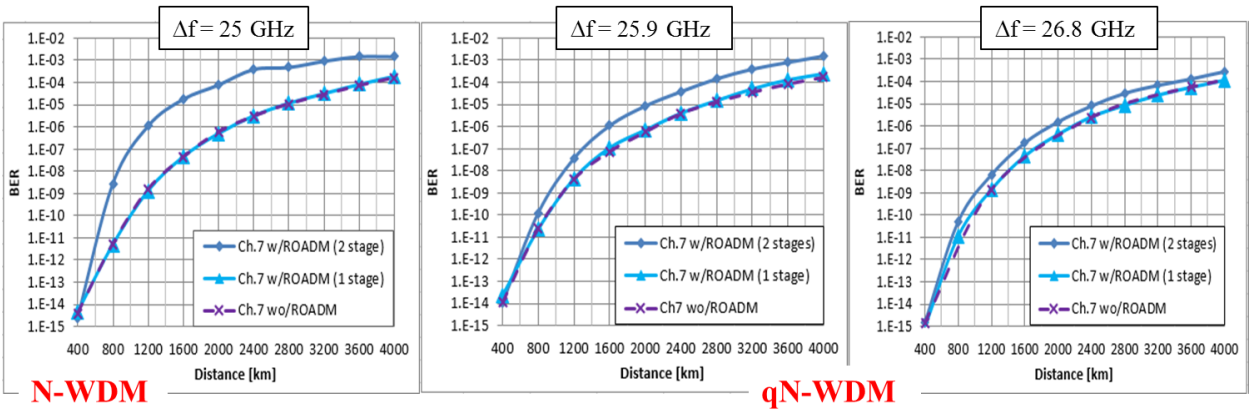

Figure 2.23 – BER vs distance of Ch7 in three scenarios: point-to-point transmission (w/o ROADM), transmission with only coarse filtering (w/ ROADM (1 stage)) and transmission with both coarse and fine filtering (w/ ROADM (2 stage)). In the third scenario, Ch3 is dropped and a new Ch3 is added at each ROADM with N- and qN-WDM transmission. In all cases, the evaluated sub-channels belong to the middle SCh.

2.3.3 Maximum transmission reach estimation in a multi-link scenario with FOX-C nodes

In Figure 2.24 and Figure 2.25 we show the maximum transmission reach as a function of the launch power estimated with the QoT Tool using the OSNR values for BER = 10^{-3} from Figure 2.16 for N-WDM and qN-WDM transmission of a super-channel with sub-channel spacing of 25 GHz and 26.8 GHz in three scenarios: point-to-point (blue), multi-link (green) and multi-link with FOX-C nodes (red), where the influence of the ASE noise due to the WSS amplification was considered (the filtering effect of adding/dropping sub-channels hasn't been included in the transmission estimating tool).

Even though the only difference between the point-to-point and the multi-link scenarios is that for the first one we used the algorithm based on Equation (*2.10*) and for the second one we used Equation (*2.14*), we see that the maximum reach is reduced in the multi-link scenario by a few hundred kilometres. We should note that in the first scenario the distances increase in multiples of 80 km and in the second case in multiples of 400 km, which undoubtedly has an impact on the accuracy of the results. Furthermore, the assumption regarding the summation of the OSNR values for the individual optical links across the lightpath presented in Equation (*2.14*) is valid for the case of the ASE noise term, which has purely Gaussian characteristics, but is in general invalid for the case of NLI. In spite of this, we have found that the difference in terms of Q factor performance is relatively small, especially at the optimum operation conditions, but obviously increases for higher launch powers because of the NLI noise contribution increase.

In the multi-link scenario with FOX-C nodes utilising the correction factor deduced in subsection 2.3.1 (Equation (*2.17)*), we can observe that the result is very good in the case of q-NWDM (Figure 2.25) if we compare it with the maximum distance obtained with VPI shown in Figure 2.21 (left) and Figure 2.22 (left), but the maximum distance was severely underestimated in the case of NWDM (Figure 2.24). This may be explained by two facts. On the one hand, the aforementioned circumstance that the distance is now determined in multiples of 400 km (which reduces the precision), on the other hand, the strong dependence of the distance on the back-to-back OSNR. By varying the OSNR values obtained in Figure

2.16 by ±0.5 dB we can achieve a match with the values obtained in Figure 2.21 and Figure 2.22 in all cases.

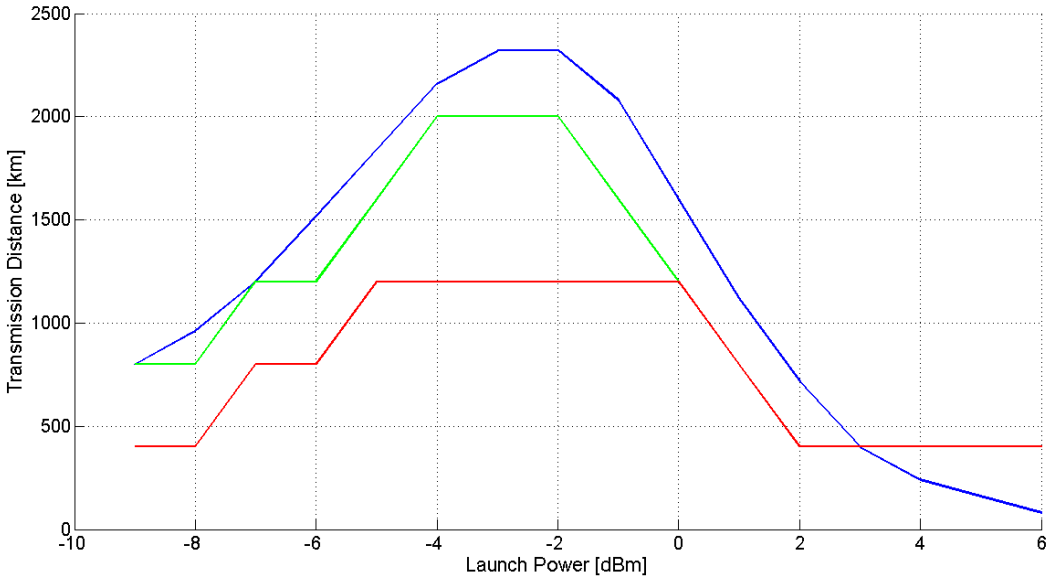

Figure 2.24 – Maximum transmission reach vs launch power estimated with the QoT Tool using the OSNR values for BER = 10^{-3} from Figure 2.16 (left) for N-WDM transmission of a super-channel composed of 7 sub-channels with a Baud rate of 25 GBaud, modulation format QPSK and channel spacing of 25 GHz in three scenarios: point-to-point (blue), multi-link (green) and multi-link with FOX-C nodes (red).

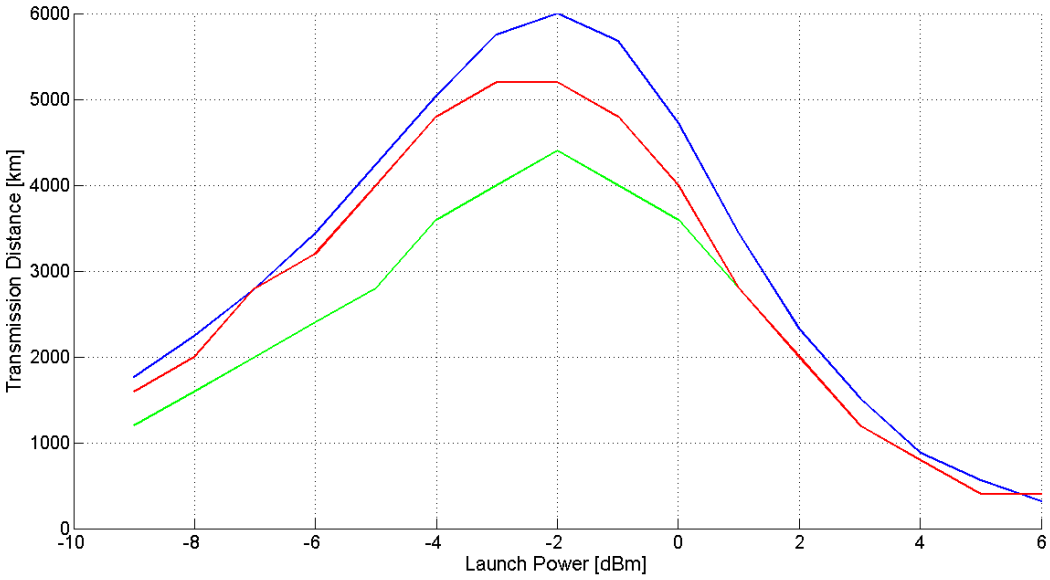

Figure 2.25 – Maximum transmission reach vs launch power estimated with the QoT Tool using the OSNR values for BER = 10^{-3} from Figure 2.16 (right) for qN-WDM transmission of a super-channel composed of 7 sub-channels with a Baud rate of 25 GBaud, modulation format QPSK and channel spacing of 26.8 GHz in three scenarios: point-to-point (blue), multi-link (green) and multi-link with FOX-C nodes (red).

3 Cost and power consumption reference model

This chapter sums up the transceiver designs for the different all-optical and electrical multiplexing schemes evaluated in WP3 and the FOX-C-enabling optical cross connect designs resulting from the work carried out in WP4. These designs are used to estimate the cost and power consumption of the modules for the techno-economic evaluation presented in section 4.5.

3.1 Transceivers

In this section we present the designs of the single-carrier and super-channel transceivers used to estimate the cost and power consumption of the modules for the multiplexing schemes analysed in T3.2 and T3.3. We divide the different multiplexing schemes into the following categories:

- Electrical multiplexing schemes: NFDM and e(f)OFDM
- Optical multiplexing schemes:
  - (q)NWDM with optical filtering
  - O-OFDM with dual quadrature modulation
  - O-fOFDM with single quadrature modulation

3.1.1 Electrical multiplexing schemes

Figure 3.1 shows a design of the type of single-carrier transceivers considered in the networking studies presented in chapters 4 and 5. This transceiver will be used for the benchmarking cases (both in the single line rate (SLR) and multiple line rate (MLR) scenarios) and, connected to the Add/Drop cards, for the addition and extraction of sub-channels to/from a super-channel based on NFDM or e(f)OFDM. It consists of:

- a DSP chip with
  - four low frequency RF power dividers ($1k-$1.5k and 2-10W depending on the frequency range and on included amplifiers for loss compensation, if considered separately)
  - four DAC/ADC (1.5W per DAC/ADC for integrated solution and 2W for standalone solution. The DAC should be running at 64GSa/s)
- a four-port RF amplifier as modulator drivers
- four RF LP filters after the modulator drivers to remove the aliasing components. These can be dispensed with if the sampling rate of the DSP chip is sufficiently high in comparison with the electrical bandwidth. Additionally, four optional RF LP filters can be used in front of the ADCs, depending on the sampling rate and electrical bandwidth of the ADCs, to remove unwanted spectral components. An increased sampling rate of the ADCs would allow getting rid of the aliasing spectra in the DSP, but it would come at the price of increasing the amount of data to be processed at the receiver. We have considered RF LP filters both at the transmitter and the receiver.
- one polarisation-multiplexed IQ modulator
- two narrow-linewidth lasers (one at the transmitter and the other one at the receiver)
- one integrated, dual-polarisation coherent receiver, including a 90º hybrid, four balanced photodiodes and four transimpedance amplifiers (TIA)

For more details, please refer to D3.2 and D3.3.

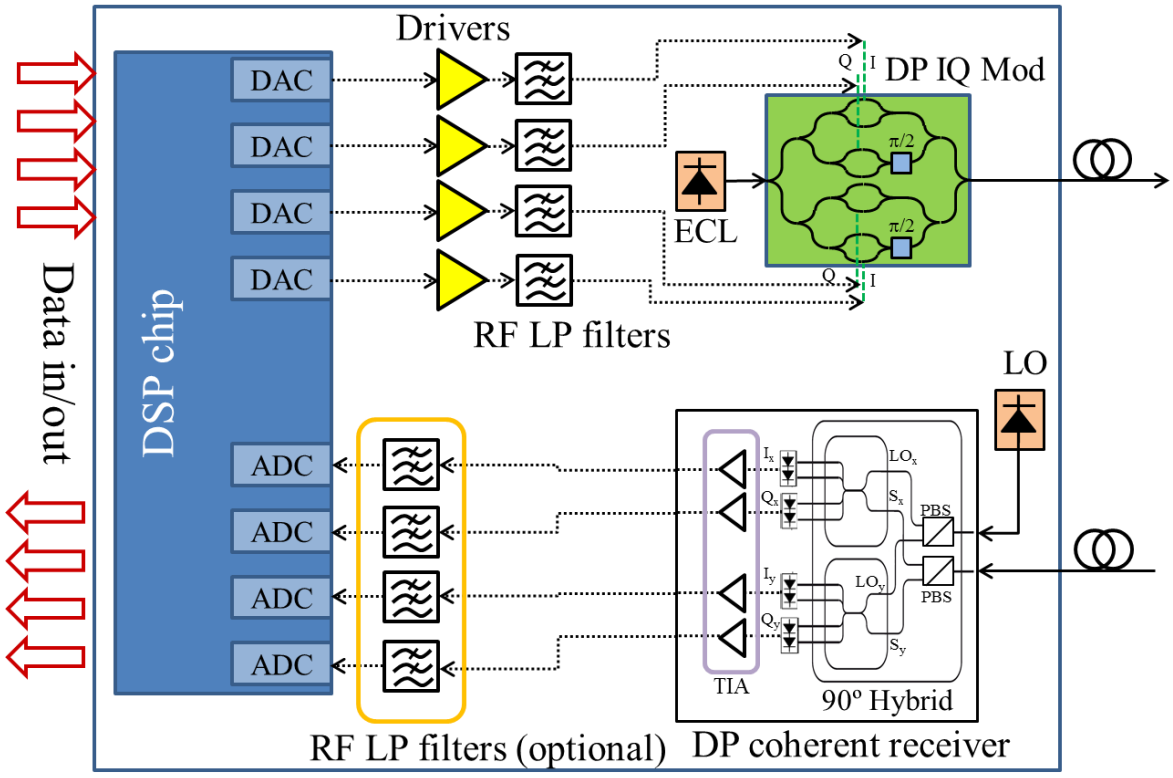

Figure 3.1 – Design of a single-carrier transceiver for SLR, MLR and the addition/extraction of one sub-carrier to/from super-channels based on the electrical multiplexing schemes.

Table 3.1 shows the cost and power consumption associated with the single-carrier transceiver depicted in Figure 3.1. The cost is expressed in absolute values (k$) and also relative to the cost of the 100G transceiver (*) or the 10G transceiver (**).

Table 3.1 – Cost and power consumption of a single-carrier transceiver to be used in the SLR and MLR benchmarking scenarios as well as for the addition/extraction of sub-channels to/from super-channels based on the electrical multiplexing schemes.(*) Relative to cost of 100G transceiver. (**) Relative to cost of 10G transceiver

			SLR/MLR/NFDM & MB-e(f)OFDM Sb-Ch TRx				
Component	**Unit cost (K$)**	**Power (W) [max]**	**#**	**Total cost (K$)**	**Relative cost (*)**	**Relative cost (**)**	**Total power (W)**
DSP Chip	10.00	38.5	1	10.00	0.4	1.9	38.5
PM IQ Mod	6.00	0	1	6.00	0.2	1.1	0.0
Laser (Tx & Rx LO)	1.50	1.5	2	3.00	0.1	0.3	3.0
4-Port Modulator Driver	2.00	6	1	2.00	0.1	0.4	6.0
RF LP filter	0.10	0	8	0.80	0.0	0.0	0.0
DP Coherent Receiver	6.00	1.5	1	6.00	0.2	1.1	1.5
				27.80	1.0	5.2	49.0

The cost of the DSP excludes the development cost. It includes analogue front-end, i.e. 4× ADC and 4× DAC (64GSa/s) as well as first stage of AGC amplification and 4× low frequency RF power dividers. The power consumption of the DSP/FEC <35W, that of the four ADC/DAC is 1.5W, and that of the four power dividers equals 0.5 W.

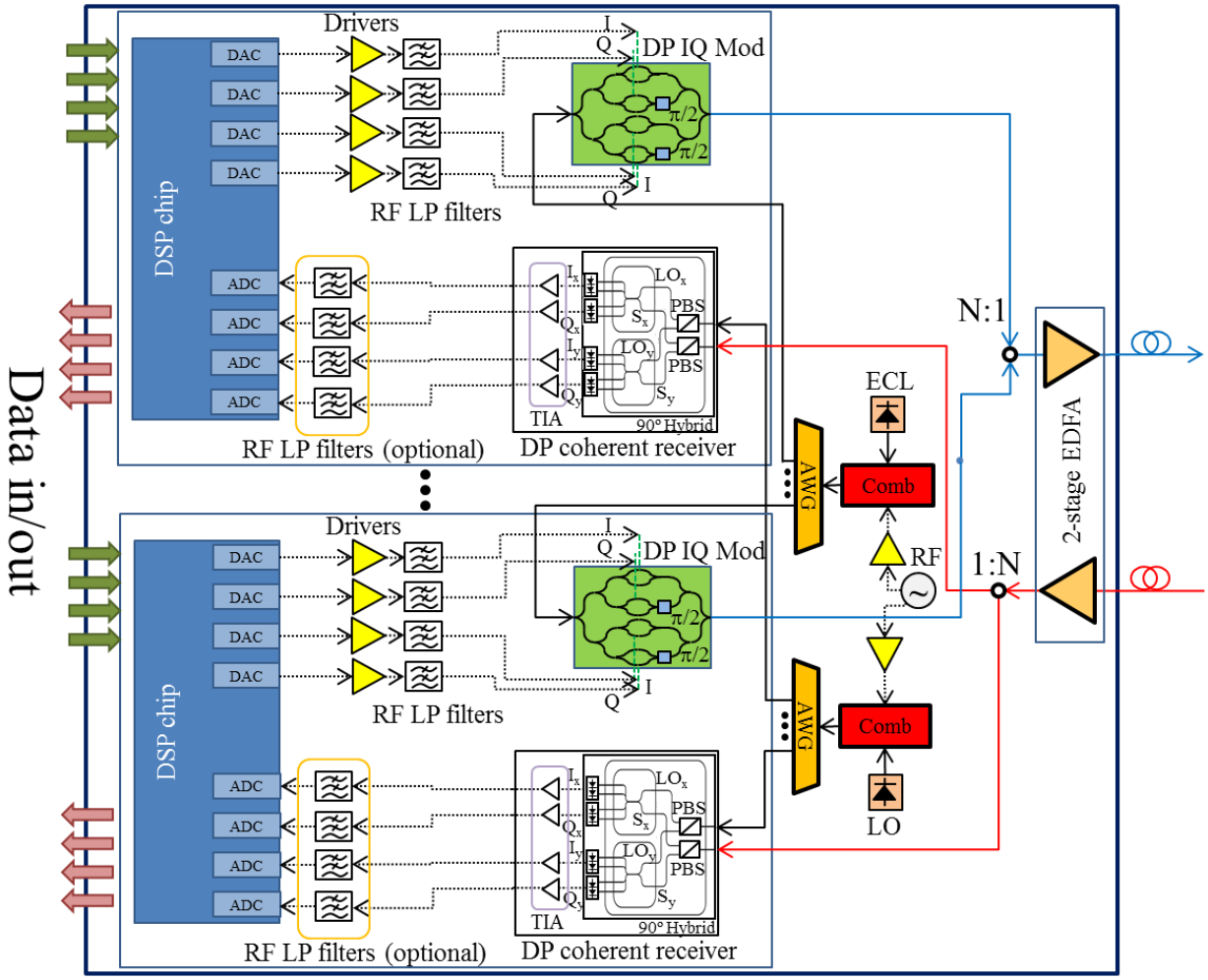

Figure 3.2 – Design of a super-channel transceiver for the electrical multiplexing schemes.

Figure 3.2 shows the design of a super-channel transceiver for the electrical multiplexing schemes. It employs a comb generator modulator driven by a sinusoidal signal, two AWGs, an N:1 combiner and a 1:N splitter. As mentioned before, we have assumed for the cost and power consumption evaluation that the maximum number of sub-channels is 8.

In the cost model presented in Table 3.2 we have assumed a reduction of 40% in the cost of all components, except for the DSP, due to electronic integration, including integrated photonic circuit development and integration with active and passive RF electronics. In an alternative design, the variable gain dual-stage amplifier may not be integrated for practical reasons, in which case the integration reduction factor would not affect this component and the overall cost of the super-channel transceiver device would be $166.84k, or 6.0 times the cost of a 100G transceiver or 31.4 times the cost of a 10G transceiver (1.2% more expensive).

Table 3.2 – Cost and power consumption of a super-channel transceiver for the electrical multiplexing schemes.(*) Relative to cost of 100G transceiver. (**) Relative to cost of 10G transceiver

			Sp-Ch TRx (total)					
Component	**Unit cost (K$)**	**Power (W) [max]**	**#**	**Integration reduction factor**	**Total Cost (K$)**	**Relative cost (*)**	**Relative cost (**)**	**Total power (W)**
DSP Chip	10.00	38.5	8	0	80.00	2.9	15.0	308.0
PM IQ Mod	6.00	0.00	8	0.4	28.80	1.0	5.4	0.0
Laser (Tx & Rx LO)	1.50	1.50	2	0.4	1.80	0.1	0.3	3.0
4-Port Modulator Driver	2.00	6.00	8	0.4	9.60	0.3	1.8	48.0
RF LP filter	0.10	0.00	64	0.4	3.84	0.1	0.7	0.0
DP Coherent Receiver	6.00	1.50	8	0.4	28.80	1.0	5.4	12.0
Variable gain dual-stage amplifier	5.00	12.00	1	0.4	3.00	0.1	0.6	12.0
Comb generator modulator	5.00	0.00	2	0.4	6.00	0.2	1.1	0.0
Comb generator mod. driver	2.00	2.00	2	0.4	2.40	0.1	0.5	4.0
1:N AWG	0.50	0.00	2	0.4	0.60	0.0	0.1	0.0
					164.84	5.9	31.0	387

3.1.2 (q)NWDM with optical filtering

This is, together with O-(f)OFDM, a type of optical multiplexing scheme. Because the spectrum filtering is done in the optical domain, the RF LP filters are replaced with a 1x1 HSR filter followed by an amplifier to compensate for the losses. Apart from that, there are no other changes in the transceiver design, presented in Figure 3.3, with respect to the electrical multiplexing case.

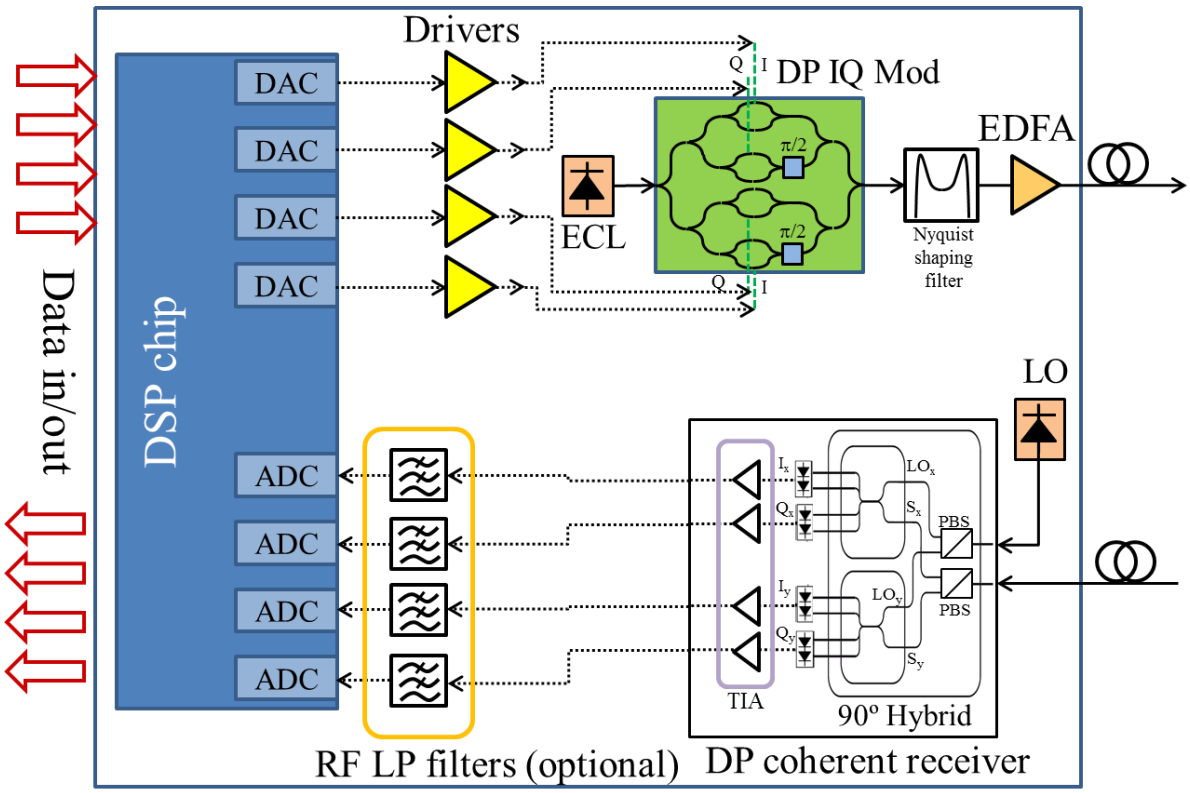

Figure 3.3 – Design of a sub-channel transceiver for the addition/extraction of one sub-carrier to/from super-channels based on (q)NWDM with optical filtering.

In Table 3.3 we show a breakdown of the cost and power consumption of the sub-channel transceiver to be used in conjunction with the ultra-fine resolution add/drop cards of the nodes to add or drop sub-channels from a super-channel. Its cost is ~50% higher than the cost of the sub-channel transceiver for electrical multiplexing schemes due to the high cost of the HSR filter. In the cost model presented in this chapter we assume a cost premium for newly created technology, but we expect the HSR filter cost to scale down to that of conventional 1×9 WSS (5-6 k$). A sensitivity analysis of the sub-channel transceiver cost on the HSR filter cost is shown in Figure 3.4. In our model, the power also increases by over 1/4 due to the HSR filter and the associated EDFA to compensate for the high insertion loss of this component, but the power dissipation and insertion losses are also expected to scale down in future developments.

Table 3.3 – Cost and power consumption of a sub-channel transceiver for the addition/extraction of sub-channels to/from super-channels based on (q)NWDM with optical filtering.(*) Relative to cost of 100G transceiver. (**) Relative to cost of 10G transceiver

			Sb-Ch TRx				
Component	**Unit cost (K$)**	**Power (W) [max]**	**#**	**Total cost (K$)**	**Relative cost (*)**	**Relative cost (**)**	**Total power (W)**
DSP Chip	10.00	38.5	1	10.00	0.4	1.9	38.5
PM IQ Mod	1.50	0.0	1	1.50	0.1	0.3	0.0
Laser (Tx & Rx LO)	1.50	1.5	2	3.00	0.1	0.6	3.0
4-Port Modulator Driver	2.00	6.0	1	2.00	0.1	0.4	6.0
RF LP filter	0.10	0.0	4	0.40	0.0	0.1	0.0
DP Coherent Receiver	6.00	1.5	1	6.00	0.2	1.1	1.5
Variable gain amplifier	3.00	9.0	1	3.00	0.1	0.6	9.0
1x1 HSR filter	15.00	4.0	1	15.00	0.5	2.8	4.0
				40.90	1.5	7.7	62.0

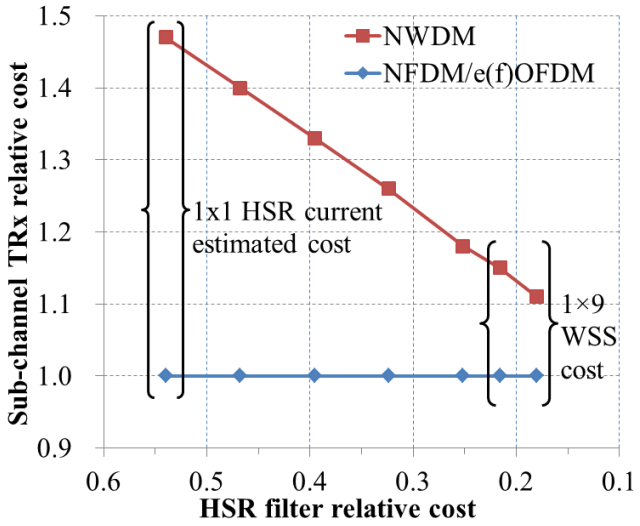

Figure 3.4 – Sensitivity analysis of the relative cost of the single-carrier/sub-channel transceiver for electrical multiplexing schemes (NFDM/e(f)OFDM) and N-WDM with optical filtering on the relative cost of the HSR filter. The HSR filter cost is assumed to vary from a relative cost of 0.54 (equivalent to $15k) to ~0.2 (current cost of a 1x9 WSS). Relative costs to cost of 100G transceiver.

Figure 3.5 shows the super-channel transceiver design. To reduce the cost, odd and even sub-channels are multiplexed separately and fed into two 1x1 HSR filters. An interleaver (ITL) is used to combine the two sets of sub-channels prior to amplification. Alternatively, a coupler can be used.

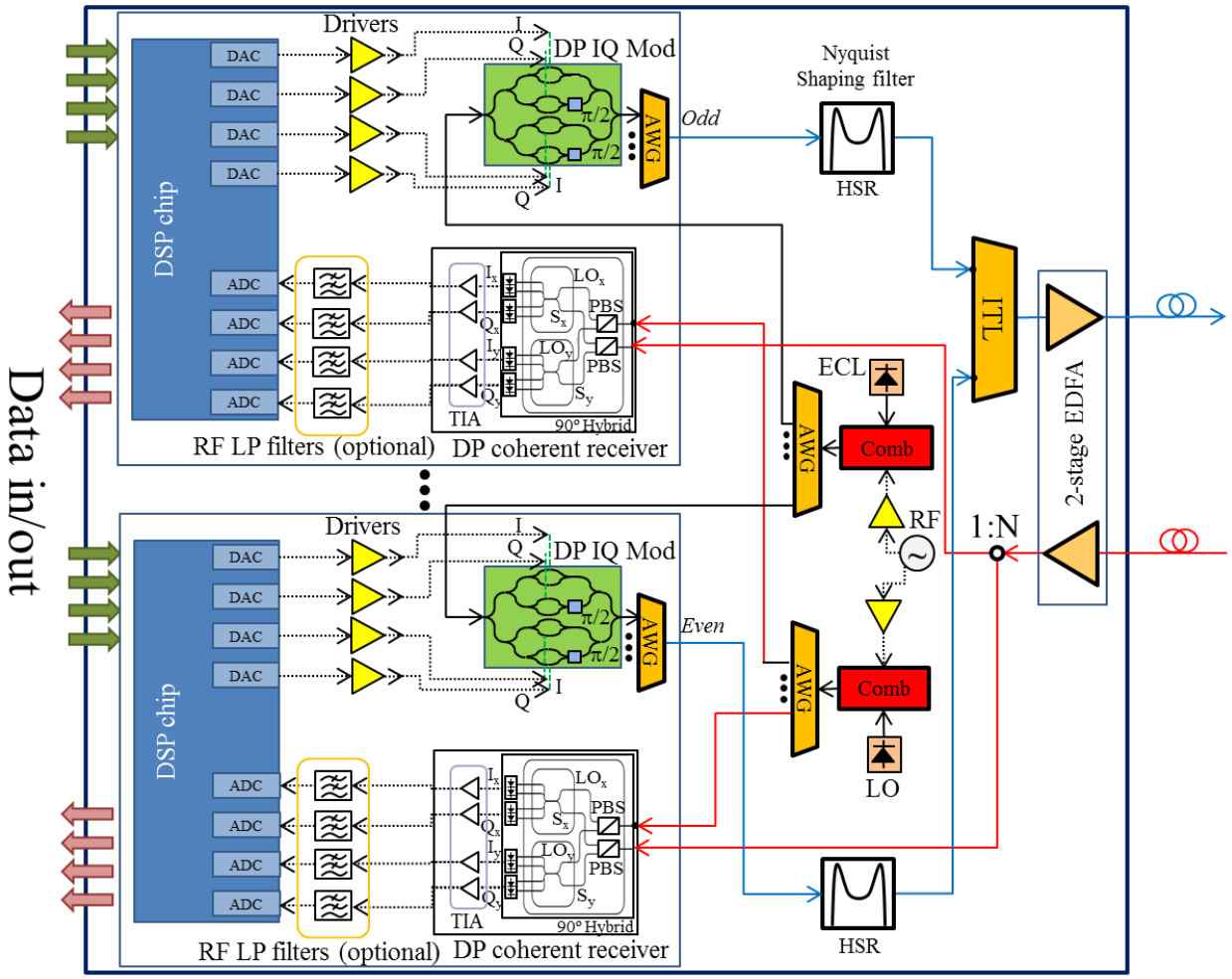

Figure 3.5 – Design of a super-channel transceiver for (q)NWDM with optical filtering.

In Table 3.4 the cost and power consumption for the super-channel transceiver are presented. Compared with the super-channel transceiver for the electrical multiplexing schemes, the cost is less than 5% higher (down from ~50% higher for the sub-channel transceiver) and the power consumption is ~2% higher (down from ~25% higher for the sub-channel transceiver). This reduction in comparison with the sub-channel transceiver is due to the sharing of HSR filters between the even and odd sub-channels. Note that in this design the DSP chip and the HSR filter do not benefit from a 40% cost reduction on account of the integration process. We can anticipate that further technology development may lead to the integration of both HSR filters (for even and odd sub-channels) in one, so only a single Nx1 HSR filter would be required, with the associated cost and power consumption reduction. We can estimate the cost of an 8x1 scalable bulk-grating-based HSR (being developed by partner HUJI) to be ~$20k. In this case, the total cost of the super-channel transceiver would come down to $161.32k (30.3 times the cost of a 10G transceiver or 5.8 times the cost of a 100G transceiver) and the power consumption would be 391W. This N-WDM super-channel transceiver cost comparison is shown in Figure 3.6, both for the current cost of the HSR filters and following a sensitivity analysis on the cost of the HSR filters.

Table 3.4 – Cost and power consumption of a super-channel transceiver for (q)NWDM with optical filtering.(*) Relative to cost of 100G transceiver. (**) Relative to cost of 10G transceiver

			Sp-Ch TRx (total)					
Component	**Unit cost (K$)**	**Power (W) [max]**	**#**	**Integration reduction factor**	**Total Cost (K$)**	**Relative cost (*)**	**Relative cost (**)**	**Total power (W)**
DSP Chip	10.00	38.5	8	0	80.00	2.9	15.0	308.0
PM IQ Mod	1.50	0.0	8	0.4	7.20	0.3	1.4	0.0
Laser (Tx & Rx LO)	1.50	1.5	2	0.4	1.80	0.1	0.3	3.0
4-Port Modulator Driver	2.00	6.0	8	0.4	9.60	0.3	1.8	48.0
RF LP filter	0.10	0.0	32	0.4	1.92	0.1	0.4	0.0
DP Coherent Receiver	6.00	1.5	8	0.4	28.80	1.0	5.4	12.0
Variable gain dual-stage amplifier	5.00	12.0	1	0.4	3.00	0.1	0.6	12.0
Comb generator modulator	5.00	0.0	2	0.4	6.00	0.2	1.1	0.0
Comb generator mod. driver	2.00	2.0	2	0.4	2.40	0.1	0.5	4.0
1:N AWG	0.50	0.0	4	0.4	1.20	0.0	0.2	0.0
Interleaver	0.70	0.0	1	0.4	0.42	0.0	0.1	0.0
1x1 HSR filter	15.00	4.0	2	0	30.00	1.1	5.6	8.0
					172.34	6.2	32.4	395.0

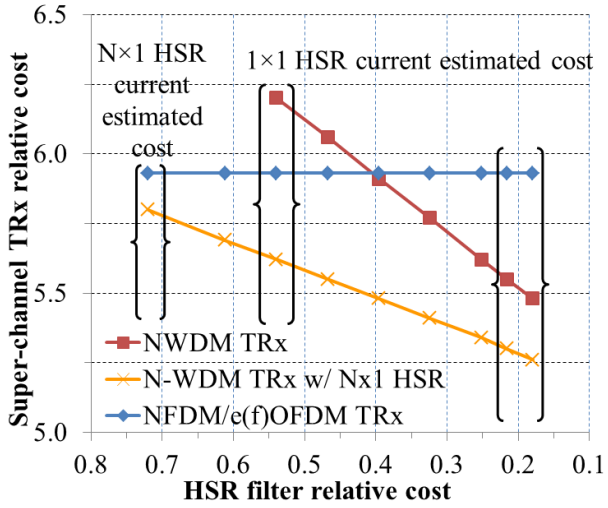

Figure 3.6 – Sensitivity analysis of the relative cost of the super-channel transceiver for electrical multiplexing schemes (NFDM/e(f)OFDM) and N-WDM with optical filtering (with either two 1x1 HSR filters and an interleaver, as shown in Figure 3.5, or with one Nx1 HSR filter) on the relative cost of the HSR filter. The HSR filter cost is assumed to vary from a relative cost of 0.54 (equivalent to $15k) to ~0.2 (current cost of a 1x9 WSS). Relative costs to cost of 100G transceiver.

3.1.3 O-OFDM with dual quadrature modulation

A second case of optical multiplexing scheme is O-OFDM. As is depicted in Figure 3.7, because we need as high a bandwidth as possible, the RF low pass filters are removed and so could the four DACs. However, in our current cost evaluation we are considering them for pre-emphasis of the electrical signal. The sub-channel transceiver now has three ports: an add port, a drop port and a carrier port

connected to the carrier extraction unit of the TIDE processor in the add/drop card. The ILL and the circulator are optional components (they could be included in the TIDE processor).

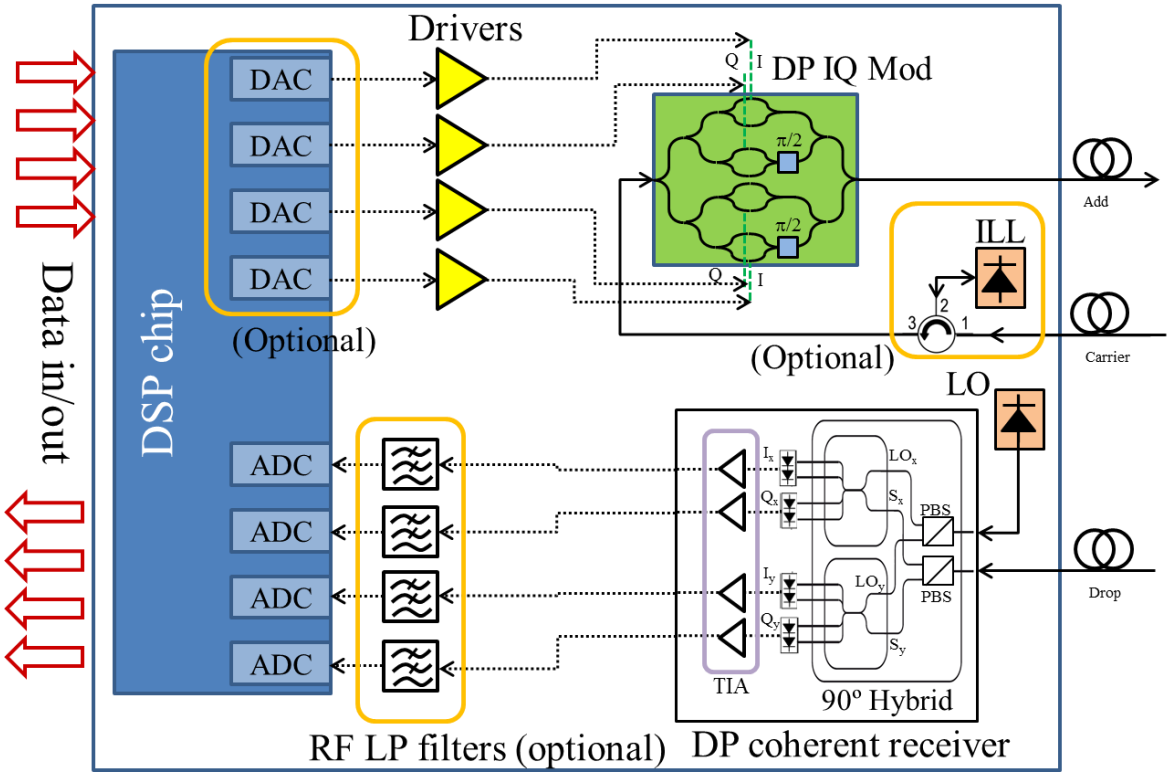

Figure 3.7 – Design of a sub-channel transceiver for the addition/extraction of one sub-carrier to/from super-channels based on O-OFDM.

Table 3.5 shows the cost and power consumption of the sub-channel transceiver. They are essentially the same as those for the electrical multiplexing schemes. Without the ILL the total cost would be $25.90k (4.9 times the cost of a 10G transceiver or 0.9 times the cost of a 100G transceiver) and the power consumption would slightly reduce to 47.5W.

Table 3.5 – Cost and power consumption of a sub-channel transceiver for the addition/extraction of sub-channels to/from super-channels based on O-OFDM.(*) Relative to cost of 100G transceiver. (**) Relative to cost of 10G transceiver

			Sb-Ch TRx (for A/D)				
Component	**Unit cost (K$)**	**Power (W) [max]**	**#**	**Total cost (K$)**	**Relative cost (*)**	**Relative cost (**)**	**Total power (W)**
DSP Chip	10.00	38.5	1	10.00	0.4	1.9	38.5
PM IQ Mod	6.00	0.00	1	6.00	0.2	1.1	0.0
Laser (ILL & Rx LO)	1.50	1.50	2	3.00	0.1	0.6	3.0
4-Port Modulator Driver	2.00	6.00	1	2.00	0.1	0.4	6.0
RF LP filter	0.10	0.00	4	0.40	0.0	0.1	0.0
DP Coherent Receiver	6.00	1.50	1	6.00	0.2	1.1	1.5
				27.40	1.0	5.2	49.0

Based on the above sub-channel transceiver, in Figure 3.8 we present the O-OFDM super-channel transceiver. Again, the results of the cost and power consumption evaluation, shown in Table 3.6, are essentially the same as those for the super-channel transceiver for the electrical multiplexing schemes.

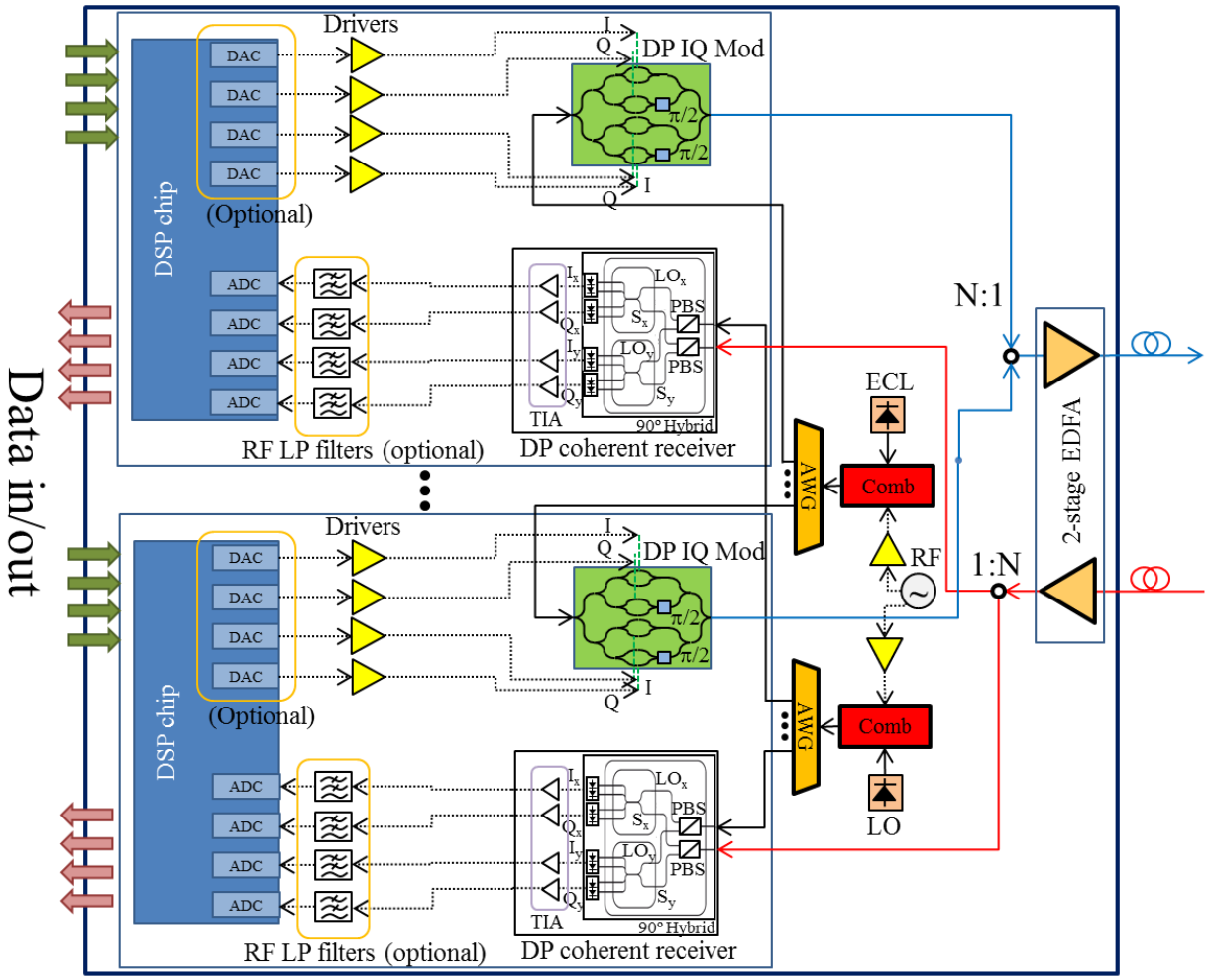

Figure 3.8 – Design of a super-channel transceiver for O-OFDM.

Table 3.6 – Cost and power consumption of a super-channel transceiver for O-OFDM.(*) Relative to cost of 100G transceiver. (**) Relative to cost of 10G transceiver.

			Sp-Ch TRx (total)					
Component	**Unit cost (K$)**	**Power (W) [max]**	**#**	**Integration reduction factor**	**Total Cost (K$)**	**Relative cost (*)**	**Relative cost (**)**	**Total power (W)**
DSP Chip	10.00	38.5	8	0	80.00	2.9	15.0	308.0
PM IQ Mod	6.00	0.00	8	0.4	28.80	1.0	5.4	0.0
Laser (Tx & Rx LO)	1.50	1.50	2	0.4	1.80	0.1	0.3	3.0
4-Port Modulator Driver	2.00	6.00	8	0.4	9.60	0.3	1.8	48.0
RF LP filter	0.10	0.00	32	0.4	1.92	0.1	0.4	0.0
DP Coherent Receiver	6.00	1.50	8	0.4	28.80	1.0	5.4	12.0
Variable gain dual-stage amplifier	5.00	12.00	1	0.4	3.00	0.1	0.6	12.0
Comb generator modulator	5.00	0.00	2	0.4	6.00	0.2	1.1	0.0
Comb generator mod. driver	2.00	2.00	2	0.4	2.40	0.1	0.5	4.0
1:N AWG	0.50	0.00	2	0.4	0.60	0.0	0.1	0.0
					162.92	5.9	30.6	387.0

3.1.4 O-fOFDM with single quadrature modulation

In Figure 3.9 we depict the super-channel transceiver design for O-fOFDM with single quadrature modulation. As in the previous section, the RF low pass filters are eliminated and the four DACs are optional, but we consider them in our cost model for pre-emphasis of the electrical signal. The sub-channel transceiver (not shown) should also have three ports, and the use of an ILL and a circulator is optional (see Figure 3.7).

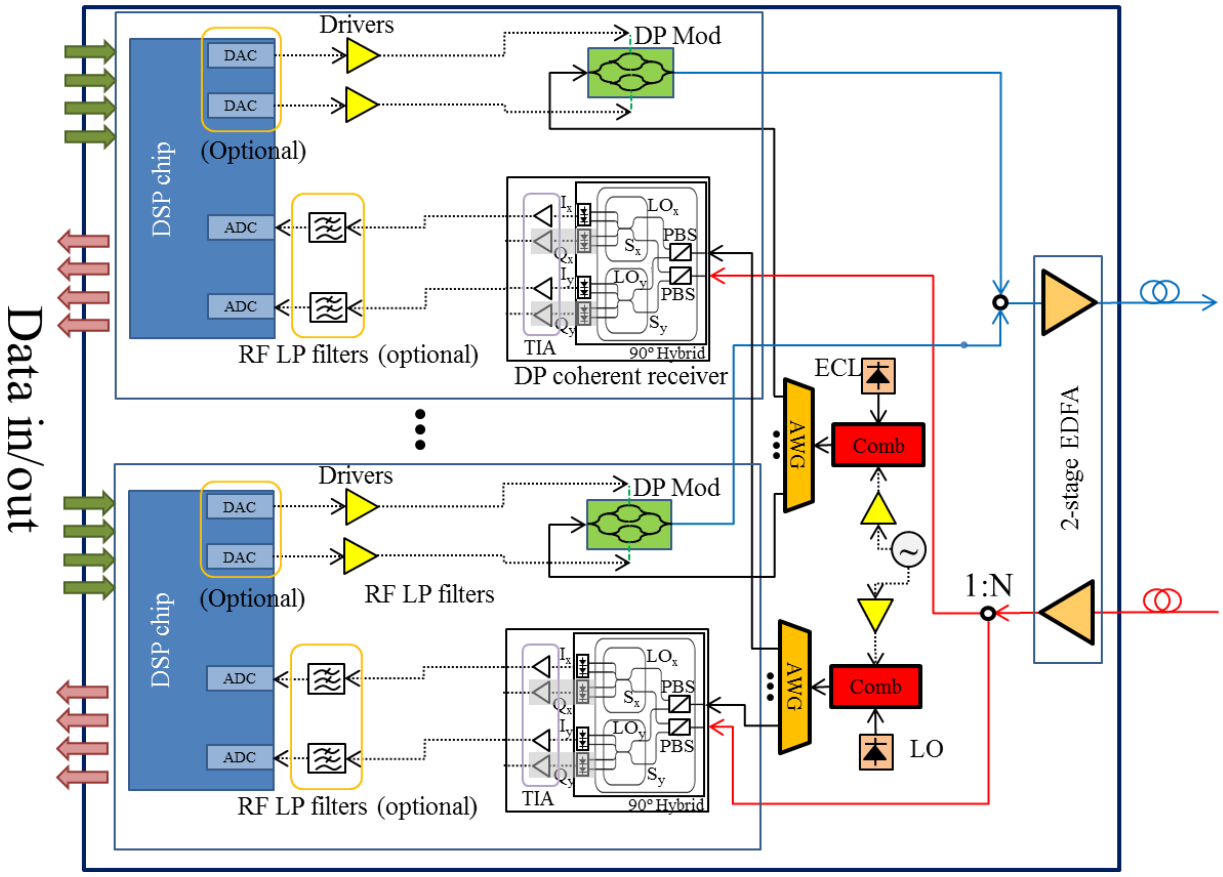

Figure 3.9 – Design of a super-channel transceiver for O-fOFDM.

Two single Mach-Zehnder modulators are used for the polarisation-multiplexed single quadrature signal, which means that the four-port modulator driver used in the previous designs could be replaced with a two-port driver. In the same way, the number of optional RF low pass filters at the receiver could be reduced to 2. The dual polarisation coherent receiver is nonetheless made up of the same components, and its cost remains the same, as reflected in Table 3.7. Without the ILL the total cost would be $22.40k (4.2 times the cost of a 10G transceiver or 0.8 times the cost of a 100G transceiver) and the power consumption would come down to 44.5W.

Table 3.7 – Cost and power consumption of a sub-channel transceiver for the addition/extraction of sub-channels to/from super-channels based on O-fOFDM.(*) Relative to cost of 100G transceiver. (**) Relative to cost of 10G transceiver.

			Sb-Ch TRx				
Component	**Unit cost (K$)**	**Power (W) [max]**	**#**	**Total cost (K$)**	**Relative cost (*)**	**Relative cost (**)**	**Total power (W)**
DSP Chip	10.00	38.50	1	10.00	0.4	1.9	38.5
Modulator	1.50	0.00	2	3.00	0.1	0.6	0.0
Laser (ILL & Rx LO)	1.50	1.50	2	3.00	0.1	0.6	3.0
2-Port Modulator Driver	1.50	3.00	1	1.50	0.1	0.3	3.0
RF LP filter	0.10	0.00	4	0.40	0.0	0.1	0.0
DP Coherent Receiver	6.00	1.50	1	6.00	0.2	1.1	1.5
				23.90	0.9	4.5	46.0

The cost and power consumption of the O-fOFDM super-channel transceiver is presented in Table 3.8. Compared with the dual quadrature O-OFDM super-channel transceiver, O-fOFDM is ~10% less expensive and uses about ~7% less power.

Table 3.8 – Cost and power consumption of a super-channel transceiver for O-fOFDM.(*) Relative to cost of 100G transceiver. (**) Relative to cost of 10G transceiver.

			Sp-Ch TRx (total)					
Component	**Unit cost (K$)**	**Power (W) [max]**	**#**	**Integration reduction factor**	**Total Cost (K$)**	**Relative cost (*)**	**Relative cost (**)**	**Total power (W)**
DSP Chip	10.00	38.50	8	0	80.00	2.9	15.0	308.0
Modulator	1.50	0.00	16	0.4	14.40	0.5	2.7	0.0
Laser (Tx & Rx LO)	1.50	1.50	2	0.4	1.80	0.1	0.3	3.0
2-Port Modulator Driver	1.50	3.00	8	0.4	7.20	0.3	1.4	24.0
RF LP filter	0.10	0.00	32	0.4	1.92	0.1	0.4	0.0
DP Coherent Receiver	6.00	1.50	8	0.4	28.80	1.0	5.4	12.0
Variable gain dual-stage amplifier	5.00	12.00	1	0.4	3.00	0.1	0.6	12.0
Comb generator modulator	5.00	0.00	2	0.4	6.00	0.2	1.1	0.0
Comb generator mod. driver	2.00	2.00	2	0.4	2.40	0.1	0.5	4.0
1:N AWG	0.50	0.00	2	0.4	0.60	0.0	0.1	0.0
					146.12	5.3	27.5	363.0

3.2 Optical cross connects

In the previous section, we presented the transceiver cost model for the FOX-C project, where different single-carrier and super-channel transceiver implementations were compared. To summarise the results of this cost model, in Figure 3.10 we present a sensitivity analysis of the cost of the single-carrier and the super-channel transceiver (assuming eight sub-channels per super-channel) on the HSR filter cost. We can observe that, by using super-channel transceivers, a substantial reduction in the relative cost of transmitting one sub-channel, with respect to the cost of transmitting single-carrier signals, can be achieved. The relative cost of a sub-channel for super-channel transceiver implementations supporting different numbers of sub-channels is shown in Table 3.9. From a cost perspective, it is then clear that in a heterogeneous traffic scenario in which a majority of the connections is not sufficiently big to justify the exclusive use of super-channel transmission, we can anticipate that using super-channel transceivers at the source and destination nodes to serve connections from the source node to the end node and any intermediate nodes, as well as from any intermediate node to the end node, together with the capability of extracting and adding sub-channel constituents from/to super-channels at the intermediate nodes should be beneficial.

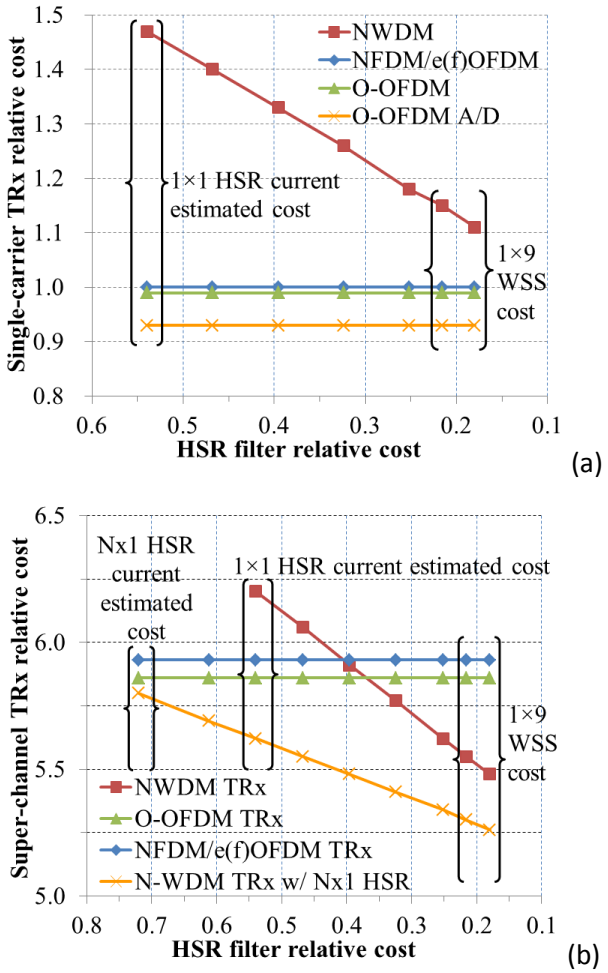

Figure 3.10 – Sensitivity analysis of the relative cost of the (a) single-carrier and (b) super-channel transceivers for electrical multiplexing schemes (NFDM/e(f)OFDM), N-WDM with optical filtering (with either two 1x1 HSR filters and an interleaver, as shown in Figure 3.5, or with one Nx1 HSR filter) and O-OFDM (according to the designs presented in Figure 3.1 (without RF LP filters at the transmitter), Figure 3.7 and Figure 3.8) on the relative cost of the HSR filter. The HSR filter cost is assumed to vary from a relative cost of 0.54 (equivalent to $15k) to ~0.2 (current cost of a 1x9 WSS). Relative costs to cost of 100G transceiver.

Table 3.9 – Super-channel transceiver relative cost and power (per sub-channel) for implementations supporting from 4 to 12 sub-channels. Relative costs to cost of 100G transceiver.

	NFDM/e(f)OFDM		NWDM		AO-OFDM	
Number of sub-channels	**Cost**	**P (W)**	**Cost**	**P (W)**	**Cost**	**P (W)**
4	0.80	50.8	0.98	52.8	0.79	50.8
6	0.76	49.2	0.84	50.5	0.75	49.2
8	0.74	48.4	0.77	49.4	0.73	48.4
10	0.73	47.9	0.73	48.7	0.72	47.9
12	0.72	47.6	0.71	48.3	0.71	47.6

This section is dedicated to the cost and power consumption evaluation of the switching node implementations with all-optical sub-channel add/drop capability investigated in T4.1 and T4.2 and reported in D4.3 and D4.5 enabling the proposed super-channel transmission scenario.

Let us start with the design of the flexible optical cross connect node under consideration, which we present in Figure 3.11. In it a node with degree D = 3 (north, west and south) and number of sub-channel add/drop cards M = 4 is shown. The express/through traffic and the locally added super-channels addressed towards W, N and S are represented with dark red, blue and green solid lines, respectively. Similarly, the dropped unprocessed super-channels coming from W, N and S are represented with dark red, blue and green solid lines, respectively.

The super-channels that need to be processed by the sub-channel add/drop cards are represented with black solid lines. Once processed, the dropped sub-channels from the drop ports are connected to sub-channel transceivers with orange, light blue and light green solid lines if they are coming from W, N or S, respectively. Finally, the added sub-channels are represented in grey. The resulting super-channels are sent through two switches (each with switching states D-1) hard-wired to the other degrees (if D=2, meaning conventional line system ROADM, switches are not needed). In the case of the processed super-channels coming from the west, because one of the sub-channel add/drop cards is unpaired, one of the outputs of the first switch is directly connected to the north WSS (this is represented with a dashed black line).

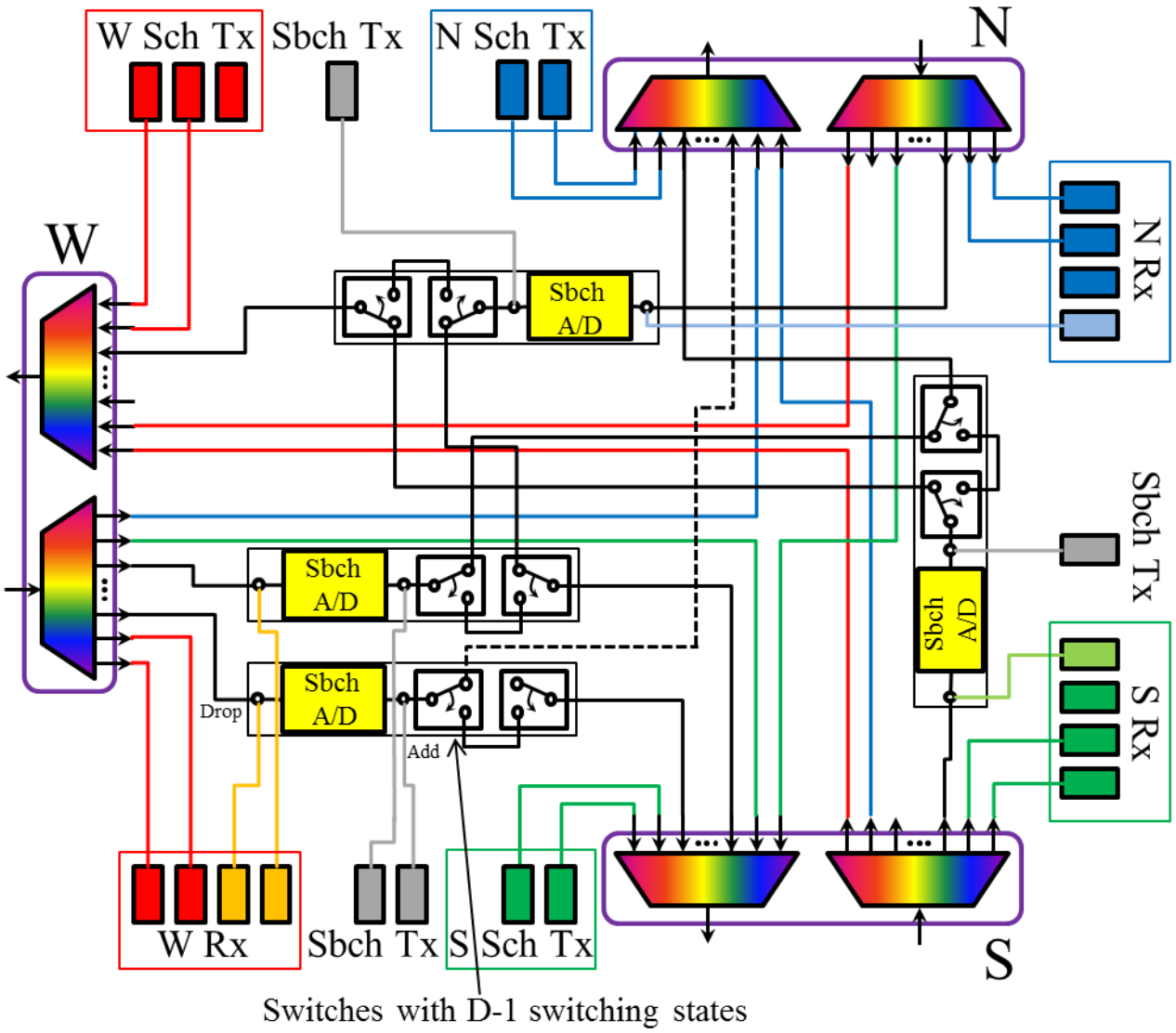

Figure 3.11 – Design of a flexible optical cross connect with degree D = 3 and number of sub-channel add/drop cards M = 4, with N and S having one card each and W having two.

The optical cross connects analysed in this section are based on the Flex-WSS and ultra-fine resolution filters reported in D4.3 and D4.5. The Flex-WSS has an optical resolution of 7.5 GHz, a pixel spectral addressability of 6.25 GHz and an insertion loss of < 5 dB. The AWG-based high spectral resolution (HSR) filter developed by HUJI has an optical resolution of 0.8 GHz, a spectral addressability of 400 MHz and an insertion loss in the region of 15 dB. For the all-optical OFDM schemes, a Terabit Interferometric Drop, Add and Extract (TIDE) processor developed by ASTON is used, which is composed of 2 1x1 AWG-based HSR filters or 2 1xN scalable bulk grating based HSR filters, where N is the number of gates. In the latter case, the optical resolution is 1.5 GHz and the spectral addressability is ~150 MHz (design values), whereas the insertion loss is still being investigated.

For the benchmarking scenarios studied in chapter 4, we consider conventional super-channel transmission without addition or extraction of sub-channels from super-channels at intermediate nodes (therefore, the number of sub-channel A/D cards M is set to zero in those scenarios). Table 3.10 shows the cost and power consumption of a conventional node with nodal degree D = 3.

Table 3.10 – Cost and power consumption of an optical cross connect with degree D = 3.(*) Relative to cost of 100G transceiver. (**) Relative to cost of 10G transceiver (^) Due to sharing of management between amplification modules.

Flexible OXC with degree D = 3								
Component	**Unit cost (K$)**	**Power (W)**	**#**	**Total cost (K$)**	**Relative cost (*)**	**Relative cost (**)**	**Power reduction factor (^)**	**Total Power (W)**
WSS	15.00	4.00	6	90.00	3.2	16.9		24.0
Variable gain dual-stage amplifier	5.00	12.0	3	15.00	0.5	2.8	0.1	33.6
				105.00	3.8	19.7		57.6

The cost and power consumption values are given by the following expressions as a function of the node degree D:

$$\text{Cost [k\$]} = 35D \tag{3.1}$$

$$\text{Power consumption [W]} = 8D + 12(1 - PRF)(D - 1) + 12 \tag{3.2}$$

where PRF is the power reduction factor, shown in Table 3.10 with a value of 0.1. This factor is due to the fact that some of the control and management can be shared between the different amplification modules present within a node. In the power model we have assumed that this 10% power reduction can be applied to all amplifiers minus 1. We can achieve more power reduction by sharing the same pump laser between different EDFAs. A common pump is simply divided N-ways and a cheap VOA is added to each copy to control power/gain. The pump sharing scenario is expected to give an additional 30% power reduction per node. This translates into an overall node power consumption of 50.4W for a 3-degree node, which represents a reduction of 12.5% with respect to the estimation shown in Table 3.10.

3.2.1 High spectral resolution filter based optical cross connect

In Figure 3.12 we show a FOX-C node design with sub-channel add/drop cards based on the HSR filtering technology. The design is the same as the one depicted in Figure 3.11 but here we also present compensating amplification as well as signal powers and attenuation values at different locations inside the node. The numbers in black show the gain or loss of each component. The numbers in green indicate the power values in dBm. In the case of unprocessed super-channels (dark red, blue and green lines) two values are given. The first one is the power corresponding to a 50-GHz bandwidth. The second one refers to the power over the entire C band. For the processed super-channels (black lines) and added/dropped sub-channels (orange, light blue and light green lines) only the power over a 50-GHz bandwidth is shown.

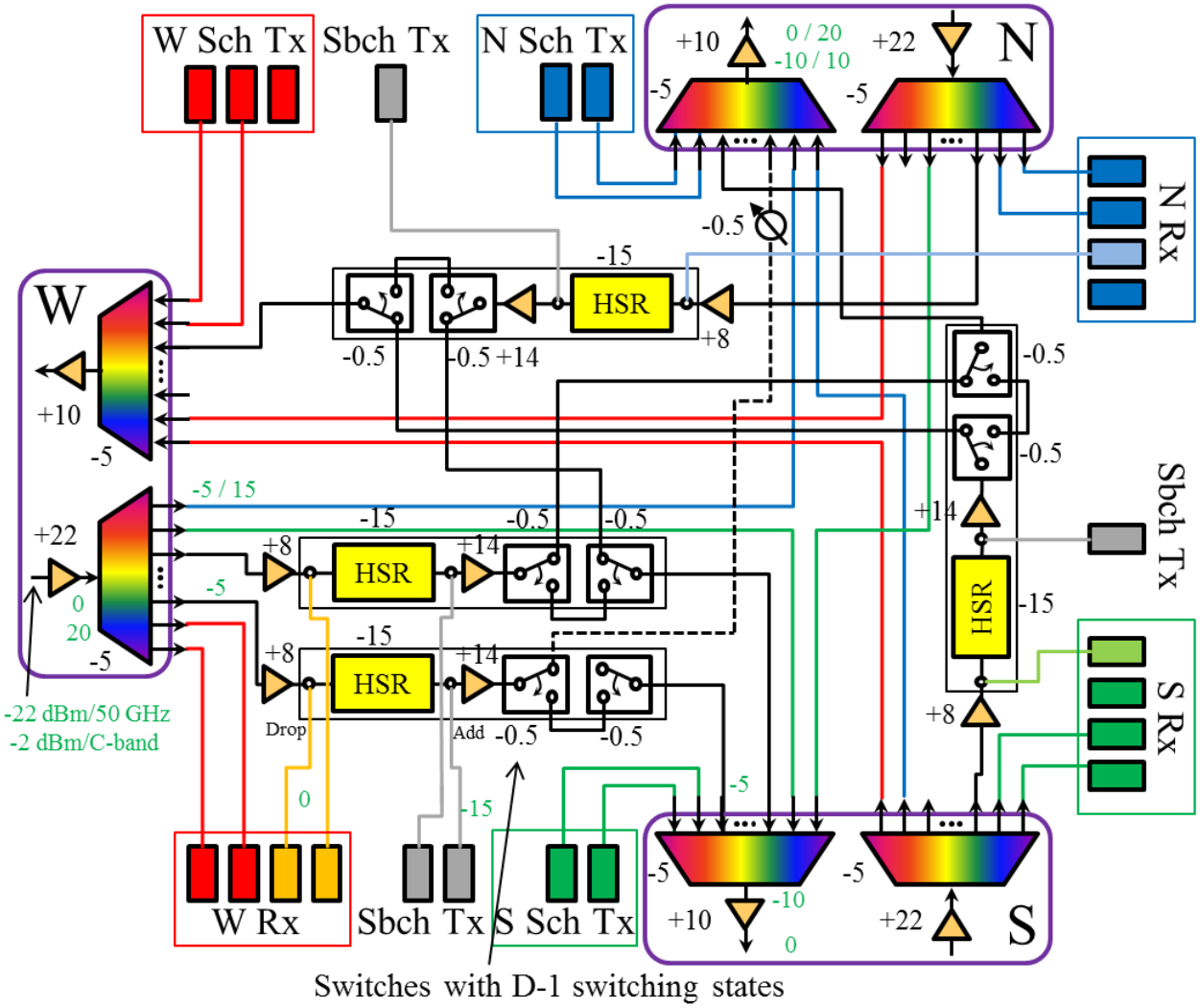

Figure 3.12 – Design of a flexible optical cross connect with degree D = 3 and number of HSR-based sub-channel add/drop cards M = 4. Shown is the total optical power (over 50GHz bandwidth and the entire C-band) at different locations together with insertion loss values of the different node components.

The breakdown of cost and power consumption of the exemplary flexible OXC node presented in Figure 3.12 with degree $D = 3$ and $M = 4$ HSR filters is detailed in Table 3.11.

In general, the cost and power consumption of the FOX-C node for D degrees and a number of HSR-based sub-channel add/drop cards M are given by the following expressions:

$$\text{Cost [k\$]} = \begin{cases} 35D + 20.8M, & \text{if } D > 2 \\ 35D + 20M, & \text{if } D = 2 \end{cases} \tag{3.3}$$

$$\text{Power consumption [W]} = 20D + 16M - 12PRF(D + M - 1) \tag{3.4}$$

In Equation (*3.4*) two expressions are shown for the power consumption due to the fact that the switches are only necessary when the number of degrees is greater than 2. The second expression does not take them into account.

Table 3.11 – Cost and power consumption of an optical cross connect with degree D = 3 and number of HSR-based sub-channel add/drop cards M = 4.(*) Relative to cost of 100G transceiver. (**) Relative to cost of 10G transceiver (^) Due to sharing of management between amplification modules.

HSR-based flexible OXC with degree D = 3 and M = 4 HSR filters									
Component	**Unit cost (K$)**	**Power (W)**	**#**	**Total cost (K$)**	**Relative cost (*)**	**Relative cost (**)**	**Relative cost (***)**	**Power reduction factor (^)**	**Total Power (W)**
WSS	15.00	4.00	6	90.00	3.2	16.9	2.6		24.0
1x1 HSR filter	15.00	4.00	4	60.00	2.2	11.3	1.7		16.0
Variable gain dual-stage amplifier	5.00	12.00	7	35.00	1.3	6.6	1.0	0.10	76.8
1x(D-1) switch	0.40	0.00	8	3.20	0.1	0.6	0.1		0.0
				188.20	6.8	35.4	5.4		116.8

Table 3.12 shows the cost (in k$) and power consumption (in W) of the flexible OXC node for different values of *D* and *M* using Equations (*3.3*) and (*3.4*).

Table 3.12 – Cost and power consumption of an optical cross connect for several node degrees D and M HSR-based sub-channel add/drop cards, with M in the range [0,8]. M = 0 is the benchmarking case without sub-channel add/drop capability.

	HSR-based flexible OXC									
	Cost [k$]	Power [W]	Cost [k$]	Power [W]	Cost [k$]	Power [W]	Cost [k$]	Power [W]	Cost [k$]	Power [W]
D M	2		3		4		5		6	
0	70.00	38.8	105.00	57.6	140.00	76.4	175.00	95.2	210.00	114.0
1	90.00	53.6	125.80	72.4	160.80	91.2	195.80	110.0	230.80	128.8
2	110.00	68.4	146.60	87.2	181.60	106.0	216.60	124.8	251.60	143.6
3	130.00	83.2	167.40	102.0	202.40	120.8	237.40	139.6	272.40	158.4
4	150.00	98.0	188.20	116.8	223.20	135.6	258.20	154.4	293.20	173.2
5	170.00	112.8	209.00	131.6	244.00	150.4	279.00	169.2	314.00	188.0
6	190.00	127.6	229.80	146.4	264.80	165.2	299.80	184.0	334.80	202.8
7	210.00	142.4	250.60	161.2	285.60	180.0	320.60	198.8	355.60	217.6
8	230.00	157.2	271.40	176.0	306.40	194.8	341.40	213.6	376.40	232.4

3.2.2 Terabit interferometric Drop, Add and Extract based optical cross connect

In Figure 3.13 we present a FOX-C node design with sub-channel add/drop cards based on the Terabit Interferometric Drop, add and Extract (TIDE) technology. We also show the compensating amplification as well as the signal powers and attenuation values at different locations inside the node. A more detailed design can be seen in Figure 3.14 (in which the add/drop card is realised with two 1x*N* HSR filters and *N* gates) and in Figure 3.15 (where the add/drop card is realised with two 1x1 HSR filters and one gate).

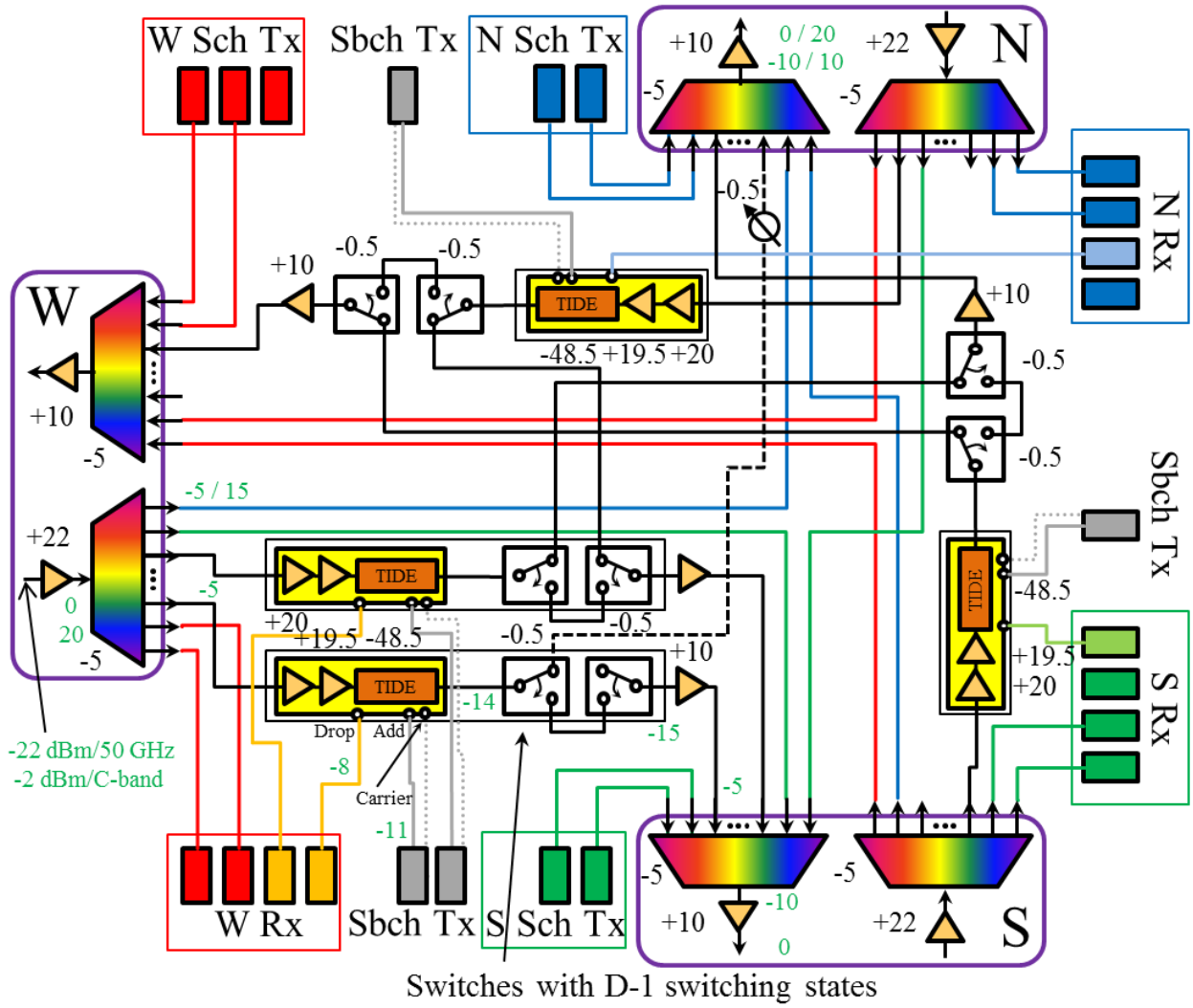

Figure 3.13 – Design of a flexible optical cross connect with degree D = 3 and number of TIDE-based sub-channel add/drop cards M = 4. Shown is the total optical power (over 50GHz bandwidth and the entire C-band) at different locations together with insertion loss values of the different node components.The sub-channel add/drop cards are only represented schematically. For a more detailed design see Figure 3.14 (add/drop card with 1xN HSR filters and N gates) or Figure 3.15 (add/drop card with 1x1 HSR filters and one gate).

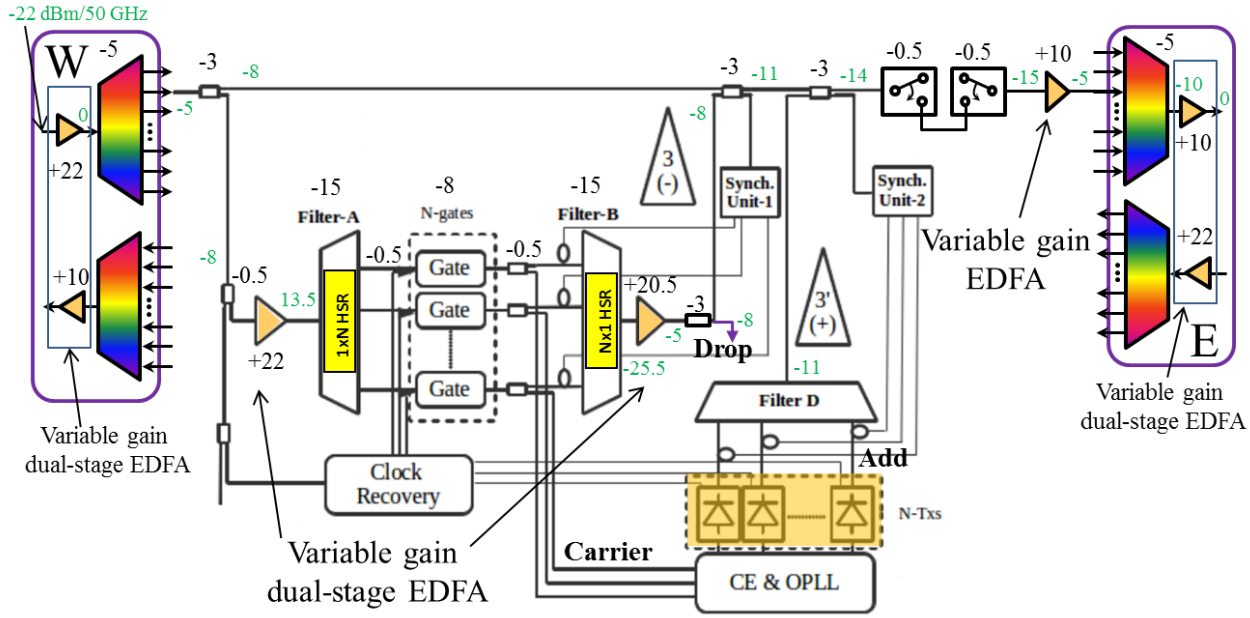

Figure 3.14 – Design of a TIDE-based sub-channel add/drop card with two 1xN HSR filters and N gates. Shown is the total optical power (over 50GHz bandwidth) at different locations together with insertion loss values of the different node components.

The breakdown of cost and power consumption of the exemplary FOX-C node presented in Figure 3.13 with degree *D* = 3 and *M* = 4 TIDE filters with four gates each (design depicted in Figure 3.14) is detailed in Table 3.13. Regarding the TIDE processor, an integrated module approach is used since building the all-optical interferometric node from discrete components is costly and bulky, occupying very expensive shelf place. The development of the integrated solution requires non-recurring engineering (NRE) of about $1M and the developed unit price is ~$3k vs $10k for the discrete component-based solution.

Table 3.13 – Cost and power consumption of an optical cross connect with degree D = 3 and number of HSR-based sub-channel add/drop cards M = 4 with N = 4 gates each.(*) Relative to cost of 100G transceiver. (**) Relative to cost of 10G transceiver (^) Due to sharing of management between amplification modules.

			Flexible OXC based on TIDE with N = 4 gates						
Component	**Unit cost (K$)**	**Power (W)**	**#**	**Total cost (K$)**	**Relative cost (*)**	**Relative cost (**)**	**Relative cost (***)**	**Power reduction factor (^)**	**Total Power (W)**
WSS	15.00	4.00	6	90.00	3.2	16.9	2.6		24.0
1xN HSR filter	20.00	4.00	8	160.00	5.8	30.1	4.6		32.0
Integrated TIDE	3.00	4.00	16	48.00	1.7	9.0	1.4		64.0
Variable gain amplifier	3.00	9.00	4	12.00	0.4	2.3	0.3	0.10	32.4
Variable gain dual-stage amplifier	5.00	12.00	7	35.00	1.3	6.6	1.0	0.10	76.8
1x(D-1) switch	0.40	0.00	8	3.20	0.1	0.6	0.1		0.0
				348.20	12.5	65.5	9.9		229.2

In general, the cost and power consumption of the FOX-C node for *D* degrees and a number of TIDE-based *N*-gated sub-channel add/drop cards *M* are given by the following expressions:

$$\text{Cost [k\$]} = \begin{cases} 35D + (48.8 + 3N)M, & \text{if } D > 2 \\ 35D + (48 + 3N)M, & \text{if } D = 2 \end{cases} \quad (3.5)$$

$$\text{Power consumption [W]} = 20D + (29 + 4N)M - 12PRF(D + (21/12)M - 1) \quad (3.6)$$

Table 3.14 shows the cost (in k$) and power consumption (in W) of the TIDE-based flexible OXC node for different values of *D* and *M* using Equations (*3.5*) and (*3.6*) with *N* = 4.

Table 3.14 – Cost and power consumption of an optical cross connect for several node degrees D and M TIDE-based sub-channel add/drop cards comprising N = 4 gates, with M in the range [0,8]. M = 0 is the benchmarking case without sub-channel add/drop capability.

	TIDE-based flexible OXC with N = 4 gates. M = 0 is the benchmarking case without sub-channel add/drop capability.									
	Cost [k$]	Power [W]	Cost [k$]	Power [W]	Cost [k$]	Power [W]	Cost [k$]	Power [W]	Cost [k$]	Power [W]
D / M	2		3		4		5		6	
0	70.00	38.8	105.00	57.6	140.00	76.4	175.00	95.2	210.00	114.0
1	130.00	81.7	165.80	100.5	200.80	119.3	235.80	138.1	270.80	156.9
2	190.00	124.6	226.60	143.4	261.60	162.2	296.60	181.0	331.60	199.8
3	250.00	167.5	287.40	186.3	322.40	205.1	357.40	223.9	392.40	242.7
4	310.00	210.4	348.20	229.2	383.20	248.0	418.20	266.8	453.20	285.6
5	370.00	253.3	409.00	272.1	444.00	290.9	479.00	309.7	514.00	328.5
6	430.00	296.2	469.80	315.0	504.80	333.8	539.80	352.6	574.80	371.4
7	490.00	339.1	530.60	357.9	565.60	376.7	600.60	395.5	635.60	414.3
8	550.00	382.0	591.40	400.8	626.40	419.6	661.40	438.4	696.40	457.2

The breakdown of cost and power consumption of the exemplary flexible OXC node presented in Figure 3.13 with degree *D* = 3 and *M* = 4 single-gated TIDE filters (as depicted in Figure 3.15) is detailed in Table 3.15.

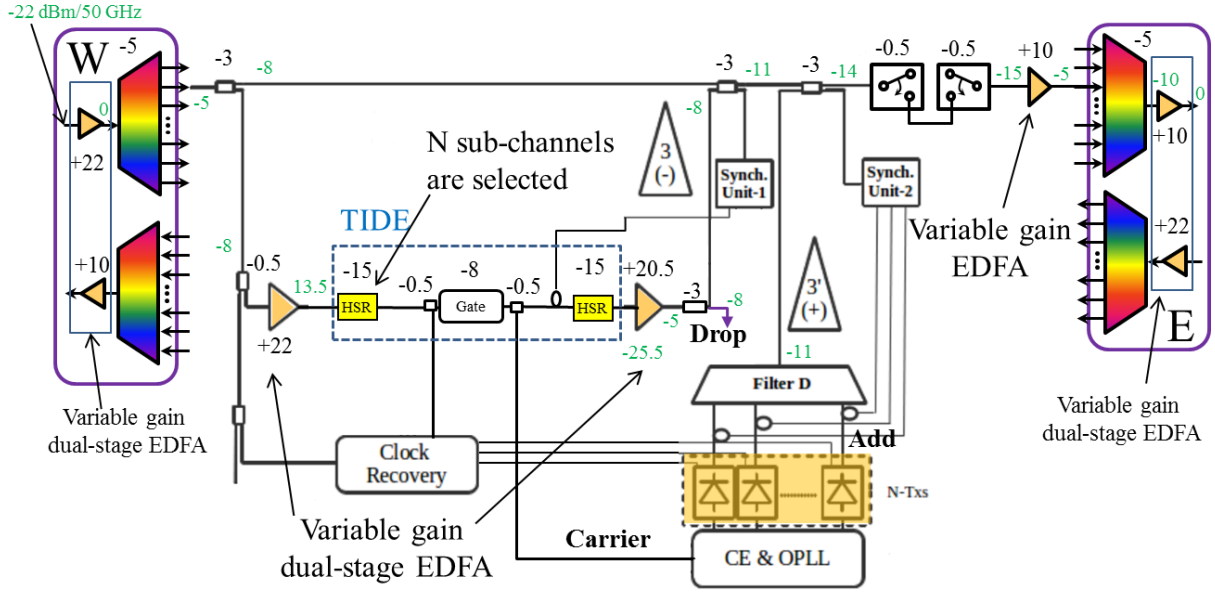

Figure 3.15 – Design of a TIDE-based sub-channel add/drop card with two 1x1 HSR filters and one gate. Shown is the total optical power (over 50GHz bandwidth) at different locations together with insertion loss values of the different node components.

Table 3.15 – Cost and power consumption of an optical cross connect with degree D = 3 and number of TIDE-based single-gated sub-channel add/drop cards M = 4.(*) Relative to cost of 100G transceiver. (**) Relative to cost of 10G transceiver (^) Due to sharing of management between amplification modules.

			Flexible OXC based on TIDE with one gate							
Component	**Unit cost (K$)**	**Power (W)**	**#**	**Total cost (K$)**	**Relative cost (*)**	**Relative cost (**)**	**Relative cost (***)**	**Power reduction factor (^)**	**Total Power (W)**
WSS	15.00	4.00	6	90.00	3.2	16.9	2.6		24.0
1x1 HSR filter	15.00	4.00	8	120.00	4.3	22.6	3.4		32.0
Integrated TIDE	3.00	4.00	4	12.00	0.4	2.3	0.3		16.0
Variable gain amplifier	3.00	9.00	4	12.00	0.4	2.3	0.3	0.10	32.4
Variable gain dual-stage amplifier	5.00	12.00	7	35.00	1.3	6.6	1.0	0.10	76.8
1x(D-1) switch	0.40	0.00	8	3.20	0.1	0.6	0.1		0.0
				272.20	9.8	51.2	7.8		181.2

In general, the cost and power consumption of the FOX-C node for *D* degrees and a number of TIDE-based single-gated sub-channel add/drop cards *M* are given by the following expressions:

$$\text{Cost [k\$]} = \begin{cases} 35D + 41.8M, & \text{if } D > 2 \\ 35D + 41M, & \text{if } D = 2 \end{cases} \tag{3.7}$$

$$\text{Power consumption [W]} = 20D + 33M - 12PRF(D + (21/12)M - 1) \tag{3.8}$$

Table 3.16 – Cost and power consumption of an optical cross connect for several node degrees D and M TIDE-based single-gated sub-channel add/drop cards, with M in the range [0,8]. M = 0 is the benchmarking case without sub-channel add/drop capability.

	TIDE-based flexible OXC with one gate. M = 0 is the benchmarking case without sub-channel add/drop capability.									
	Cost [k$]	Power [W]	Cost [k$]	Power [W]	Cost [k$]	Power [W]	Cost [k$]	Power [W]	Cost [k$]	Power [W]
D / M	2		3		4		5		6	
0	70.00	38.8	105.00	57.6	140.00	76.4	175.00	95.2	210.00	114.0
1	111.00	69.7	146.80	88.5	181.80	107.3	216.80	126.1	251.80	144.9
2	152.00	100.6	188.60	119.4	223.60	138.2	258.60	157.0	293.60	175.8
3	193.00	131.5	230.40	150.3	265.40	169.1	300.40	187.9	335.40	206.7
4	234.00	162.4	272.20	181.2	307.20	200.0	342.20	218.8	377.20	237.6
5	275.00	193.3	314.00	212.1	349.00	230.9	384.00	249.7	419.00	268.5
6	316.00	224.2	355.80	243.0	390.80	261.8	425.80	280.6	460.80	299.4
7	357.00	255.1	397.60	273.9	432.60	292.7	467.60	311.5	502.60	330.3
8	398.00	286.0	439.40	304.8	474.40	323.6	509.40	342.4	544.40	361.2

Table 3.16 shows the cost (in k$) and power consumption (in W) of the TIDE-based flexible OXC node for different values of *D* and *M* using Equations (*3.7*) and (*3.8*).

4 Network level performance evaluation

Despite the potential performance enhancements that the introduction of a new technology may have, operators seeking to migrate to the next generation optical network are likely to select a solution by taking the required capital expenditures into account. This chapter aims to evaluate the expected improvement of performance and cost saving introduced by FOX-C technology from the networking perspective. All studies are done over the network topologies described in section 4.2. Legacy technologies, as detailed in section 4.3, are used for benchmarking purposes. Possible FOX-C solution based scenarios along with a novel traffic grooming capable routing and spectrum allocation algorithm are introduced in section 4.4. Finally, section 4.5 presents the techno-economic study methodology and results.

Before moving to any further detail, let us briefly review the problem of Resource Allocation (RA) in optical networks, since solving it is a crucial step toward performing techno-economic evaluations.

4.1 Resource allocation problem in optical networks

The introduction of flexible optical architecture poses additional challenges in the networking level, especially on the efficient connection establishment [2]. Figure 4.1 projects a comprehensive overview of this issue. In a very general perspective, a possible solution for the RA problem is an algorithm that can select a route and allocate a spectrum portion to every incoming connection request to the network. By considering some inputs such as: connection level performance requirements, control plane capabilities, network topology, traffic demand with the related service level agreement and cost and power consumption of the network equipment, an efficient RA solution is able to optimally utilize the capabilities of the advanced physical layer from the network level. The ultimate goal is to achieve better results on one or more network level performance metrics, such as required network equipment/resources, blocking probability, connection provisioning time, energy efficiency and the network cost.

Based on the abovementioned discussion, RA solutions can be divided into the following broad categories:

a) In fixed grid WDM networks, the conventional routing and wavelength assignment (RWA) algorithms [19]. Here, the main issue is to maintain the consistency of the connection between source and destination, unless the usage of wavelength converters is assumed.

b) In flexible optical networks with multitude degrees of freedom, more complicated routing and resource allocation schemes are necessary. For example, assuming only the flexibility on the number of assigned subcarriers to a connection - while all other transmission parameters such as Baud rate and modulation level are fixed – routing and spectrum assignment (RSA) algorithms are utilized [2]. Nevertheless, by considering additional degrees of freedom such as modulation format and level selection, symbol rate and FEC more complex solutions such as routing, modulation level and spectrum assignment (RMLSA) algorithms are needed [21]. It is worth to note that despite the desired degree of freedom, unless the usage of wavelength converters is assumed, the RA solution should serve the connection over a spectrum portion that complies with the spectrum continuity and contiguity constraints.

There are two main approaches for solving the RA problem, a) considering both route selection and spectrum assignment jointly and b) breaking the problem into two sub-problems, 1) routing sub-problem and 2) spectrum assignment sub-problem, and solve them separately. The solutions for the first approach are mainly with the help of Integer Linear Programing (ILP) or Mixed ILP (MILP) formulations.

Although these solutions are accurate, they are very complex, time consuming and in general, inapplicable for the real size networks. Alternatively, in the second approach in order to provide faster and easier solutions, normally heuristic algorithms are employed. A heuristic solution is a technique designed for solving a problem more quickly when classic methods are too slow, or for finding an approximate solution when classic methods fail to find any exact solution. This is achieved by trading optimality, completeness, accuracy, or precision for speed. Having this in mind, in FOX-C project to fulfill the requirements of a practical solution, the main focus is put on disjoint heuristic algorithms.

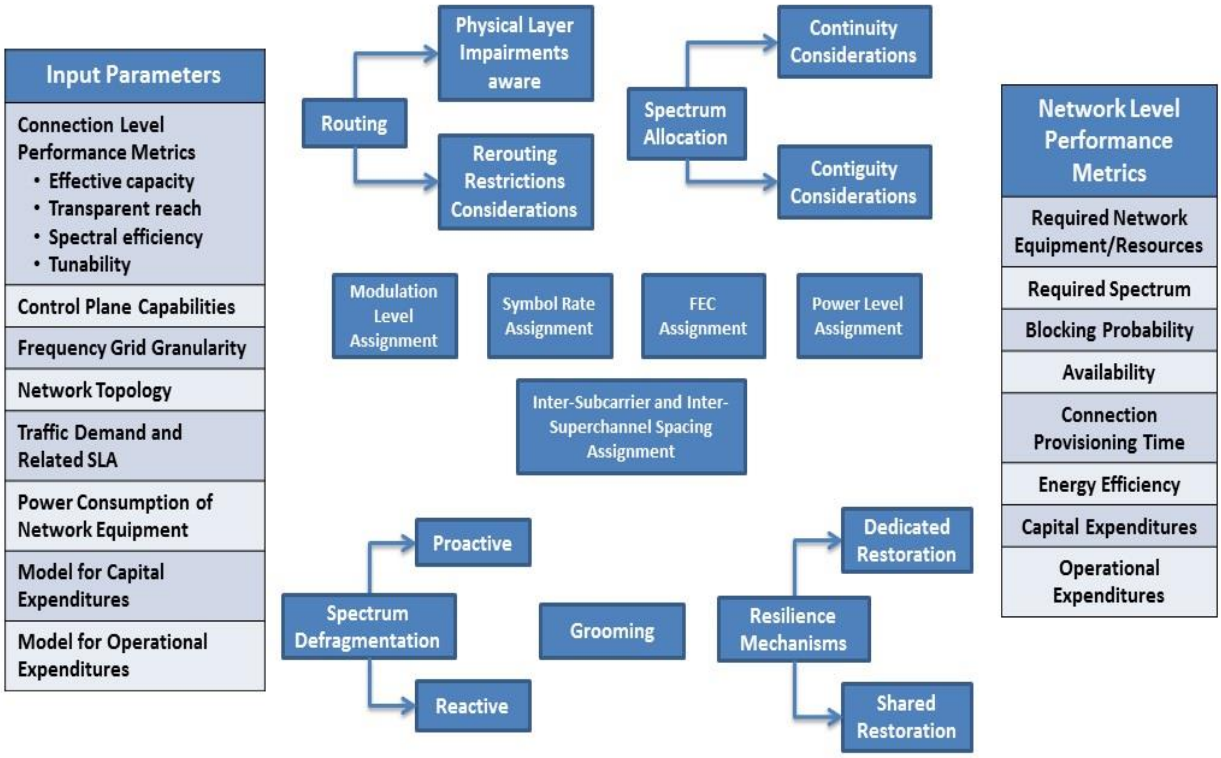

Figure 4.1 – Resource allocation in optical networks.

Based on the application, RA solutions can also be classified into two main categories: 1) static RA solutions utilized for offline network planning and 2) dynamic RA solutions capable to dynamically serve incoming connection requests over the network. In this deliverable, since the main objective is to verify the benefits of FOX-C solution trough Total Cost of Ownership (TOC) evaluations, a static solution has been developed.

It is also important to note that regardless of the details in any RA solution, there are some important issues that need to be considered (especially on flexible optical architectures). Of course, respecting to the traffic profile, quality of service, cost and energy consumption it is possible to enhance the RA algorithm to address one or more of these issues.

4.1.1 Spectral fragmentation

Figure 4.2 shows scattered spectral fragments in four links of a typical flexible optical network. As shown, the available spectrum in the network links is fragmented into small non-contiguous spectral bands. In a dynamic scenario, this situation can occur due to the randomness in the connection setup and tear down processes over the network. Also, in a static scenario by taking both continuity and contiguity constraints into account along with the possibility of having connections traversing more than one hop, such a fragmented spectral status is expected. The spectrum fragmentation significantly decreases the probability of finding enough contiguous spectrum for establishing new incoming connections, especially those traversing multi-hop paths (e.g., traversing links 1 to 4 in Figure 4.2)

and/or requesting large amounts of bandwidth. In fact, new connection requests can be blocked in spite of having enough spectral resources if these are non-contiguous.

Since an efficient utilization of the limited spectral resources in the network is an important issue for network operators, this problem has grabbed the research community attention. To address it, the proposal of spectral defragmentation has appeared in the literature. In general, spectral defragmentation means arranging the spectral resources, either re-routing them along alternative routes and/or retuning them onto different spectrum portions, in order to consolidate the available spectral fragments contiguously, so that they can be used for serving new incoming connection requests. Spectral defragmentation reduces connection blocking probability, and maximizes the service capacity of the network. In addition, it enables better network maintenance, more efficient network restoration and enhances the quality of service for a given spectral capacity.

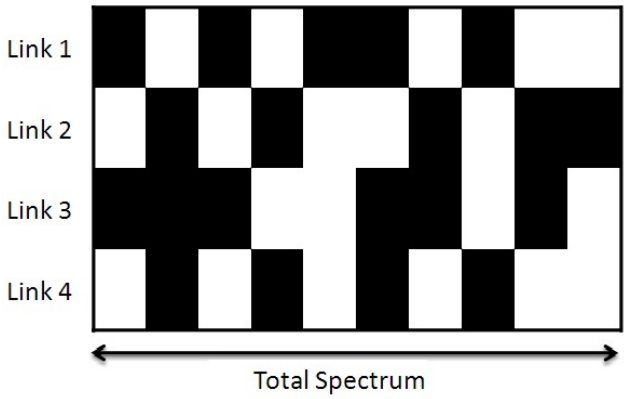

Figure 4.2 – Scattered spectral fragments in four links of a typical flexible optical networks.

In a very general perspective, there are two main ways to perform the defragmentation operation, reactive and proactive. Reactive operations are invoked when a request cannot be accommodated given the network-wide spectrum allocation. In proactive operations, the spectrum allocation is performed in a manner that unused spectrum slots are proactively preserved for future use, such as defragmenting periodically or according to some fragmentation threshold [22]. These mechanisms usually operate with the goal of confining the spectral usage to one side of the spectrum, and require the entire network to be considered for defragmentation simultaneously. It is worth mentioning that, in either case, it is very important to perform the re-allocation of connections in a hitless fashion, i.e. without terminating a connection or affecting other running connections in the network.

4.1.2 Time-varying traffic

Demands are not only dynamic in terms of arrival and duration but they are also (usually) dynamic in terms of bandwidth [23]. For instance, a service provider may request more bandwidth from the network in some time periods to support the data backup service during night hours or to support video on-demand services during evening hours. In conventional WDM networks, connections are over-provisioned in order to support changes in traffic demand. Whenever significant traffic changes are observed or expected, additional wavelengths are provisioned. On the contrary, in flexible optical networks, the allocated optical spectrum of a lightpath is tailored to the actual width of the transmitted signal. This new feature creates an additional problem, with respect to the adaptation of the spectrum allocated to each lightpath so as to follow the traffic bandwidth variations, in particular, expansion of the spectrum when the required bit rate of a demand increases.

To enable time-varying traffic service, additional contiguous spectrum portion need to be necessarily (pre-) allocated to the demands. In such a way, connections can accommodate increased bit rate by expanding their spectrum to such additional slots and return to the original state by contracting them. Different variants of spectrum expansion/contraction strategies exist. The easiest solution is to assign a

fixed number of spectrum slots to each demand subject to time-traffic varying. Such additional slots can be used exclusively by certain connections or shared among any connections. More complex approaches cannot only expand/contract the spectrum but can also move its central frequency either within a short range, or along the whole spectrum range. Such cases are clearly more challenging as the algorithms must be robust enough to prevent conflicting resource allocation in case many connections require resource re-allocation at the same time.

4.1.3 Resilience

As services impose high availability requirements, it is of vital importance to design resilient networks. Resilience can be provided via dedicated and shared protection schemes. In contrast to dedicated protection, shared protection schemes allow sharing of the protection resources among connections with disjoint working resources. Recent works have examined the potential benefits that can be gained when deploying different protection schemes in flexible optical networks for both the static and the dynamic scenarios. It is shown that the flexible network with shared protection has better performance than the fixed grid networks with same protection scheme in terms of energy efficiency.

4.1.4 Traffic grooming

Traffic grooming is the process of grouping many low capacity demands into larger units, which can be processed as single entities. The main objective of traffic grooming is to minimize the cost and spectrum resource consumption of the network. There are two main approaches to preform traffic grooming in the network. The first approach relies on the O/E/O conversion and electronic signal processing (electrical traffic grooming). However, perform traffic grooming in the electrical domain has some drawbacks such as high energy consumption, big device footprint and scalability. More importantly, by moving to the higher bit rates such as 1Tbps, 10 Tbps and more, the electronic devices cannot keep pace with the traffic demands, thus, it is quite impossible to process such a huge amount of information in the electrical domain. Alternatively, optical grooming techniques enable the aggregation and the distribution of the traffic directly at the optical layer, i.e. multiple low capacity demands can be grouped together (in a contiguous way) to form a super channel.

Depending on where traffic grooming is performed, it is possible to classify the operation into two main categories: source aggregation and intermediate nodes grooming. The source aggregation proposal is based on the idea of better utilization of transmitter capacity. In flexible optical networks, Bandwidth Variable (BV) transmitters should support flexible central frequency tuning and elastic spectrum allocation, which can be achieved thanks to recent technology advances. To realize traffic accommodation, the bandwidth of transmitters is discretized in spectrum units, referred as spectrum slots. The spectrum variability of lightpaths is achievable by tuning the number of allocated spectrum slots. The incoming traffic is mapped onto individual BV transmitters generating the appropriate-sized optical lightpaths between end nodes. However, the capacity of a transmitter may remain underutilized when the traffic demands are lower than the transmitter's full capacity. In simple words, despite the crucial role of BV transmitters in increasing the spectrum efficiency of network, their full capacity cannot be utilized efficiently. It is therefore essential to introduce a solution for maximizing the capacity utilization of BV transmitters. To address the problem, the idea of source aggregation has been proposed [24]. In general, this proposal tries to aggregate multiple sub-wavelength connections into one transmitter and serves them as a whole over the network. This solution has been taken into account as a quasi-FOX-C solution presented in subsection 4.4.1.

In addition to the above mentioned process, it is possible to perform the traffic grooming, all optically in the network intermediate nodes. However, implementing such a proposal over flexible optical networks from the technology point of view was so far impossible. Thanks to the efforts in FOX-C, now realizing all optical traffic grooming in the network intermediate nodes is not a dream. This case will be detailed in subsection 4.4.2. Along with it and in order to highlight the benefits of FOX-C technology, it is very important to develop and design a new RA solution that efficiently exploits all

optical traffic grooming functionality at network nodes. The proposed Traffic grooming capable routing and spectrum allocation (TG-RSA) algorithm will be explained in subsection 4.4.3. However, let's first review the reference network topologies and characteristics as well as benchmarking cases.

4.2 Reference network topologies and characteristics

This section describes the reference network structures as well as considered traffic demands that are used for the feasibility, techno-economic and energy consumption analysis. Two reference networks are considered in this study:

a) A large national-scale network: Orange group national network with 51 nodes.

b) A continental network: GÉANT Pan-European network with 34 nodes.

The diversity of the reference network topologies allows us to capture a better picture of the applicability of the FOX-C technology, while examinining the scalability tolerances in terms of cost and power consumption. Moreover, such a wide selection of reference network topologies pave the way for finding a gradual network migration path which will be investigated in the deliverable D2.4.

4.2.1 The Orange group national network

The Orange group national network, which is representative of a typical transmission backbone network encountered in one European country, has been selected as a large national-scale network, Figure 4.3. This network is composed of 51 nodes connected together through 75 links, each of them having a pair of fibres (one fibre per direction). Although, the mean nodal degree in this topology is 2.9, it is important to note that 3 out of the 51 nodes are particularly sensible with a rather high degree of meshing (nodes 21, 32 and 33) which makes this topology an interesting case for study. The majority of links (80%) are either very short (25% of links are less long than 50km and most of the time correspond to intra-city links), either lower than 300 km. The average link length is 217 km. However, two links (among green links on Figure 4.3) on this topology are much longer than the average (1300km and 2427km) and corresponds to possible paths towards international connections. Also, it is worth mentioning that the whole C-band has been considered available in all network links. For more detail please see [25].

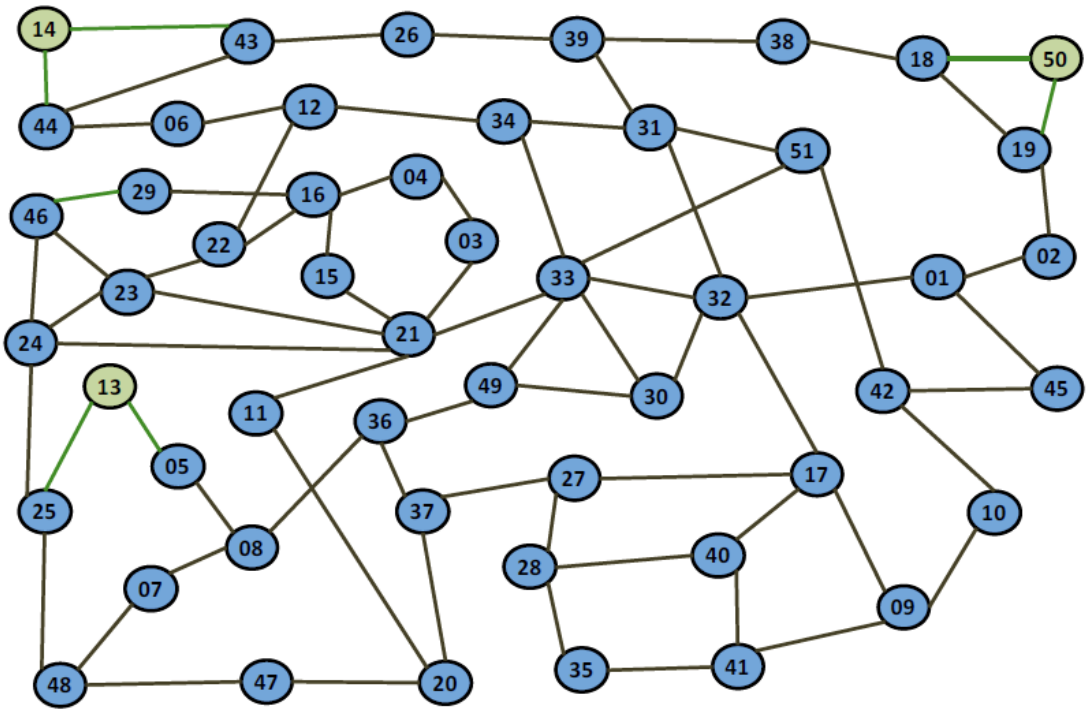

Figure 4.3 – The Orange group national network.

The traffic demand matrix for the first year under study is included to provide reference data for simulations, Figure 4.4. Each column shows the total traffic demand per node. It is possible to observe that, some nodes are almost pure transit (i.e. core network) nodes since they don't support considerable edge node service demand (e.g. node 41). Moreover, it is worth to notice that the traffic is not uniformly spread over the network and there is a considerable difference between the highest and the lowest traffic demand. In this study, the evaluation is preformed over a period of 7 years. To model the traffic growth, in line with [25], the growth rate of 1.2 per year has been considered.

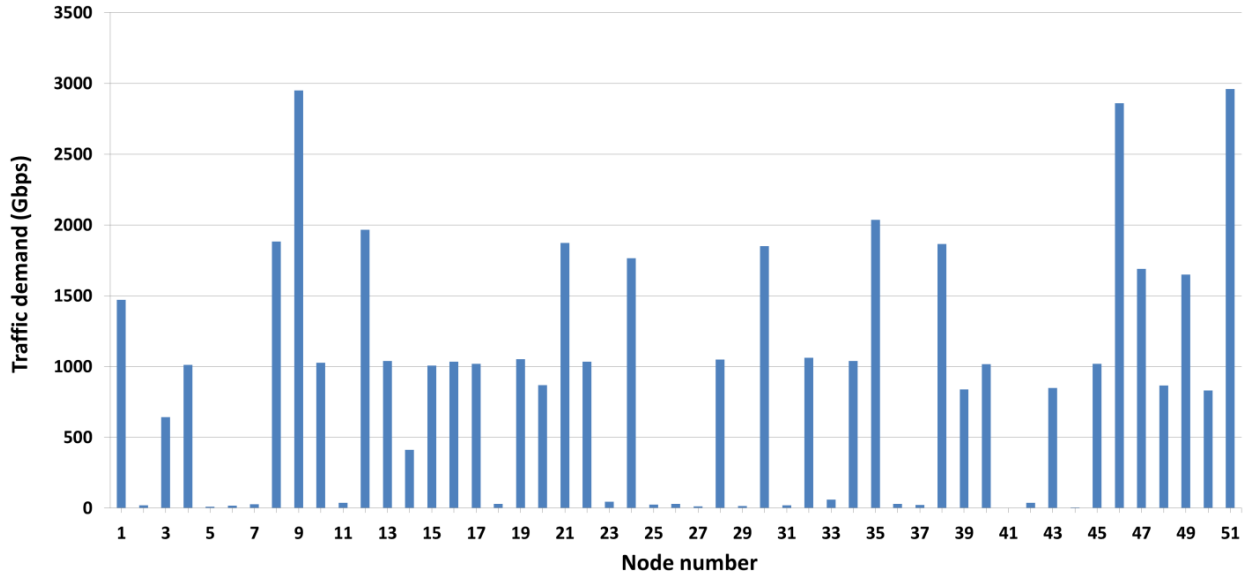

Figure 4.4 – Traffic demand matrix (Gbps) of Orange group national network.

4.2.2 The GÉANT2 Pan-European reference network

The selected continental network topology in this study is the Pan-European GÉANT2 reference network, presented in Figure 4.5. As a successor to GÉANT, the pan-European multi-gigabit research network, GÉANT2 is the seventh generation of pan-European research and education network. The GÉANT2 network connects 34 countries through 30 national research and education networks (NRENs), using multiple 10Gbps WDM links. The first links came into service in early December 2005, between Switzerland and Italy, and Switzerland and Germany, respectively. Multiple 10Gbps wavelengths are being employed in the network's core. The total numbers of links of GÉANT2 is 52 which more than 40% of them have lengths less than 500 km. Also, around 80% of the links have lengths less than 1300 km and except some few links the rest have lengths less than 2100 km. Also, it is worth mentioning that the whole C-band has been considered available in all network links. For more detail please see [25].

The reference traffic matrix for the GÉANT 2 network is presented in Figure 4.5. Similar to the previous case, there are some nodes with no traffic demands (transit nodes), while there are some nodes with considerable edge node service demands. The 7 years study period has also assumed here. To model the traffic growth same 1.2 ratio as above is applied.

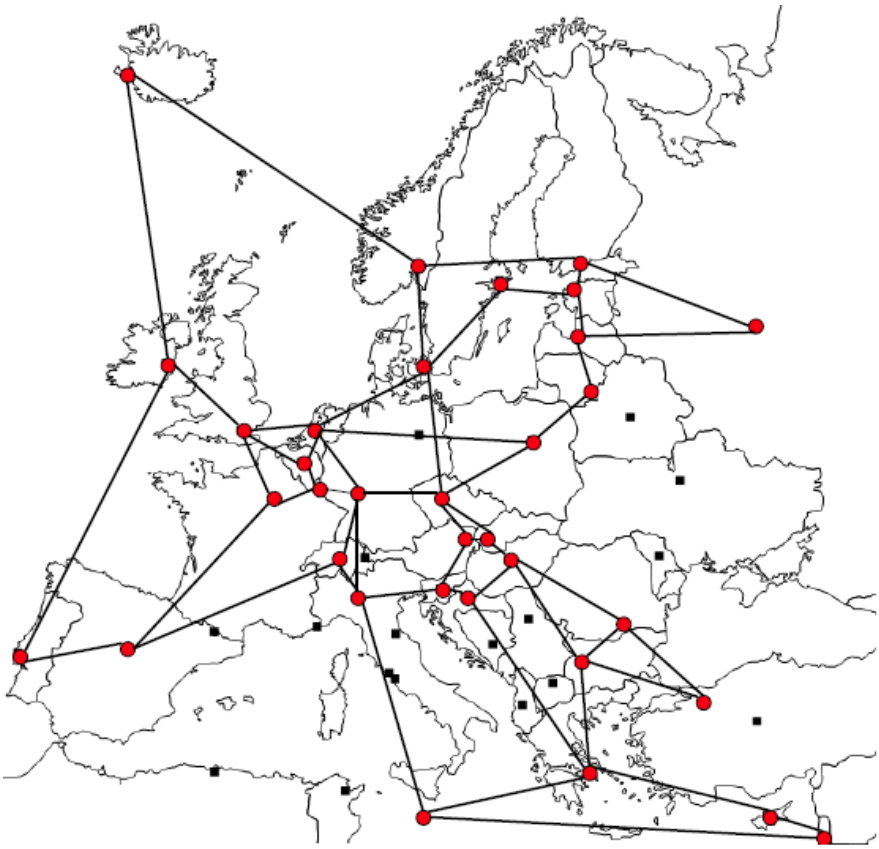

Figure 4.5 – The GÉANT2 Pan-European reference network.

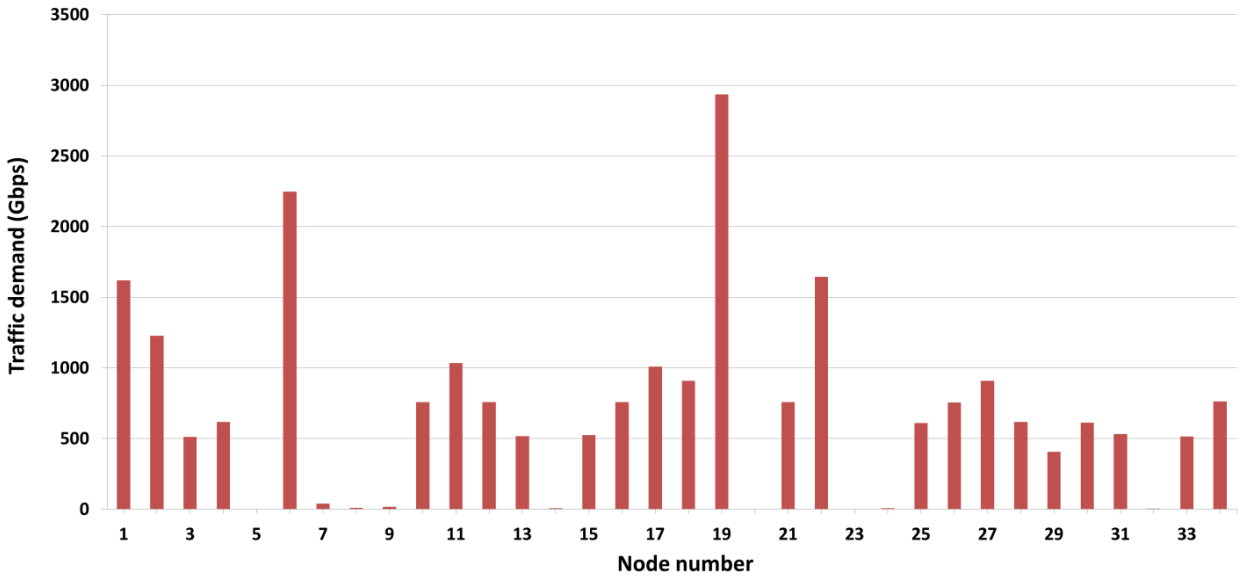

Figure 4.6 – Traffic demand matrix (Gbps) of GÉANT2 Pan-European reference network.

4.3 Benchmarking cases

In the following, the benchmarking scenarios under study are described. Different options are considered with respect to the current state of optical networking technology. This gives us a good opportunity to capture a better image of the FOX-C solution benefits over other technologies.

4.3.1 SLR transceiver over fixed grid

The Single Line Rate (SLR) scenario, as shown in Figure 4.7, employs only a single type of transceiver to serve all demands over the network. Of course, the selected modulation format for transmission should be able to guarantee the quality of transmission (QoT) at the receiver side of all connection requests. In this study, DP-BPSK is the selected modulation format for the SLR case. Moreover, in this scenario, the fixed 50-GHz ITU-T frequency grids are assumed to be in place.

To solve the routing sub-problem, the Fixed Alternate Routing (FAR) approach has been adopted, which considers K-disjoint (K = 3) routes between source-destination pairs. Each node in the network has to maintain a routing table that contains an ordered list of routes to each destination node. The routes include the shortest, the second-shortest and the third-shortest path calculated by Dijkstra's algorithm from the source node *s* to the destination node *d*. It is important to note that a link-disjoint approach has been applied in the path calculations, i.e. the second-shortest path between *s* and *d* is any route that does not share any links (is link-disjoint) with the shortest path. In the same way, the third-shortest path is any route that does not share any links with already existing routes (shortest and second-shortest path) in the routing table of *s*. Note that considering some critical issues such as network topology and nodal degree, there is a maximum number of possible routes between each source-destination pair.

Regarding the spectrum allocation sub-problem, the First Fit (FF) approach has been selected, which is a well-known and widely used spectrum allocation scheme. In a fixed grid scenario, all wavelengths are initially numbered. When searching for available wavelengths, a lower-numbered wavelength is considered before a higher numbered wavelength. The first available wavelength is then selected. This scheme requires no global information, which guarantees small computational overhead, low complexity and small communication overhead. By utilizing FF, it is possible to pack all in-use wavelengths toward the lower end of the wavelength space, and therefore longer continuous paths at the higher end of the wavelength space will remain available for future traffic requests.

Also it is worth mentioning that since the main focus of this deliverable is on the static RA solutions, the way that connections are ordered in the serving list plays an important role in the final outcome. To enhance the results in all cases under study, the simulated annealing (SimAn) meta-heuristic has been employed to find an appropriate ordering that yields a near-optimal result [21]. The SimAn procedure is detailed in subsection 4.4.3.

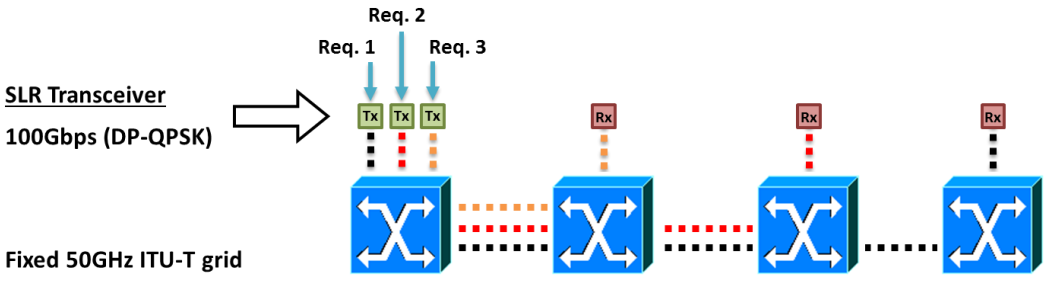

Figure 4.7 – SLR transceiver over fixed grid.

4.3.2 MLR transceiver over fixed grid

Unlike the SLR scenario, the Multi Line Rate (MLR) scenario employs more than one transceiver type to serve connections, i.e. transceivers with different bit rates and different performance in terms of the maximum transparent optical reach. It gives the provider the possibility to select transceivers with different characteristics depending on the connection requirements. As shown in Figure 4.8, four transceiver types, DP-BPSK, DP-QPSK, DP-8QAM and DP-16QAM, have been considered. In addition, as in the SLR scenario, the fixed 50-GHz ITU-T frequency grid is assumed. Also, to accommodate

connections over the network the abovementioned RA algorithm for routing and spectrum allocation is used.

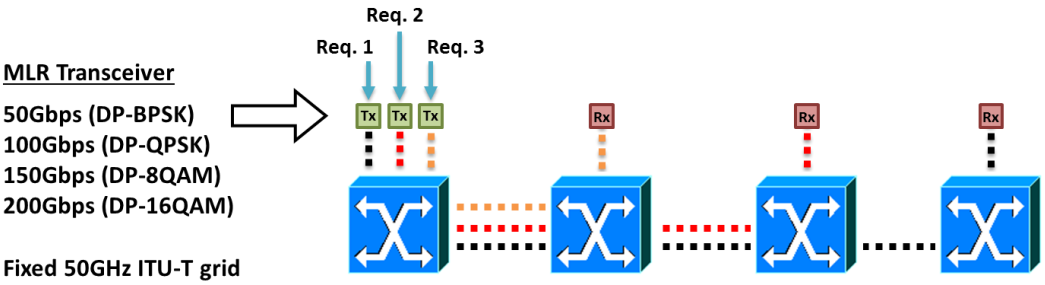

Figure 4.8 – MLR transceiver over fixed grid.

4.3.3 MLR transceiver over flexi-grid

This scenario is the conventional understanding of flexible optical network offering further degrees of flexibility compared to MLR networks –as it is able to allocate an appropriately-sized portion of optical spectrum to a connection request depending on the demand requirements–. It means that, unlike the previously mentioned fixed grid scenarios, here a lightpath can expand and contract according to the traffic volume and user request. In this way, incoming traffic demands can be served in a spectrally efficient manner.

As mentioned previously, instead of assigning a certain wavelength to each connection in a flexi-grid scenario, a number of contiguous spectrum slots, which have a finer granularity than the 50-GHz wavelengths (e.g. 12.5 GHz), are used to accommodate a connection. Moreover, the continuity of these spectrum slots should be guaranteed in a similar manner as the wavelength continuity constraint is imposed in fixed-grid networks. As discussed, this leads to the development of RMLSA algorithms. In the current study, the RMLSA algorithm [21] consists of the previously mentioned FAR routing scheme and a modified version of the FF spectrum allocation algorithm. The new FF initially calculates the required spectrum for each incoming connection request regarding the traffic volume and the optical reach of the available modulation formats: DP-BPSK, DP-QPSK, DP-8QAM and DP-16QAM. Next, it searches for the necessary consecutive slots in ascending order of the spectrum slot index. The first slot set found fulfilling the requirements of connection request is selected. Similar to subsection 4.3.1, SimAn meta-heuristic has also been included in the RA solution.

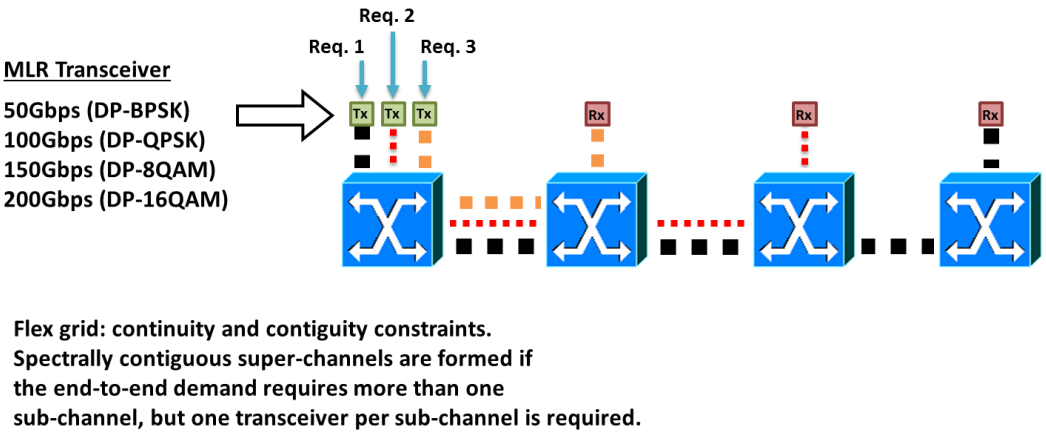

Figure 4.9 – MLR transceiver over flexi-grid.

It is also important to note that in a flexi-grid scenario, leaving some intact spectral portion between adjacent connections to guaranty the quality of signal in the receiver side is crucial. It is customary that the assigned spectrum portion between adjacent connections should be regarded as a multiple of the

spectrum slot (12.5GHz). However, such a "blind" spectrum dedication may lead to spectrum overutilization. In the following, this issue is investigated.

4.3.3.1 Impact of filter sharpness on performance

Both transceivers and WSS, as discussed in section 2.1, present imperfect optical filter shapes that degrade the transmitted signal quality. Filter cascading was seen to strongly affect the total reach of the lightpath —or equivalently the maximum number of node hops that can be traversed with adequate quality of transmission (QoT) —. To circumvent this problem, a larger amount of spectrum can be reserved for a connection, thus guaranteeing the signal quality by restraining the signal to the filter flat central region and avoiding the filter transition region.

Likewise, Adjacent Channel Interference (ACI), a form of power leakage from adjacent channels attributed to the physical impairments on the fibre as well as the imperfect shape of filters [27][28], negatively affects channel transmission. As discussed in [29], to mitigate ACI, guard bands (GBs) are needed between adjacent channels.

This results in overutilization of the network resources, which is one of the main concerns for network operators. In this section, we take this issue into account and also investigate the effect of reducing the FS size to improve the GB assignment and, consequently, the network spectrum utilization in a dynamic network scenario.

I. Filter shape and guard band

A. Filter models

In this study we assume Nyquist pulse shaping at the transmitter (Tx), as was done in D3.4 for NWDM and NFDM transmission, on account of its capability to enable high spectral efficiency transmission. A family of filters that satisfies the Nyquist theorem is the raised cosine filters [30]. For any given roll-off value, the total reserved spectrum after filtering (BW_{Tx}) is given by [31]

$$BW_{Tx} = (1 + \beta)BW \tag{4.1}$$

where β is the roll-off value of the filter and BW equals the Baud rate of the signal. In this formulation, the spectral penalty due to the imperfect shape of the filter amounts to β · BW/2 (on each side of the connection). These filters have therefore very sharp rising/falling edges for small β.

At the intermediate nodes, flex-grid LCoS-based WSS are assumed, whose spectral roll off can be modeled as an error function defined by the spectral granularity and optical resolution of the filter, as explained in D4.1. The filter granularity depends on the LCoS pixel size and the spatial dispersion, whereas the channel passband shape is given by the optical resolution of the WSS dispersive optics. In this study we have considered four different values for the optical resolution, namely, 2.5, 5.0, 7.5 and 10.0 GHz, such that the finer the resolution, the wider and flatter the passband characteristic across the allocated channel bandwidth. The spectral penalty (or GB required on each side of the connection) due to the imperfect shape of the WSS filter was calculated as the width between f = BW/2 (i.e. the edge of the ideal Nyquist channel) and the frequency at which a -35dB block bandwidth is achieved.

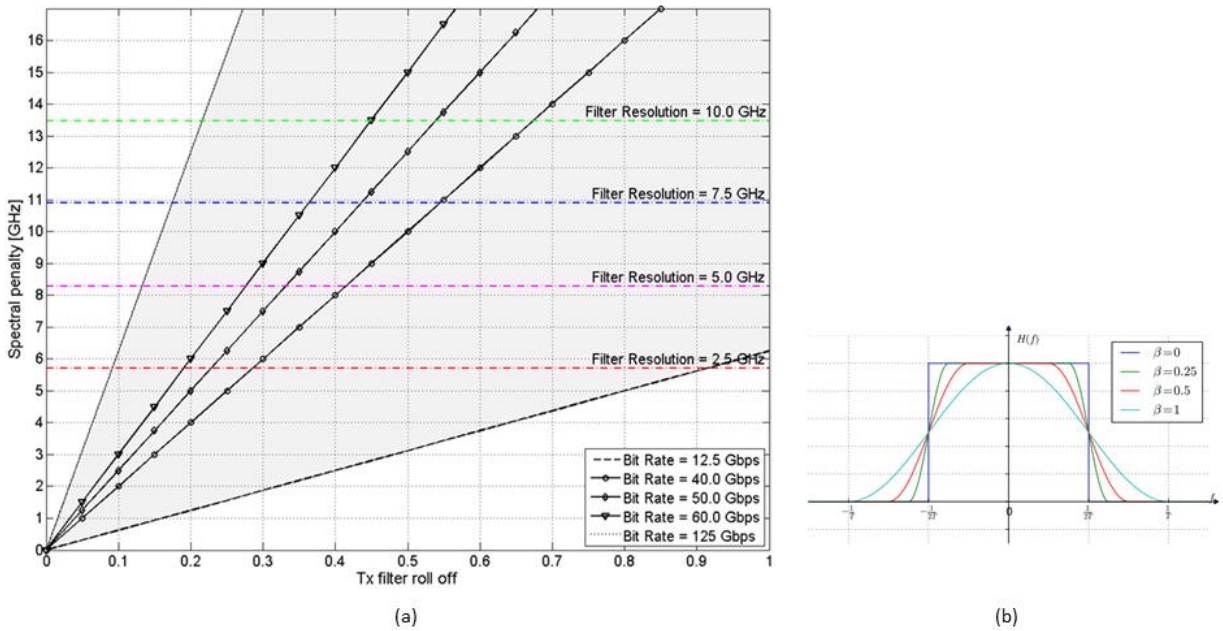

Figure 4.10 – (a) Spectral penalty for different Tx and WSS filter characteristics and offered load values ranging from 12.5 to 125 Gbps (gray area) (b) Schematic of a Nyquist channel with different beta roll-off values .

Figure 4.10 shows the spectral penalty (or GB) as a function of the transmitter filter roll-off value and the intermediate-node WSS filter resolution for different bit rates per connection. The grey area indicates the range of bit rates per connection considered in this study, which goes from 12.5 (bottom line) to 125 Gbps (top line), and we have singled out three bit rates, namely, 40, 50 and 60 Gbps. The raised cosine filters at the Tx are load aware, while the LCoS-based WSS filters are load agnostic. Thus, the GB allocated to a certain channel is dependent on which filter is dominant for a given bit rate per connection, Tx filter roll off and WSS filter optical resolution. Let us define a *load-agnostic region* as the area in the graph in which the WSS filter spectral penalty is dominant for a given optical resolution (and therefore the GB value must be made equal to this spectral penalty value). Conversely, a *load-aware region* can be defined as the area in which the Tx raised-cosine filter penalty is dominant for a given WSS optical resolution and offered load. In both cases, the region reduces to a vertical line when a specific Tx filter roll-off value is considered. These definitions will be used in discussing the simulation results in subsection II.

B. Filter cascading

The transmitted optical signal may experience multiple optical filtering along its route. In this case, the effect of signal distortion due to cascaded optical filters has to be taken into account. The dominant signal distortion factor is unwanted spectral clipping arising from the narrowing of the filter passband [32]. This effect is more destructive for lightpaths traveling through larger numbers of node hops [33]. In order to compensate for this issue, filters with sufficiently large bandwidths are used to guarantee that the received signal is not distorted. From the networking point of view, this effect can be translated into more reserved spectrum for connections.

While the conventional way to cope with this issue is to consider the worst-case design (i.e. considering enough spectrum to guarantee the QoT for the lightpath with the longest path length), in this study a quasi-dynamic scheme is introduced. We assume that for every lightpath with path length equal to P (expressed as the number of transparent hops), the extra reserved spectrum for the connection due to the cascading effect (CRS) is given by [32]:

$$CRS = \lfloor (P-1)/4 \rfloor \times 6.25\ [GHz] \quad (4.2)$$

For example, if we have a connection travelling over six links, an extra amount of spectrum equal to 6.25 GHz is reserved for the connection in order to compensate for the effect of filter cascading.

C. Efficient spectrum allocation

The amount of GB assigned between channels to alleviate the spectral penalty stemming from filter cascading and ACI is traditionally a multiple of the FS size (12.5GHz). While it may seem like a reasonable approach to calculate the GB size, it is not always spectrally efficient. For example, by considering two connections of 25 Gbps and 37.5 Gbps and a roll-off value of 0.10 in a scenario with ideal filters at intermediate nodes (i.e. optical resolution = 0), a filter spectral penalty of 1.25 and 1.875 GHz, respectively, on each side of the connections is observed, as shown in Fig. 2 (a). Therefore, considering the conventional FS size, a spectrum portion equal to 25 GHz has to be left unused between the shown adjacent connections (12.5 GHz per connection). In this way, roughly 22 GHz of spectrum are wasted (25 - (1.25 + 1.875) = 21.875 GHz). By moving to finer FS sizes, for instance, 6.25 GHz or 3.125 GHz, the spectrum utilization can be improved by reducing the amount of wasted spectrum. As shown in Figure 4.11(b), with FS size = 6.25 GHz, the wasted spectrum would reduce to 9.375 GHz (12.5 - 3.125 = 9.375 GHz). In the same way, an FS size equal to 3.125 GHz leads to almost 65% less wasted spectrum compared to the previous case (Figure 4.11(c)).

In light of this discussion, one could infer that better spectrum utilization could be achieved by moving to finer FS granularities. This claim, nevertheless, needs to be examined for different filter characteristics and load profiles in order to quantify the gain obtained when moving toward lower granularities. This will be analyzed, through extensive simulations, in the next subsection.

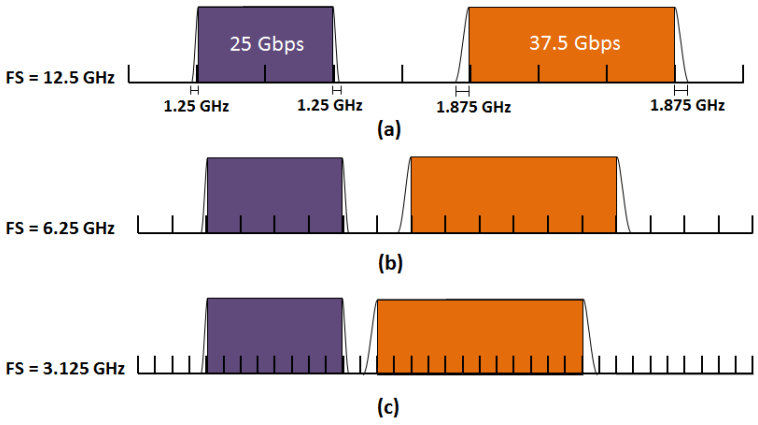

Figure 4.11 – GB assignment for two exemplary connections, considering FS size of (a) 12.5 GHz, (b) 6.25 GHz, and (c) 3.125 GHz.

II. Simulation results

Discrete event simulation studies have been carried out for performance evaluation purposes using the 34-node GÉANT2 pan-EU reference network topology with 54 links. We assumed a total optical spectrum of 4 THz per link (C-band) and considered BPSK as the modulation format due to its capability to support long reach optical transmission, which allows establishing all possible connections in the GÉANT2 pan-EU network [34]. To solve the Routing and Spectrum Allocation (RSA) problem, a k-Shortest Path computation algorithm with a First-Fit slot assignment starting with the shortest computed path was applied [2]. Additionally, unidirectional connections between end nodes were considered due to the asymmetric nature of today's Internet traffic. The load generation followed a Poisson distribution process, so that different offered loads could be obtained by keeping the mean Holding Time (HT) of the connections constant to 200s, while their mean Inter-Arrival Time (IAT) was modified accordingly (i.e. offered load = HT/IAT). Traffic demands for each source-destination pair were randomly generated

following a normal distribution over the range of 12.5 Gbps to 125 Gbps. The average traffic demand of all generated connections in the simulation (3×10^5) was used as a measure of the service granularity. The GB calculation and assignment policy, along with the effect of filter cascading, presented in the previous subsection, were considered for all cases under study.

In a first study, we investigated the effect of the filter characteristics on the performance of the network in terms of the BP (total dropped traffic (Gbps) / total offered traffic (Gbps)). To do that, three optical resolution values (2.5, 5 and 7.5 GHz) for the WSS filters at the intermediate nodes and two roll-off values (0.05 and 0.3) for the Tx filters were considered. Regarding the offered load, the average number of connections per node was fixed at 8.5 for all cases under study (the total average number of connections in the network was therefore 289) and the simulations were run for three average bit rates per connection, namely, 40, 50 and 60 Gbps. Consequently, the total average traffic generated per node was 340, 425 and 510 Gbps, respectively. We also evaluated the effect of using finer FS granularities on the BP performance of the network. For this purpose, three different FS sizes were assumed (12.5, 6.25 and 3.125 GHz).

As can be seen in Figure 4.12, a significant reduction in BP can be achieved by moving to sharper filters (e.g. Tx roll off = 0.05 and WSS optical resolution = 2.5 GHz). The remarkable difference between the network BP for the best and worst characteristics (for a given service granularity) is due to the fact that with better filter shapes connections can be allocated closer to one another without requiring a wide GB in between, and therefore the chances of finding free spectral resources for establishing new connections in the network improve. In addition, it is worth noting that in all cases under study with FS size = 12.5 GHz the network BP is higher than in the case of finer FS sizes. This result can be justified by virtue of the arguments given in the previous section: from a closer look at how the filter spectral penalty is calculated, it can be easily deduced that in most cases the total spectral penalty is lower than 25 GHz and therefore it is possible to consider just one FS (12.5 GHz) as GB (on each side of a connection) to guarantee its QoT (conventional worst-case design). Hence, generally speaking, by moving to finer FS granularities the amount of wasted spectrum as GB reduces.

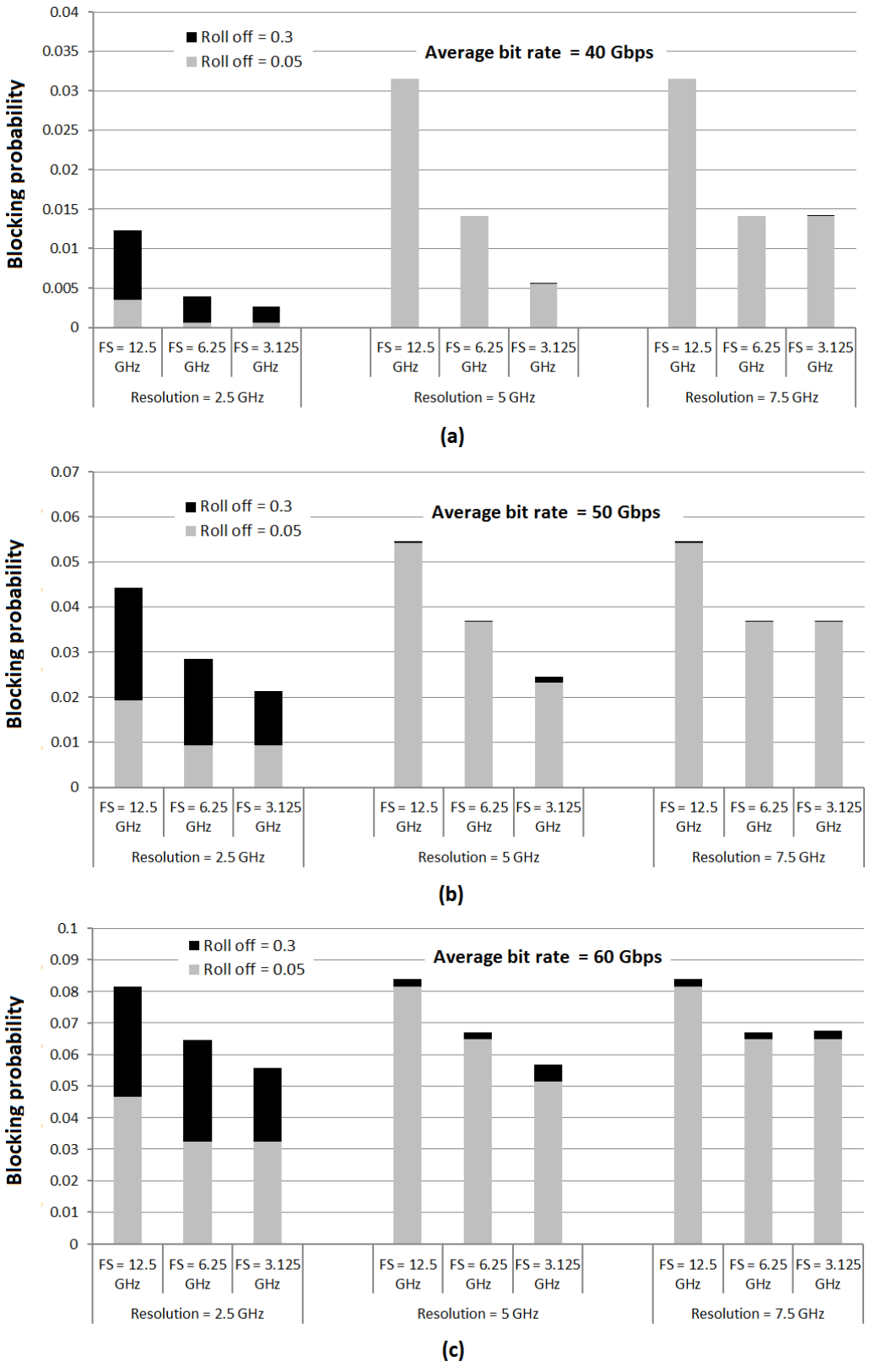

Figure 4.12 – Network blocking probability for six filter characteristics (Tx filter roll off = 0.05 and 0.3, and WSS resolution = 2.5, 5 and 7.5 GHz) and three frequency slot sizes (12.5, 6.25 and 3.125 GHz) for different offered loads. The average bit rate per connection was (a) 40 Gbps, (b) 50 Gbps, and (c) 60 Gbps.

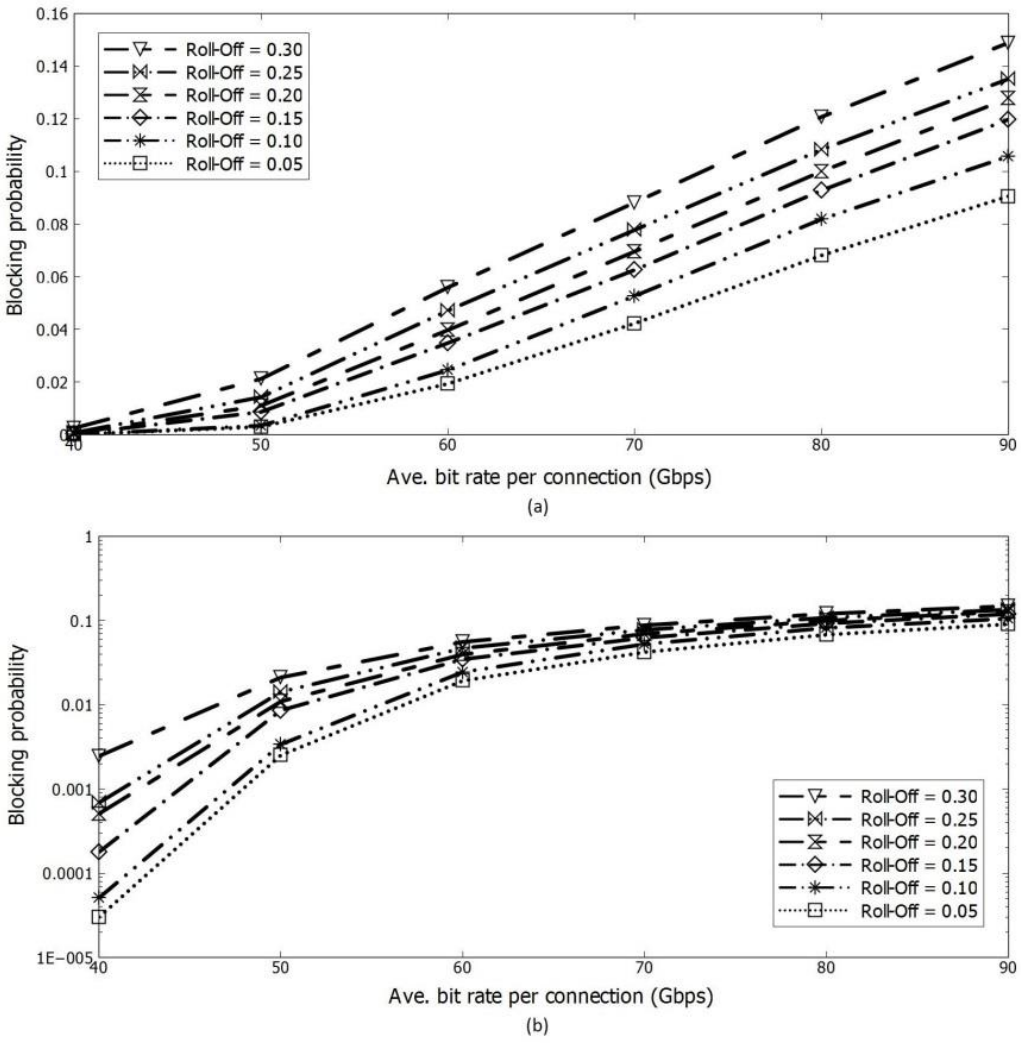

Figure 4.13 – Network BP for different roll-off values (considering ideal WSS filters) in (a) linear and (b) logarithmic scale. The offered load to the network ranges from 340 to 765 Gbps per node (i.e. average number of connections per node 8.5 and average bit rate per connection ranging from 40 to 90 Gbps).

However, this statement is not always true. To gain a better insight into this matter, let us investigate each of the filter characteristics individually. With a Tx filter roll-off value of 0.05, the GB is equal to the WSS filter spectral penalty (load agnostic region). In light of the spectral penalty for WSS optical resolutions of 2.5, 5.0 and 7.5 GHz being, respectively, ~6, 8 and 11 GHz, it is observed that employing the finest FS size (3.125 GHz) can only provide benefits if the WSS optical resolution is set to 5 GHz, there being no reason to go for finer FS sizes than 6.25 GHz in any other case. Similarly, with a Tx filter roll-off value of 0.3 and WSS optical resolutions other than 2.5 GHz, we are around the edge of the load-agnostic region, so the GB value is equal (or similar) to the WSS filter penalty. In contrast, with a WSS optical resolution of 2.5 GHz, which is the most load-aware case under study, the BP performance of the network varies considerably with the Tx filter roll-off value of the transmitter filter and a FS of 3.125 GHz brings significant gain when sharper filter functions are considered.

All in all, it can be concluded that there is undoubtedly a correlation between the BP performance and the filter sharpness at the transmitters and intermediate nodes, but this correlation must not be taken for granted and, instead, each particular case must be studied individually. Let us therefore focus on the two limiting cases explained above. In order to establish a common ground for comparison and guarantee the best performance in all cases, we will set, without loss of generality, the FS size to 3.125 GHz for the rest of the study.

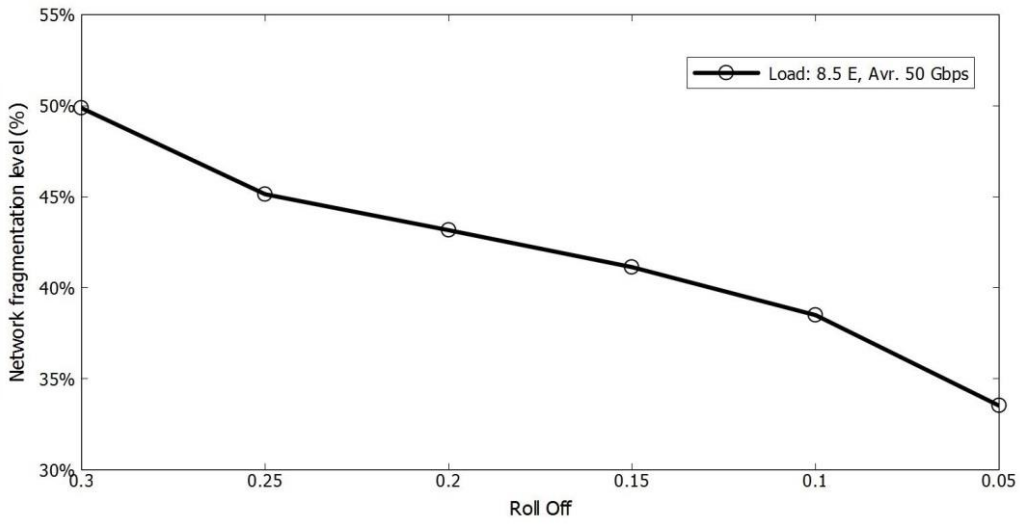

Figure 4.14 – Network fragmentation level for different Tx filter roll-off values (considering ideal WSS filters). The offered load to the network is 425 Gbps per node (i.e. average number of connections per node 8.5 and average bit rate per connection 50 Gbps).

In the case of the load-aware filters, we studied the effect of the Tx filter roll-off value on the BP performance of the network for different offered loads in a scenario with ideal WSS filters. Regarding the traffic load, a fixed average number of connections per node of 8.5 was assumed (with the total average number of connections in the network being 289). Also, we considered an average demand per connection request ranging from 40 to 90 Gbps, such that the total traffic generated per node ranged from 340 to 765 Gbps, respectively. Figure 4.13 shows the results both in (a) linear and (b) logarithmic scale. The presented results quantify the benefit of employing sharper transmitter filters in terms of BP. As illustrated, by employing the best Tx filter roll-off under study (roll off = 0.05), the BP of the network can be improved by around 40% as compared with the worst case considered (roll off = 0.3) for high offered loads (Figure 4.13(a)). This improvement is even more significant for low offered load, amounting to around two orders of magnitude (Figure 4.13(b)). To broaden our vision, we also evaluated the effect of the transmitter filter characteristics on the level of fragmentation in the network [22]. As mentioned previously, in a dynamic traffic scenario, the random connection arrival and departure process leads to the fragmentation of the spectral resources. Therefore, in medium and high loaded network scenarios, the probability of finding sufficient contiguous spectrum to establish a connection over such fragmented spectrum can be very low, leading to blocking of connection requests despite having sufficient, but non-contiguous, spectrum resources. To evaluate the level of fragmentation in the network the following steps are taken: first, the level of fragmentation in each link of the network is calculated using the following equation [35]:

$$Fragmentation\ level = 1 - \left(\frac{largest\ free\ block}{total\ free}\right)\ \% \tag{4.3}$$

where *largest free block* is the FS count for the largest contiguous free spectrum portion, and *total free* is the total number of free FSs. Second, the network fragmentation level is obtained as the mean value of the calculated fragmentation level of the network links. In light of this equation, Figure 4.14 presents the network fragmentation level as a function of the roll-off value for a given offered load to the network (with the average number of connections being 8.5 and the average bit rate per connection being 50 Gbps). As shown, reducing the filter roll off from 0.3 to 0.05 results in the reduction of the level of fragmentation in the network by more than 15%. From this result it can be inferred that not only the saved spectrum due to the smaller GB associated with lower roll-off values, but also the reduction in the level of fragmentation of the network, are responsible for the significant BP improvement observed. However, it is worth noting that improving the filter sharpness will only reduce the fragmentation level

in the network to a certain degree, since there always exists a level of fragmentation in the network due to the random nature of the connections set up and torn down in a dynamic scenario.

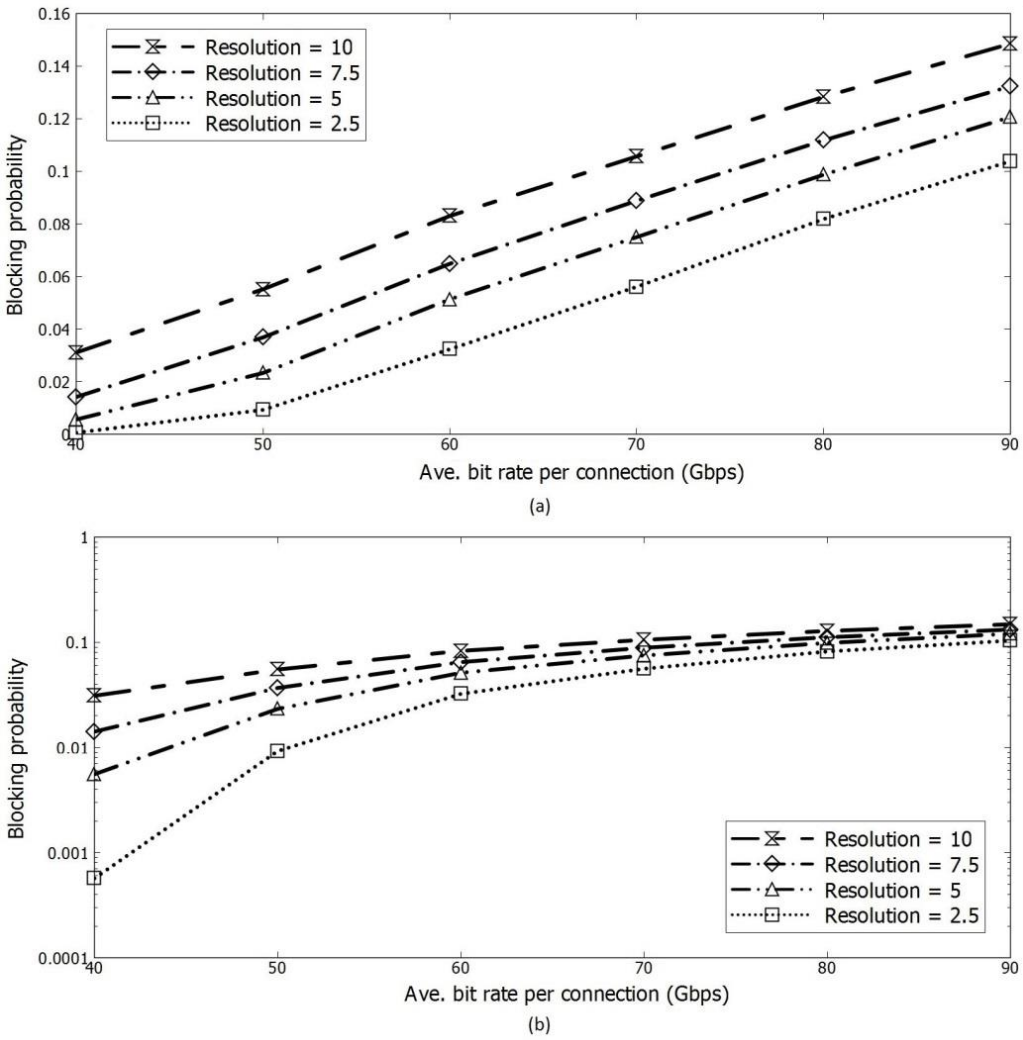

Figure 4.15 – Network BP for different resolutions (considering ideal Tx Nyquist filters) in (a) linear and (b) logarithmic scale. The offered load to the network ranges from 340 to 765 Gbps per node (i.e. average number of connections per node 8.5 and average bit rate per connection ranging from 40 to 90 Gbps).

In the case of the load-agnostic filters, similar studies have been conducted in a scenario with ideal Tx filters (roll off = 0) and intermediate-node WSS filters with resolutions from 2.5 to 10 GHz. Like in the above-mentioned study, the offered load consisted of a fixed average number of connections per node (8.5) and an average bit rate per connection ranging from 40 to 90 Gbps. As shown in Figure 4.15, a significant reduction in the BP of about 30% can be achieved for high loads (Figure 4.15(a)) and more than an order of magnitude for low loads (Figure 4.15(b)) when the results for the best (2.5 GHz) and worst (10 GHz) resolutions are compared.

Regarding the network fragmentation level, as in the previous case (Figure 4.14), we also considered an average number of connections of 8.5 and an average bit rate per connection of 50 Gbps. Figure 4.16 shows that the network fragmentation level can be improved by about 10 % by selecting sharper filters at the intermediate nodes. By comparing these results with the data shown in Figure 4.14, we observe that the effect is less strong in the second case due to the load-agnostic nature of WSS filters.

In conclusion, we have demonstrated in this study that a case could be made for going for increasingly fine spectral slot sizes in the limit of the load-aware region if the blocking probability is to

be decreased. However, in the load-agnostic region, spectral slots finer than 6.25 GHz bring no benefit for a given WSS optical resolution. Furthermore, we have demonstrated through simulations that improvement in terms of network BP and network fragmentation level can be obtained by using filters with sharper edges in both the load-aware and load-agnostic regions. These results can be used during the network planning stage to assess the practicality of moving to filters with better characteristics at the transmitters or intermediate nodes, since sharper filters or finer FS granularities could increase the cost of the technology while not necessarily yielding further improvement in terms of network level performance.

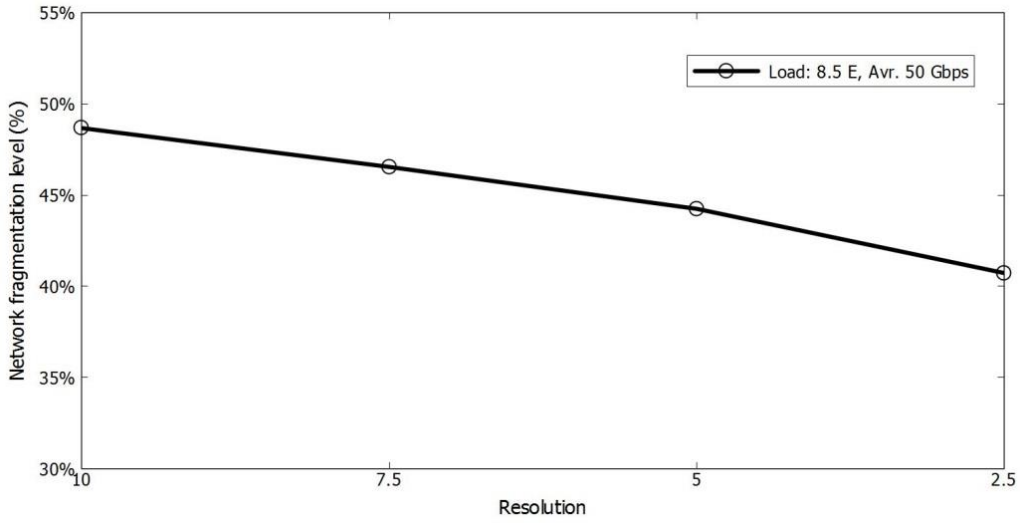

Figure 4.16 – Network fragmentation level for different resolutions (considering ideal Tx Nyquist filters). The offered load to the network is 425 Gbps per node (i.e. average number of connections per node 8.5 and average bit rate per connection 50 Gbps).

4.3.4 Non-grooming end-to-end connections supported by super-channel transceivers

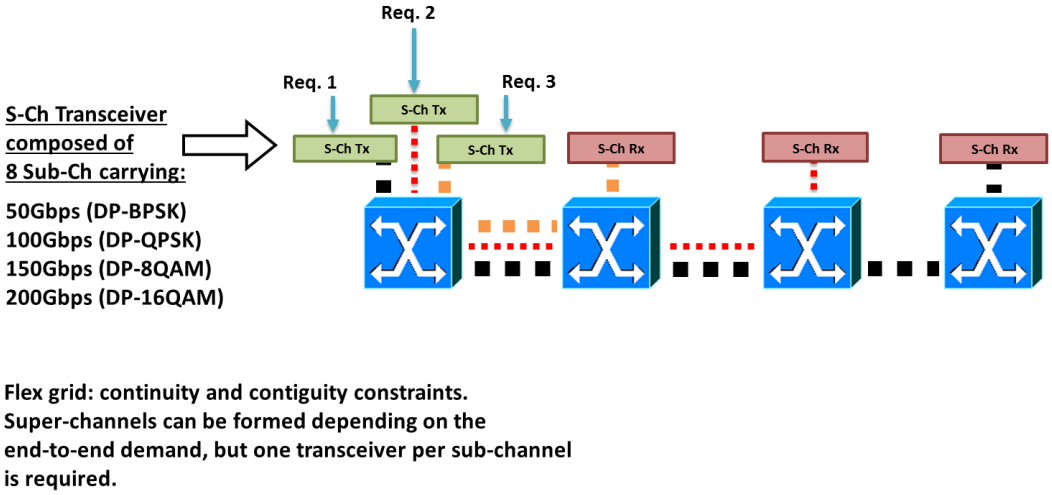

Figure 4.17 – Non-grooming end-to-end connections supported by super-channel transceivers.

So far, a set of already well-known industrial solutions has been presented. Nevertheless, it is possible to have one more imaginative scenario. The difference between this scenario and the cases explained above is the transceiver type used to serve the connections. Here, instead of having sub-channel transceivers, FOX-C super-channel transceivers are in place to support each and every end-to-end connection. As a matter of fact, this increases the cost of the network dramatically, especially for small offered load values, yet it is worth having it as a benchmarking case. The main goal is to evaluate the level of performance improvement obtained through only employing FOX-C super-channel

transceivers in the network. All abovementioned routing, modulation level selection and spectrum allocation are also used here. Finally, since the argument about spectral guard bands between adjacent channels is also valid in this case, in the following this issue is investigated, paying particular attention to the evaluation of the optimum spectral slot size for the allocation of sub-channels within a super-channel.

4.3.4.1 Evaluation of the optimum filter resolution and sub-channel spectrum granularity for qN-WDM flexible super-channels with optical filtering

Different techniques have been proposed to implement a flexible optical transmission system in a view to optimizing the use of resources by flexibly assigning spectrum, data rate and modulation format adapted to the needs of the end-to-end connection requests. One of these techniques is based on the utilization of quasi-Nyquist WDM super-channels (Sp-Ch) composed of Nyquist-shaped sub-channels (Sb-Ch), each occupying a certain portion of spectrum. To accommodate traffic, the available optical bandwidth (BW) is discretized in FS. According to the ITU-T 694.1 standard, the FS size is 12.5 GHz and the spectrum variability of the connections is achieved by tuning the number of allocated FSs. However, recent studies have been addressing the question of whether this is indeed the optimum spectral slot. E.g., in [36] it was demonstrated that, for mixed-rate signal transmission, an FS size calculated as the greatest common factor of the spectrum width of all signals would bring benefits in terms of network performance. Nevertheless, it did not address a scenario with fully flexible traffic accommodation and only evaluated the optimum FS granularity at the Sp-Ch level considering granularities down to 10 GHz. Recent developments in filter technology [13] carried out in WP4 have made it possible to move to finer FS granularities while still ensuring a good transmission performance.

This section is devoted to studying the performance of an optically-filtered qN-WDM transmission system in a fully flexible scenario from a networking perspective in order to determine the optimal spectrum granularity at the Sb-Ch level for several filter resolutions, bearing in mind that better resolution filters and finer spectrum granularity impose higher hardware requirements.

I. Bandwidth-variable transmitter characteristics and guard-band assignment policies

To carry out the network performance studies leading to the evaluation of the optimum FS sizes in multiplexing Sb-Chs to form a Sp-Ch, we have assumed a quasi-Nyquist-WDM-based transmitter like the one shown in Figure 2.13 (but with 8 sub-channel transceivers instead of 7). A maximum of 8 Sb-Chs are generated, PSK-modulated at 25 GBd by an IQ Mach-Zehnder modulator (MZM) and Nyquist-shaped by an inverse-Gaussian filter of order 2 (Figure 4.18(b)). In order to shape the signal spectrum, digital filtering (performed in the transmitter DSP) is usually employed [37], although recent advances in optical filtering technology developed in FOX-C have also made it possible to implement high-spectral-resolution optical Nyquist-shaping filters. In Figure 4.18, we have assumed an LCoS-based high spectral resolution (HSR) photonic processor with spectral roll off modeled as an error function defined by the spectral addressability and optical resolution of the filter [13], even though the results shown are applicable to digital filters with equivalent resolution. In the optical filter case, the spectral addressability depends on the LCoS pixel size and the spatial dispersion, whereas the channel passband shape is given by the optical resolution of the HSR-processor dispersive optics. In this study we have considered filters with spectral addressability of 400 MHz/pixel, as indicated in [13], and optical resolution ranging from 0.8 to 3.125 GHz.

Table 4.1 –Spectral penalty for different Nyquist-shaping filter resolutions and crosstalk values.

Res. \ Xtalk	-10 dB	-35 dB
0.8 GHz	0.40 GHz	0.90 GHz
1.0 GHz	0.42 GHz	1.12 GHz
1.2 GHz	0.50 GHz	1.34 GHz
1.5 GHz	0.61 GHz	1.66 GHz
2.0 GHz	0.79 GHz	2.19 GHz
2.5 GHz	0.95 GHz	2.70 GHz
2.75 GHz	1.02 GHz	2.95 GHz
3.125 GHz	1.13 GHz	3.32 GHz

On the subject of Sb-Ch allocation, five different spectral grids have been considered (12.5 GHz, 6.25 GHz, 3.125 GHz, 1.5625 GHz and gridless), so that the total BW of the Sb-Ch, including the inter-sub-channel GB (calculated as twice the value given by Table 4.1 for different filter resolutions and two levels of crosstalk), has to be a multiple of the minimum slot width in each case. Figure 4.18(c) illustrates this point by depicting a Sp-Ch composed of 5 Nyquist-shaped Sb-Chs in two cases: the Sb-Chs comply with the ITU-T 12.5-GHz grid (top) and the Sb-Chs are multiplexed in a gridless scenario (bottom). In both cases, the spectral penalty incurred by the signal when a maximum level of crosstalk of -35dB was allowed after Sb-Ch shaping with a 0.8-GHz resolution filter has been taken into account. A significant spectral-occupancy difference (187.5 vs. 134 GHz) can be observed.

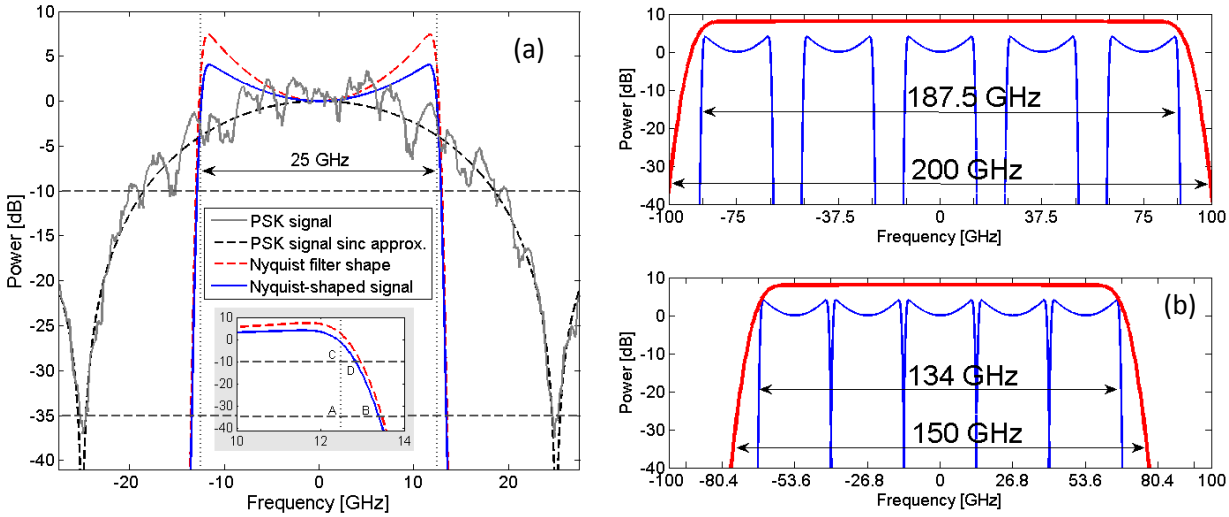

Figure 4.18 – (a) Simulated spectrum of the output signal of a MZM driven by a 25-GBd square signal with rise time 0.32 ns (gray solid); approximation of the spectrum by a sinc function (black dashed); Nyquist-shaping filter transmissivity (red dashed); filter output spectrum (blue solid); inset: detail of falling edge of filter and output signal showing segments AB and BC along elevation lines for -35 and -10 dB block BWs used to calculate the guard band (GB) between Sb-Ch. (b) Sp-Ch composed of 5 Sb-Ch spaced out according to the ITU-T 12.5-GHz grid (top) and based on gridless multiplexing (bottom). The Sp-Ch filter transmissivity is shown in red (shifted up for clarity). PPG: pulse pattern generator, PBC/PBS: polarization beam combiner/splitter.

At the intermediate nodes, the Sp-Chs go through a cascade of flex-grid LCoS-based WSSs with resolution of 7.5 GHz and spectral addressability of 6.25 GHz. On account of the WSS filtering characteristics and the sharp edges of the Sb-Chs, a GB of 12.5 GHz between Sp-Chs is regarded to be sufficient to guarantee low impact of WSS cascading, especially when the level of crosstalk is low (e.g. -35dB), in which case only degradation due to ASE noise is observed [38]. Furthermore, the Sp-Chs (as opposed to the Sb-Chs) are required to comply with the ITU-T 12.5-GHz grid, so their total BW, including GB, has to be a multiple of 12.5 GHz. Therefore, in Fig. 1(c) the 5-band Sp-Ch BW increases to 200 and 150 GHz for the 12.5-GHz FS size and the gridless scenarios, respectively.

II. Simulation results

Discrete event simulation studies were carried out for performance evaluation purposes using the 34-node GÉANT2 pan-EU reference network topology with 54 links. We assumed a total optical spectrum of 4 THz per link (C-band) and considered dual-polarization BPSK as the modulation format due to its capability to support long reach optical transmission, which allows establishing all possible connections in the network. To solve the Routing and Spectrum Allocation (RSA) problem, a k-Shortest Path computation algorithm with a First-Fit slot assignment starting with the shortest computed path was applied [2]. Additionally, unidirectional connections between end nodes were considered due to the asymmetric nature of today's Internet traffic. The load generation followed a Poisson distribution process, so that different offered loads could be obtained by keeping the mean Holding Time (HT) of the connections constant at 200s, while their mean Inter-Arrival Time (IAT) was modified accordingly (i.e. offered load = HT/IAT). Total traffic demands per Sp-Ch were randomly generated following a normal distribution over the range of 50 Gbps to 400 Gbps (corresponding to 1-8 Sb-Chs). The average traffic demand of all generated Sp-Chs in the simulation (3 × 105) was used as a measure of the service granularity. The GB calculation and assignment policy, presented in the previous sub-section, were considered for all cases under study.

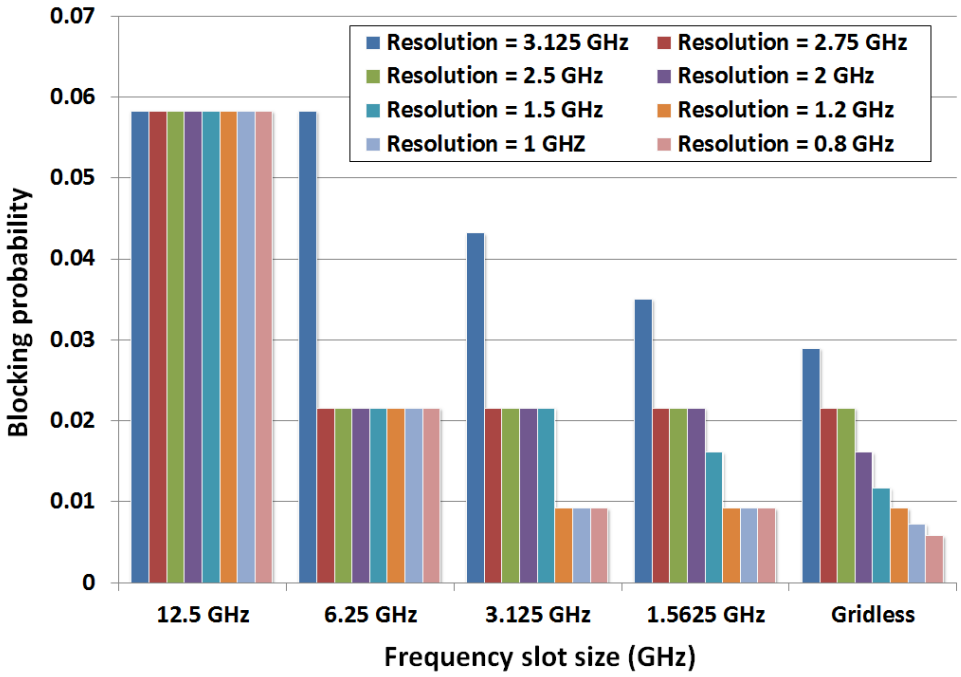

Figure 4.19 – Network BP for different filter characteristics and FS sizes.

In the first study, we investigated the effect of the filter characteristics on the performance of the network in terms of the blocking probability (BP = total dropped traffic (Gbps) / total offered traffic (Gbps)). To do that, filter resolution values from 0.8 to 3.125 GHz were considered. The average number of Sp-Chs per node was fixed at 5 for all cases under study (i.e. total average number of Sp-Chs in the network was 170) and the simulations were run for an average bit rate per Sp-Ch of 200 Gbps (i.e. total average traffic generated per node was 1 Tbps). We also evaluated the effect of using the FS granularities mentioned in the previous sub-section on the BP performance of the network.

As can be seen in Figure 4.19, a significant reduction in BP can be achieved by moving to finer FS granularities (e.g. a vast reduction in the BP is experienced when moving from 12.5 GHz to 6.25 GHz FS size with a filter resolution of 2.75 GHz and below). The difference between the network BP for the finest and coarsest FS granularities (especially for the finest filter resolutions) is due to the fact that with finer granularities Sb-Chs can be allocated closer to one another without wasting spectrum, and

therefore the probability of finding free spectral resources for establishing new Sp-Chs in the network improves.

We also investigated the network BP vs. offered loads for filter resolutions of 0.8 and 1.2 GHz in two scenarios: FS size of 3.125 GHz and gridless (and used FS = 12.5 GHz as a benchmark). To do so, along with the above-mentioned fixed average number of Sp-Chs per node (5), we considered an average demand per Sp-Ch request ranging from 150 to 300 Gbps, such that the total traffic generated per node ranged from 0.75 to 1.5 Tbps, respectively. Figure 4.20 shows that by employing the finest filter in a gridless scenario, the network BP can be improved by ~10% as compared with all other cases under study for high offered loads (Fig. Figure 4.20(a)). This improvement is more significant for low offered load, amounting to ~60% (Fig. Figure 4.20(b)).

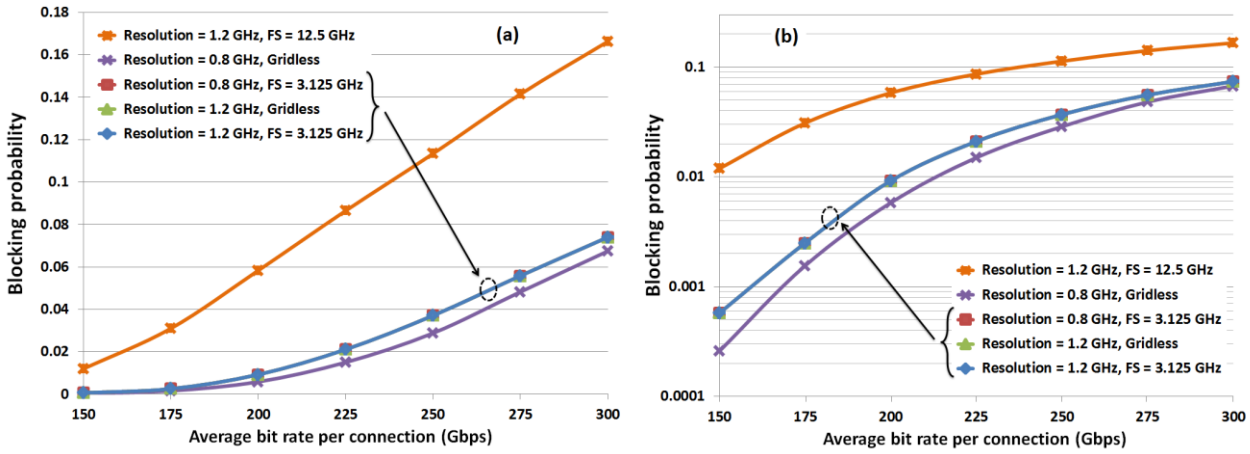

Figure 4.20 – Network BP for different filter characteristics and frequency slot sizes in (a) linear and (b) logarithmic scale. Note that the cases with FS size of 3.125 GHz and the Gridless case with filter resolution 1.2 GHz overlap.

The use of different modulation formats adapted to the connection lengths can be investigated, but we anticipate that, because longer distances for a given modulation format will be attained with finer filter resolutions and wider gaps between Sb-Chs, a performance improvement in a gridless scenario should still not be expected.

In conclusion, we have demonstrated that moving to a gridless scenario, despite showing the best performance in terms of BP when combined with very fine resolution filters, may only be justified if the additional investment in the required technology is offset by a significant turnover increase. Other than that, the results make a case for allocating sub-channels on the 3.125-GHz grid provided that filters with resolutions finer than 1.2 GHz are employed.

4.4 FOX-C solution

In this section, two possible FOX-C enabled solutions are detailed. Even though the ultimate goal of the FOX-C technology is to introduce an optical solution capable to drop and add low-rate tributaries (defined as sub-channels) directly from/to ultra-high capacity super-channels, it is still possible to have an intermediate solution. This quasi FOX-C solution tries to maximize the super-channel transmitter capacity utilization through aggregating same-source but different-destination connections. In the following, the source-aggregating scenario is first reviewed, followed by the full FOX-C solution and the Traffic Grooming capable Routing Modulation Level and Spectrum Allocation (TG-RMLA) algorithm.

4.4.1 Drop & Continue

As explained in section 4.1.4, the idea of source aggregation has been proposed to enhance the transceivers capacity utilization. To take this case into account, a quasi-FOX-C solution is introduced, namely Drop & Continue solution. Here, only the drop functionality of the FOX-C nodes is considered,

and therefore the traffic grooming is done in the network ingress nodes. The groomed traffic is served over the network using super-channels, while a number of sub-channels (i.e. one or more) within a super-channel can be dropped locally according to the demand. Due to practical concerns, e.g. control plane complexity, the spectrum portion dedicated to a super-channel remains unchanged in the entire path between connection end nodes, even though one or more sub-channels might drop locally at some intermediate node. This point has been emphasized in Figure 4.21 by indicating the unused spectrum portions. Also, it is worth pointing out that the super-channel transceivers have only been considered in source/destination nodes of the aggregated connection. To detect extracted sub-channels at intermediate nodes, sub-channel transceivers are assumed.

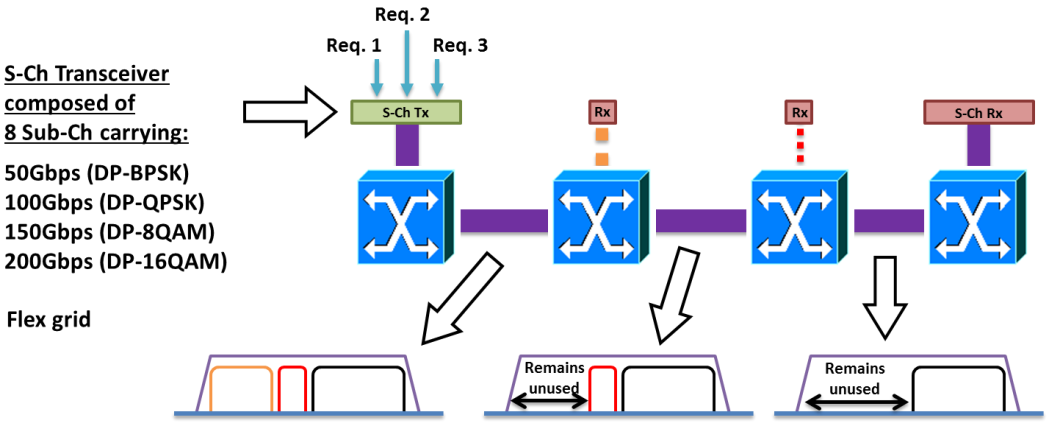

Figure 4.21 – Drop & Continue.

4.4.2 Add & Drop

To enhance the spectrum utilization, the second case considers full FOX-C node capability (add/drop). This means that, in addition to the ability to drop a number of sub-channels from a super-channel, network nodes are also able to all-optically add them. In addition, the super-channel and sub-channel transceivers count is done in the same way as explained above.

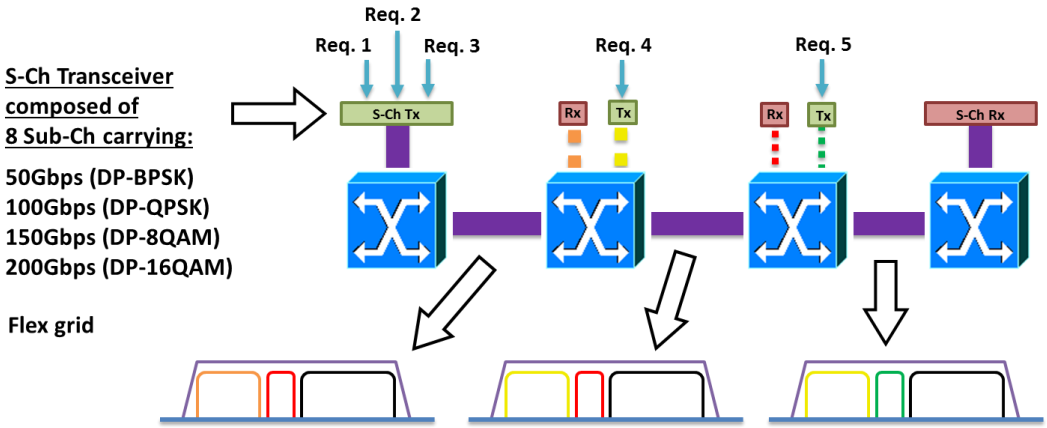

Figure 4.22 – Add & Drop.

4.4.3 Traffic grooming capable routing and spectrum allocation (TG-RMLSA)

The main body of the TG-RMLSA algorithm is similar to the previously mentioned RA algorithms, i.e. it uses FAR routing algorithm to solve the routing problem and the modified version of FF (subsection 4.3.3) to select modulation level and spectrum allocation. The main difference between the TG-RMLSA algorithm and a normal RMLSA algorithm is on steps 4 and 5 of the algorithm shown below, which introduces the capability of all-optical traffic grooming at the network nodes.

TG-RMLSA algorithm:

1. Let element R(s,d,b) be the connection request from source s to destination d, with bandwidth b. Put the elements in the serving list.
2. Sort serving list according to b in descending order (under the simulated annealing mega heuristic, make a copy of the serving list to be used as the initial solution). Set counter = 1.
3. Base element = serving list(counter). Compute k disjoint shortest paths to establish the base element.
4. For "Drop & Continue" take the following sub-steps (otherwise skip this step):
    I. For each computed path at step 3, create an empty list to register the possible elements R that can be groomed at the source node over the path. In the serving list find all unserved elements that meet the following conditions: s = same source as the base element, d = an intermediate node of the path. Register the elements in the path's source grooming list.
    II. Select the path with the highest number of registered elements on the source grooming list. In case of a tie, select the shortest path in terms of distance.
    III. Calculate the modulation level and the number of sub-channels to serve the base element. Next, calculate the modulation level and the number of sub-channels for each of the elements in the source grooming list one by one.
    IV. Calculate the required spectrum for the super-channel formed as the juxtaposition of the sub-channels in the previous sub-step. Note that each super-channel has a maximum width limit determined by the utilized filter technology (e.g. 200 GHz for the HSR filter).
5. In the case of "Add & Drop" take the following sub-steps (otherwise skip this step):
    I. For each computed path at step 3, create an empty list to register the possible elements *R* that can be groomed at the source node over the path. In the serving list find all unserved elements that meet the following conditions: *s* = same source as base element, *d* = an intermediate node of the path. Register the elements in the path's source grooming list.
    II. For each computed path at step 3, create an empty list to register the elements *R* that are groomed at the intermediate nodes. In the serving list find all unserved elements that meet the following conditions: *s* = *d* of registered element on the source grooming list of the path, *d* = same destination as the base element. Register the elements on the intermediate node grooming list.
    III. Select the path with the highest "number of registered elements on the source grooming list + number of registered elements on the intermediate node grooming list". In case of a tie, select the shortest path in terms of distance.
    IV. Calculate the modulation level and the number of sub-channels to serve the base element. Next, calculate the modulation level and the number of sub-channels for each of the elements on the source grooming list and the intermediate node grooming list one by one.
    V. Calculate the required spectrum for the super-channel formed as the juxtaposition of the sub-channels in the previous sub-step. Note that each super-channel has a maximum width limit determined by the utilized filter technology (e.g. 200 GHz for the HSR filter).

6. Find the first sufficient spectrum portion for the super-channel so that it complies with the spectrum continuity and contiguity constraints.
7. Mark all served elements on the serving list as served connection requests. Counter++ and go to step 3 while counter ≠ size of serving list.
8. If there still exist unserved elements on the serving list, consider them as blocked connections.
9. Under the simulated annealing meta-heuristic, re-arrange the copy of the serving list according to the simulated annealing rules, set counter = 1 and go to step 3. Repeat for a set number of iterations.

In line with the discussion in section 4.3, step 9 emphasizes the utilization of simulated annealing meta-heuristic in the RS solution. Under the SimAn, the algorithm starts with the initial ordering of the serving list resulting from step 2 and calculates its cost (viewed as "energy" in SimAn setting) by serving the connections one by one, using the part of the algorithm between step 3 and 8 ("fitness function"). For a particular ordering (R_1, R_2, …, R_M) of M demands, we define its neighbor as the ordering where R_i is interchanged with R_j. To generate a random neighbor, R_i and R_j are pivoted uniformly among the M demands. This random neighbor creation procedure and the fitness function are used in a typical simulated annealing iterative procedure to minimize an optimization objective. Here, the objective is to minimize the total cost of ownership, which is described in more detail in the next section.

4.5 Total cost of ownership analysis

In this study the total cost of ownership (TCO) analysis has been selected to validate the benefits of the FOX-C technology. Based on [39] and [40], the TCO comprises three main expenditures: transceiver cost, network node cost and spectrum cost, which can be extracted through a network planning study. The first two expenditures can be easily calculated by multiplying the number of network components (transceiver and optical cross connect elements) according to the presented cost model in chapter 3. To obtain the spectrum cost, initially we introduce the spectrum resource consumption measure. The average occupied spectrum per link has been selected for this purpose. This measure is a function of

1- the dedicated spectrum to connections,
2- the spectral GB between the connections, and
3- the level of defragmentation in the network link.

As a matter of fact, this parameter gives us a comprehensive view about the required spectrum per link that guaranties the accommodation of all connection requests over the network without experiencing any blocking. Thanks to the efforts in [41] and [42], it is possible to convert spectrum resource consumption into cost. To this end, the cost of a "dark" 12.5-GHz spectrum slot has been assumed to be $11.12k, or 2.08 times the cost of a 10G transceiver. Note that this "dark spectrum slot" cost corresponds only to the cost of the link infrastructure (equipment/fibre) to support a 12.5-GHz spectrum slot and excludes any cost associated with "lighting up" this channel. The spectrum cost in addition to the transceiver and the node cost gives us the TCO to have the technology in place.

The results of the TCO analysis over the two considered networks in this document will be presented in following.

4.5.1 The Orange group national network

The results of the TCO analysis for the selected national-scale network (the Orange group national network) are presented in this subsection. Figure 4.23 shows the average occupied spectrum per link vs. traffic volume for the seven years under study. It is worth reminding that $V_j = 1.2 * V_i$ where $j = i + 1$. As illustrated, by increasing the traffic volume the average occupied spectrum per link increases in all cases. However, the increment rate highly depends on the network technology. For example, in the case of SLR

over fixed grid, even a small extra traffic demand exceeding the full capacity of one channel (50 Gbps with DP-BPK) poses additional 50-GHz spectrum consumption on the links accommodating the connection. This is the reason for the significant difference between the SLR results and the rest of the cases. To have a better view on the benefits of FOX-C solution, from now on the SLR, fixed-grid scenario is ignored.

Since in all cases except the SLR scenario, transceivers are capable to select the most appropriate modulation format (DP-BPSK, DP-QPSK, DP-8QAM, DP-16QAM) according to the traffic demand and the signal quality at the receiver side, having almost flat results is not unexpected. Let's demonstrate this through an example. Assume the traffic demand between two end nodes is 35 Gbps. Also imagine that the distance between these two nodes is such that we can use all abovementioned modulation formats to serve a connection between them. With a simple calculation, it is possible to see that the most appropriate modulation format to establish this connection is DP-BPSK with a maximum capacity of 50 Gbps. Considering a growth rate of 1.2, 35 Gbps becomes 42 Gbps in the next year, which can still be served with the same modulation format. However, after a second traffic growth in year 2 (42 Gbps * 1.2 = 50.4 Gbps), the next modulation format level (DP-QPSK) has to be utilized for establishing the connection. It is worth pointing out that, in this case, even if the maximum supported capacity of the connection is multiplied by two the spectral occupancy of the connection remains unchanged. Using the same methodology, it is possible to observe that the mentioned traffic demand would need at least 10 years to surpass the maximum capacity of the highest-level modulation format (DP-16QAM). Only in this case, we would need to allocate more spectrum/transceiver to serve this demand.

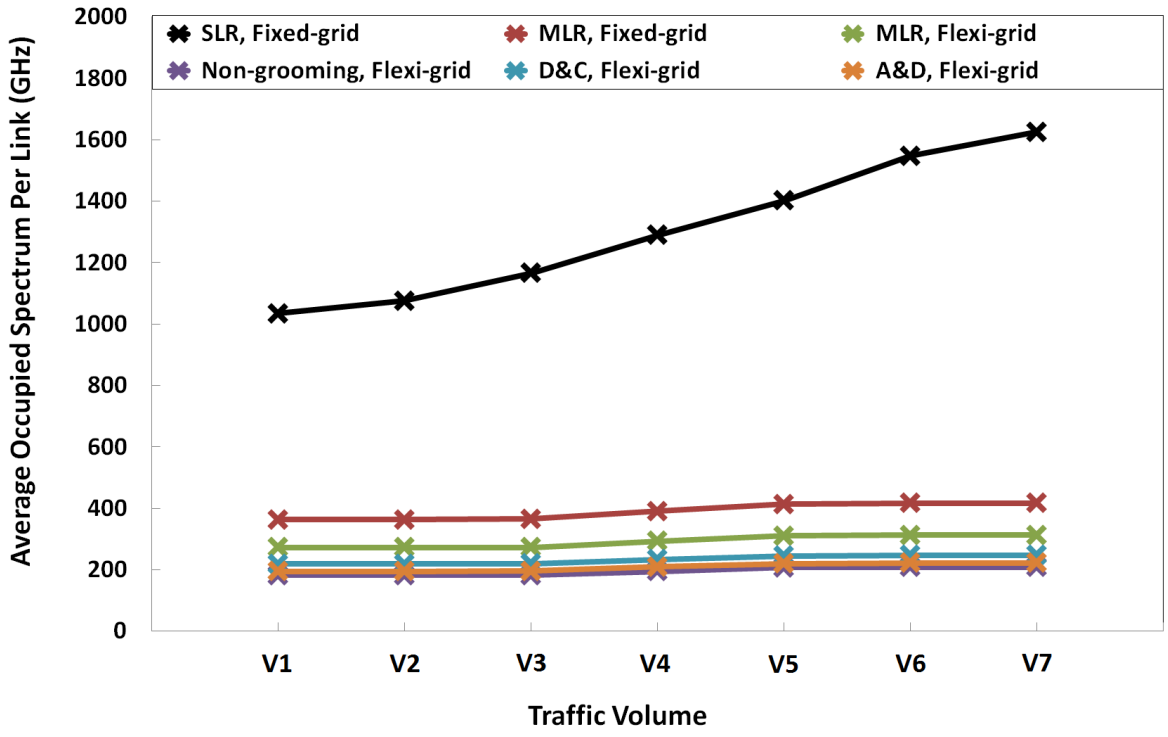

Figure 4.23 – Average occupied spectrum per link vs. Traffic volume.

By including the cost of the "dark" 12.5-GHz spectrum slot into the calculations, the spectrum cost of different cases is obtained, as shown in Figure 4.24. The most interesting fact in this figure is that the non-grooming, flexi-grid case shows the best spectral performance, even though this difference is not significant compared to the Add & Drop case. The reason is the higher fragmentation level in the network links due to performing traffic grooming. Assume we have three connections with sizes of 1, 2 and 3 slots. To accommodate them separately, we need to find three free spectrum portions with size of 1, 2 and 3 slots, respectively, while, if traffic aggregation is performed we have to search for 6 contiguous free frequency slots. In a network with a high diversity of traffic demands in terms of bit rate

and path length, finding such a big contiguous spectrum portion is difficult. Therefore, to serve the aggregated traffic demand, frequency slots with higher indices have to be allocated. In addition, it is worth noticing that in all scenarios where super-channel transceivers are utilized (i.e. non-grooming, D&C and A&D), the spectrum efficiency increases, since the internal GB between sub-channels is significantly lower than the GB between super-channels.

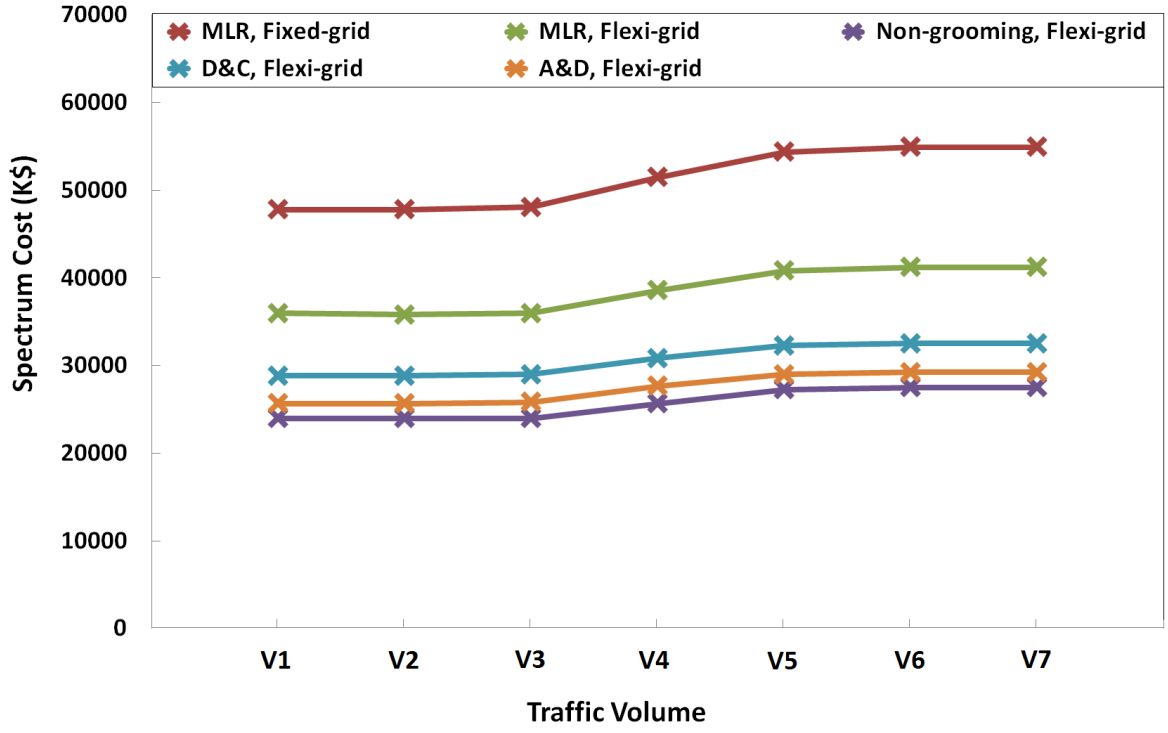

Figure 4.24 – Spectrum cost vs. Traffic volume.

Figure 4.25 presents the transceiver cost vs. the offered load for different scenarios. The non-grooming, flexi-grid case shows the worst performance since in this scenario the expensive super-channel transceivers have been utilized to support every connection. To explain the big difference between quasi and full FOX-C solutions, let us pay attention to two important points:

1) in the FOX-C solutions, we assumed that the groomed traffic in the source nodes is served by super-channel transceivers and at intermediate nodes by sub-channel transceivers,

2) with A&D, it is possible to utilize the same sub-channel transceiver to receive the dropped traffic locally and to add a new traffic demand at the same spectrum portion.

Now assume we have a super-channel between two end nodes which passes over two intermediate nodes and has some traffic to drop/add locally at each one of them. With A&D, one super-channel transceiver at each end node of the connection plus one sub-channel transceiver at each intermediate node are utilized to serve all demands. In contrast, in D&C, one super-channel transceiver at each end node of the connection plus one sub-channel transceiver at each intermediate node are utilized only to detect the super-channel at the end node and to detect the dropped sub-channels at the intermediate nodes locally. As a consequence, to accommodate the traffic demands originating from the intermediate nodes, two additional super-channel transceivers are required, which translates into substantial extra cost for the D&C scenario.

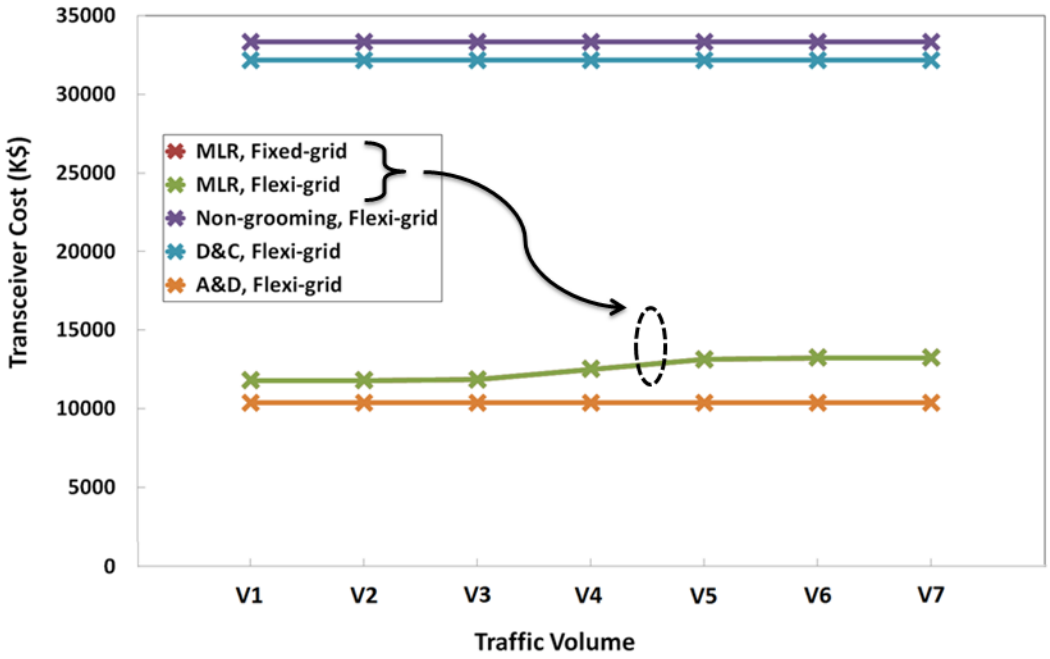

Figure 4.25 – Transceiver cost vs. Traffic volume.

Figure 4.26 presents the node cost vs. the offered load for different scenarios. All scenarios except the FOX-C solutions utilize the same type of nodes and therefore show the same node cost (indicated by the set of curves surrounded by the dash circle). To determine the node cost for the FOX-C solutions, we also need to take into account the number of dropped sub-channels per node, which can be taken as a measure for the number of HSR filters or TIDE components per node (here, we have not considered filters capable to support more than one port/sub-channel). Since, for the current traffic matrix, the number of dropped sub-channels per node in both quasi and full FOX-C solutions is the same, the node cost, calculated based on the presented cost model in section 0, for both scenarios becomes equal (as indicated by the set of curves surrounded by the solid circle).

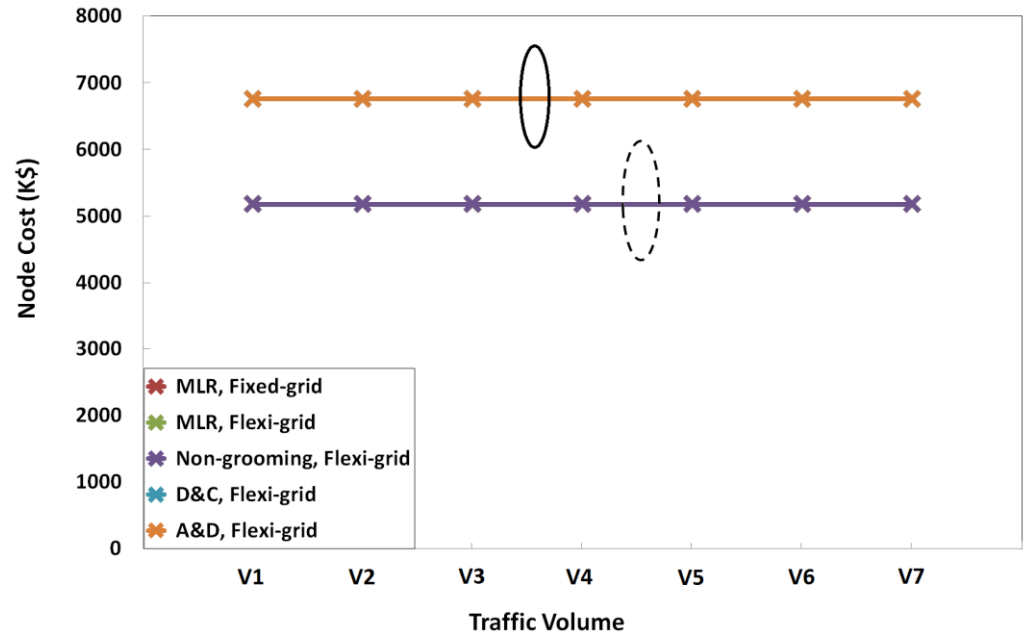

Figure 4.26 – Node cost vs. Traffic volume: node cost of all legacy solutions highlighted with the dash circule, while FOX-C solutions node cost pointed out with the solid line circule.

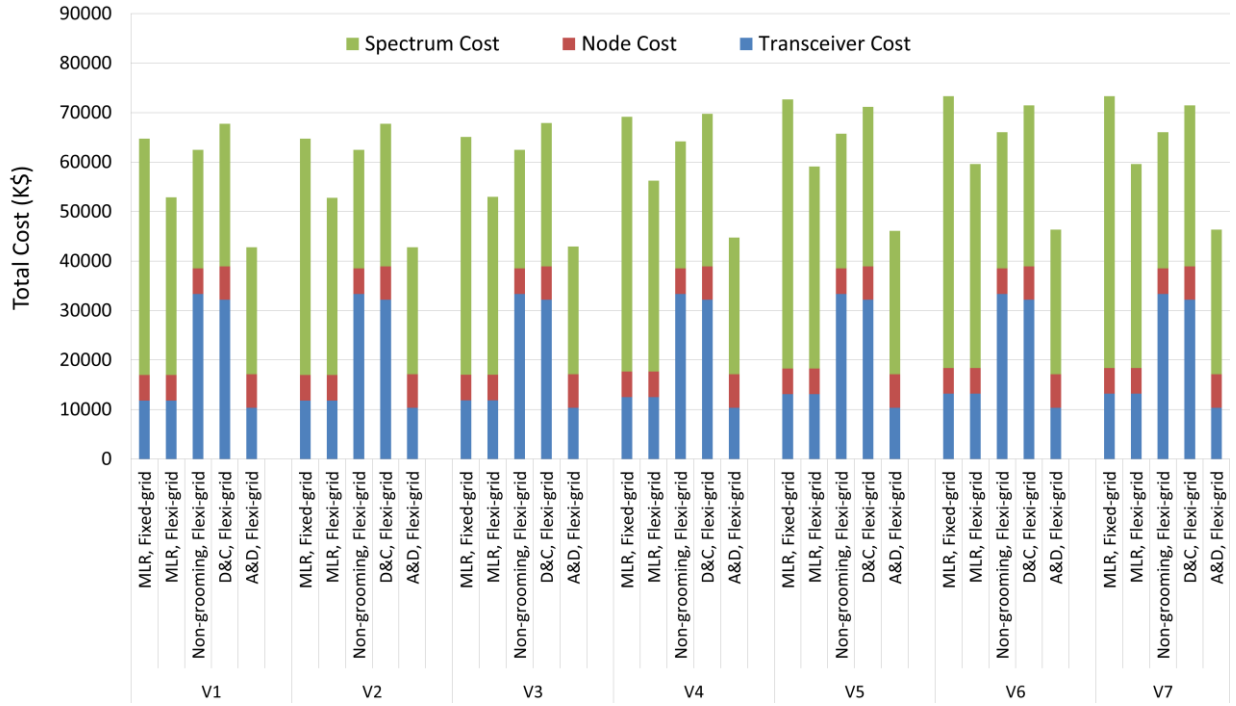

Figure 4.27 – Total cost vs. Traffic volume.

To sum up all the mentioned costs, Figure 4.27 shows the results for the total cost of all the technologies under study. As illustrated, the A&D shows the lowest cost compared to all other solutions. To quantify the benefit via TOC analysis, the area of the region bounded by each curve has to be calculated. A rough estimation shows that A&D leads to, in average, 20% cost saving compared to the MLR, flexi-grid. Table 4.2 shows the percentage of cost improvement of A&D with respect to the other possibilities.

Table 4.2 –Percentage of improvement of A&D in comparison with all other scenarios under study for the Orange group national network.

Scenario	Percent of improvement of A&D at V1	Percent of improvement of A&D at V7
SLR, fixed grid	75%	82%
MLR, fixed grid	34%	37%
MLR, flex grid	20%	22%
Non-grooming, flex grid	30%	32%
Drop & Continue, flex grid	35%	36%

4.5.2 The GÉANT2 Pan-European reference network

To get a better view, we repeat the same study for a continental-scale network, the GÉANT2 Pan-European reference network. Figure 4.28 shows the average occupied spectrum per link vs. traffic volume for the seven years under study. Once again, the difference between SLR, fixed grid and the other cases is very significant. Like in the previous study, from now on we ignore the SLR case. The rest of the results are very similar to those obtained in the previous study.

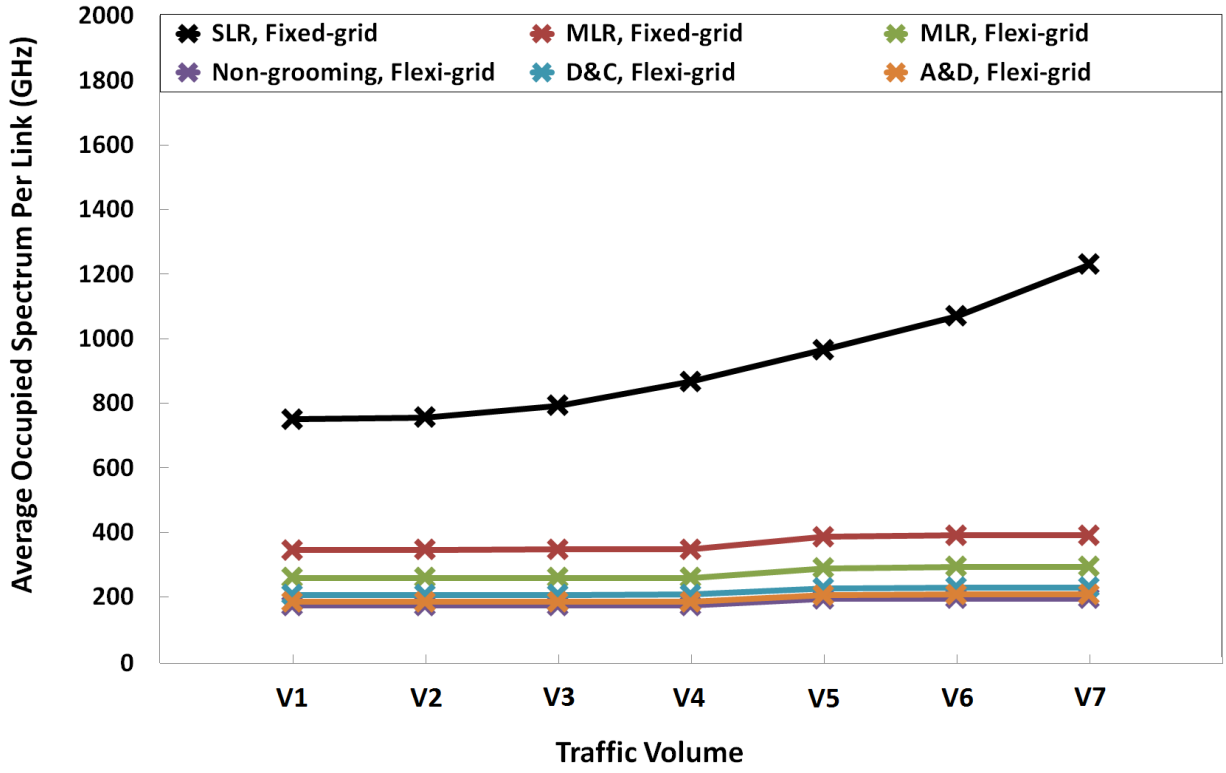

Figure 4.28 – Average occupied spectrum per link vs. Traffic volume.

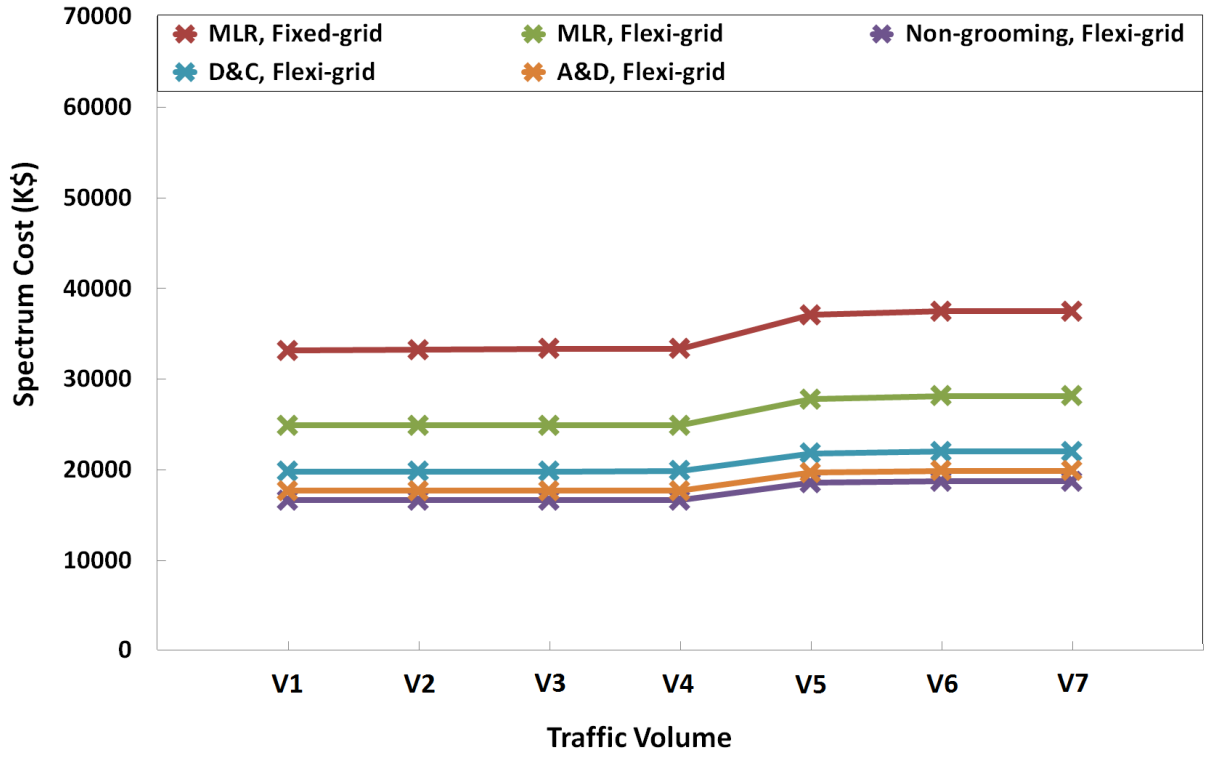

Figure 4.29 – Spectrum cost vs. Traffic volume.

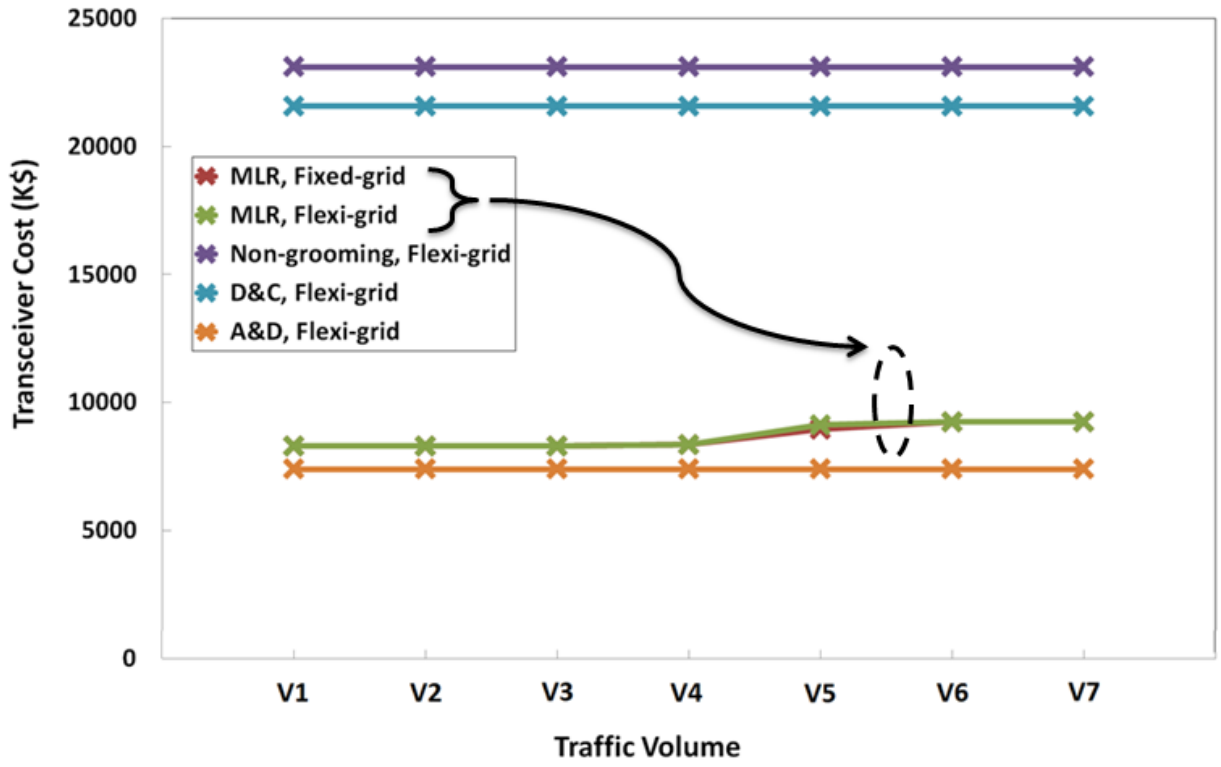

Figure 4.30 – Transceiver cost vs. Traffic volume.

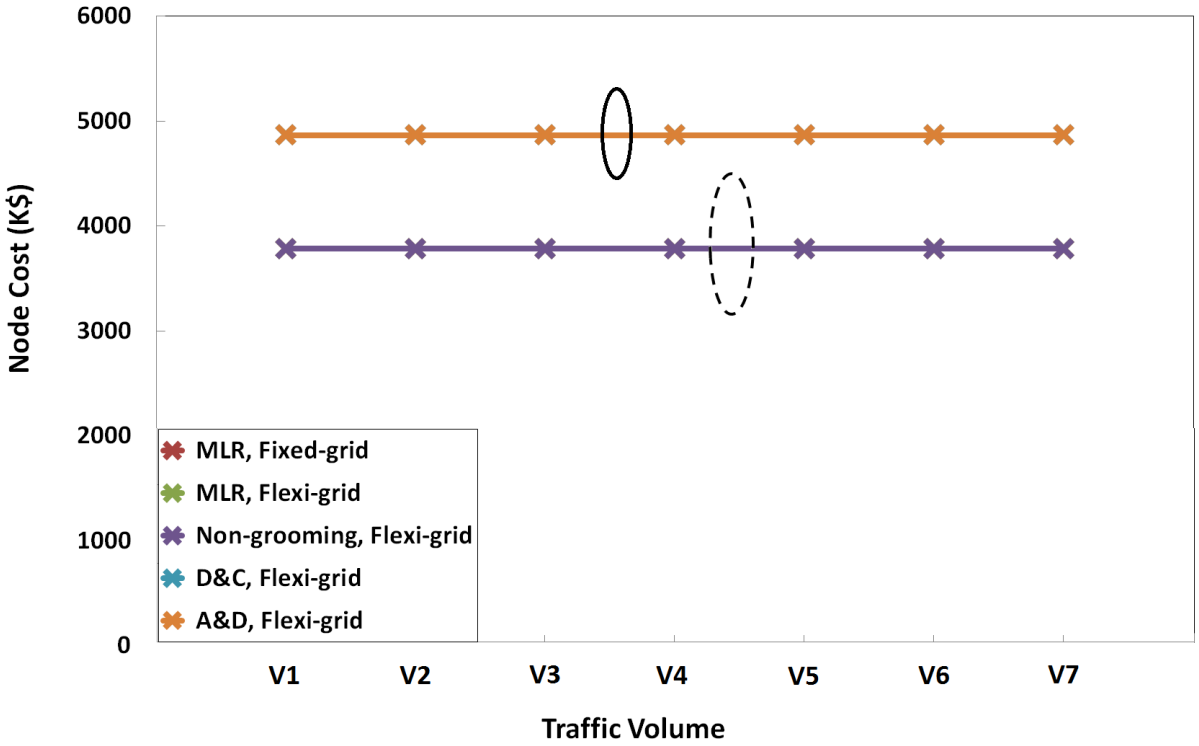

Figure 4.31 – Node cost vs. Traffic volume: : node cost of all legacy solutions highlighted with the dash circule, while FOX-C solutions node cost pointed out with the solid line circule.

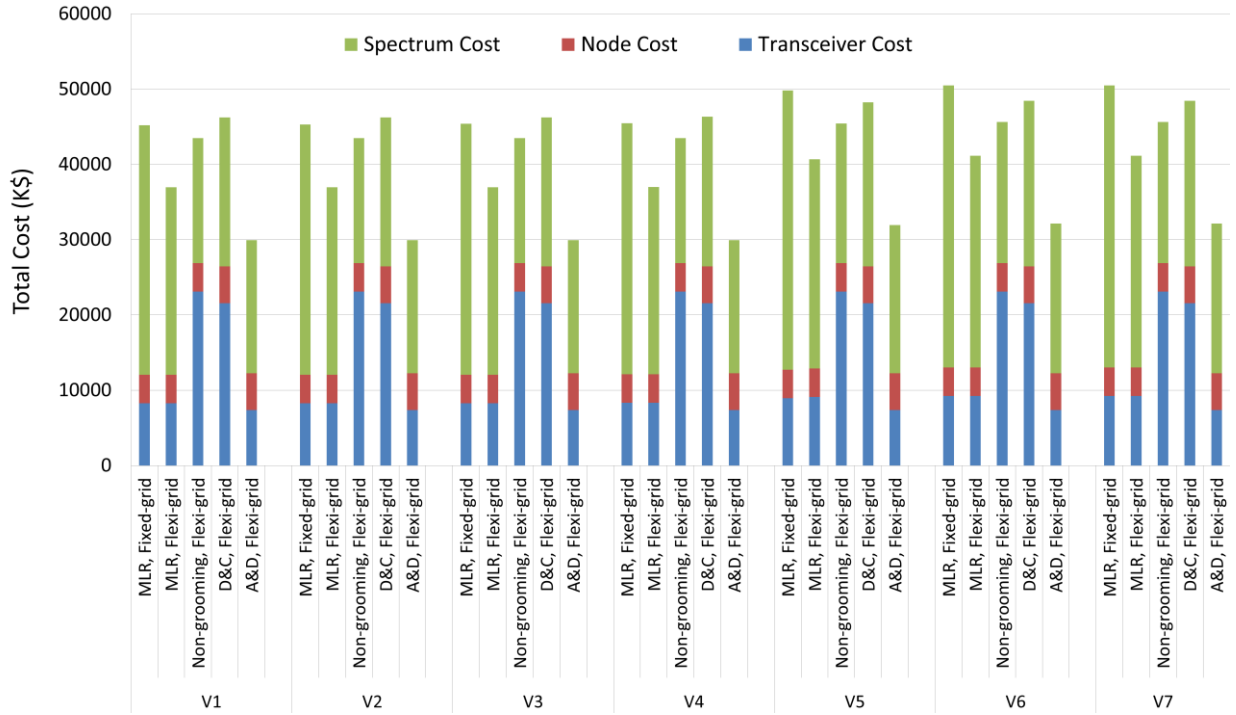

Figure 4.32 – Total cost vs. Traffic volume.

Table 4.3 –Percentage of improvement of A&D in comparison with all other scenarios under study for the GÉANT2 Pan-European network.

Scenario	Percent of improvement of A&D at V1	Percent of improvement of A&D at V7
SLR, fixed grid	67%	78%
MLR, fixed grid	33%	36%
MLR, flex grid	20%	22%
Non-grooming, flex grid	29%	31%
Drop & Continue, flex grid	33%	35%

5 Evaluation of a FOX-C based multi-layer network

The performance, power consumption and cost saving peculiar to the use of a FOX-C node have been extensively studied above. This chapter complements the previous analysis with a global Techno-Economics study, mainly focused on CAPEX aspects, considering the use of the flexible optical technology developed in the FOX-C project inside a multi-layer based transport network.

Let us note that the final FOX-C-WP2 deliverable, namely D2.4, should present some more extensive results with some OPEX considerations through migration strategy studies. Here, we evaluate the benefits in terms of CAPEX of introducing the optical flexibility offered by the FOX-C node inside a complete multi-layer transport network, as those typically encountered in the Orange Group use cases. To that end, we propose to compare different scenarios in order to highlight the advantage of the FOX-C technology in terms of optical aggregation with regard to smoother transport network solutions using electrical aggregation, as for example the OTN switching technology.

As mentioned previously, the FOX-C node offers a very high level of flexibility to a network operator, thanks to the bandwidth variability of the sub-band, and also thanks to the hierarchical level of aggregation and optical switching offered by the flexible ROADM function. The studies presented above demonstrate benefits of the FOX-C solution through a single-layer networking study. Since transport networks are not only composed of the optical layer, it is also important to evaluate, from a global architecture point of view, the benefits of managing the aggregation in the network through a multi-layer optimization of the location and dimensioning of each aggregation function. The idea is to alleviate any costly over-dimensioning at both the electrical and optical layers, and also to analyse results in order to elaborate rather coarse-grained guidelines for the operator.

5.1 Scenario presentation

In this study, we intend to position the rather disruptive solution relying on flexible optical switching as developed in the FOX C project with regards to other smooth solutions proposed by some industrial suppliers. Figure 5.1 represents the spectrum view of the optical transmission layer for the three main scenarios studied.

S0: Reference scenario: optical channels at 100Gbps (DP-QPSK), with fixed grid

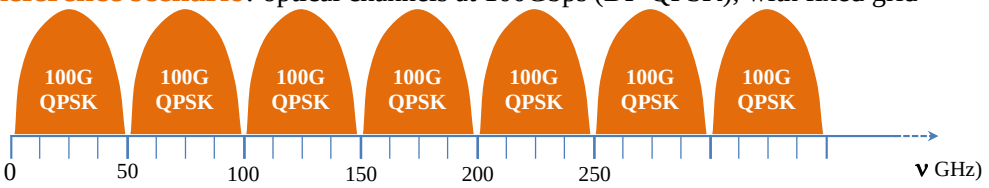

S1: Industrial scenario: use of the Nyquist WDM Multi-Band technique, with ITU-T 12,5GHz slots

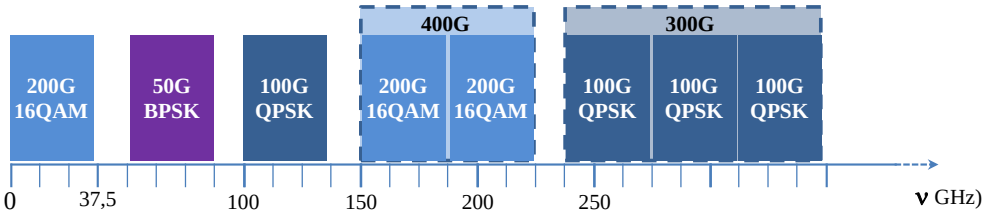

S2: FOX-C scenario: use of the MB-OFDM technique, with 12,5GHz slots

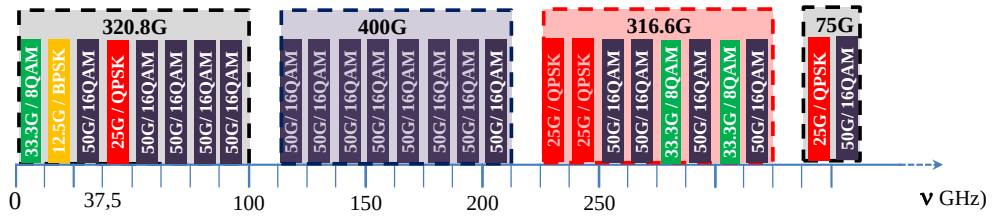

Figure 5.1 – Spectrum management of the reference scenario (S0), the Nyquist WDM super-channel as proposed today (S1) and the FOX-C solution (S2)

Scenario S0 serves as the reference because it corresponds to the currently deployed optical transport network solution. As seen in the upper part of Figure 5.1 the WDM network is deployed in its traditional way, using the ITU-T G.694.1 50-GHz spacing between each wavelength carrying 100Gbps over 2000 km using the DP-QPSK modulation format and SD-FEC.

The middle part of Figure 5.1 represents a short term approach coming from the industry to manage a first level of optical flexibility, and rather close to the benchmarking use case described in subsection 4.3.3. This solution proposes from now on the possibility to have optical channels of higher capacity while improving the spectrum efficiency. It uses a combination of Nyquist-WDM super-channels at 32 Gbauds and mixed 37.5/50-GHz spectral grid. Actually, sub-band spacing inside the super-channel is reduced to 37.5 GHz, whereas the super-channel itself remains on the traditional 50-GHz fixed grid, entailing a guard-band of typically ~18GHz between WDM super-channels. Moreover, in this approach, the super-channel is dedicated to a given traffic demand and routed as an end-to-end entity along the network without possibility to optically switch sub-bands inside the super-channel. This scenario proposes also a first level of variability for the data-rate carried inside the super-channel capacity, with a choice between 50Gbps using BPSK, 100Gbps with QPSK, 200Gbps with 16-QAM towards 400Gbps by coupling two sub-bands of 200Gbps.

The lower part of Figure 5.1 illustrates the scenario S2, which represents one utilization of the FOX-C concept, similar to the FOX-C – Add & Drop solution studied in subsection 4.4.2, with the use of the eOFDM technique to encode the sub-band or the FOX-C node tributaries. This MB-OFDM technique offers an elastic optical channel capacity, able to be closely adjusted to the exact traffic demand by "playing" with the modulation format transported by each sub-carrier constituting each eOFDM sub-band (i.e., BPSK, QPSK, 8-QAM, 16-QAM), the number of sub-carriers constituting each eOFDM sub-band, and the number of sub-band constituting the MB-OFDM signal. Even though the technology allows a very fine spectral granularity of 8 or 10 GHz per spectral slot, as was demonstrated in [43], we

intentionally align the spectrum slot of scenario S2 with the other two (S0, S1) in order to be able to compare their spectrum efficiency performances. Similarly, we keep between each super-channel a guard band of 1 slot (12.5 GHz) to allow already deployed WSS to perform the super-channel optical filtering on the fibre level. We consider that, inside the super-channel, a sub-band guard band of about ~2-4 GHz is included in the sub-band spectrum occupancy. We can observe that a high level of flexibility is offered by the optical layer to the services transported. Each eOFDM sub-band may support a very high variety of data-rates: 12.5, 25, 33.3, 50, and 100Gbps by playing with the different MB-OFDM parameters. Contrary to scenario S1, the FOX-C scenario allows aggregation of sub-bands carrying different traffic demands inside the same super-channel entity in order to enhance the spectrum utilization. It is the main objective of the project to be able to optically switch some sub-bands of a super-channel inside a transmission node thanks to the ultra-narrow and ultra-selective optical filters developed for the sub-band add & drop function.

5.2 Multi-layer network modelling

Chapter 4 presented results of networking studies carried out through simulations to evaluate the use of a flexible optical layer. Techno-Economic results show some important benefits on the optical layer itself.

However, the arrival of new aggregation functions and fine switching possibilities on the optical transmission layer sets new challenges for transport network operators, and is an opportunity for them to review and analyze the global multi-layered transport network architecture.

The goal of this study is to compare, from a techno-economic point of view, different relevant scenarios to manage a global traffic increase, particularly sustained by the IP-based communications. Let us remember that transport networks are intrinsically multi-layered, which entails subsidiary questions on overall network architectures such as, for example, the impact of all networking possibilities offered by the flexible optical transmission layer over the client electrical layers. To that end, we first model the transport network by considering its essential elements as depicted in Figure 5.2.

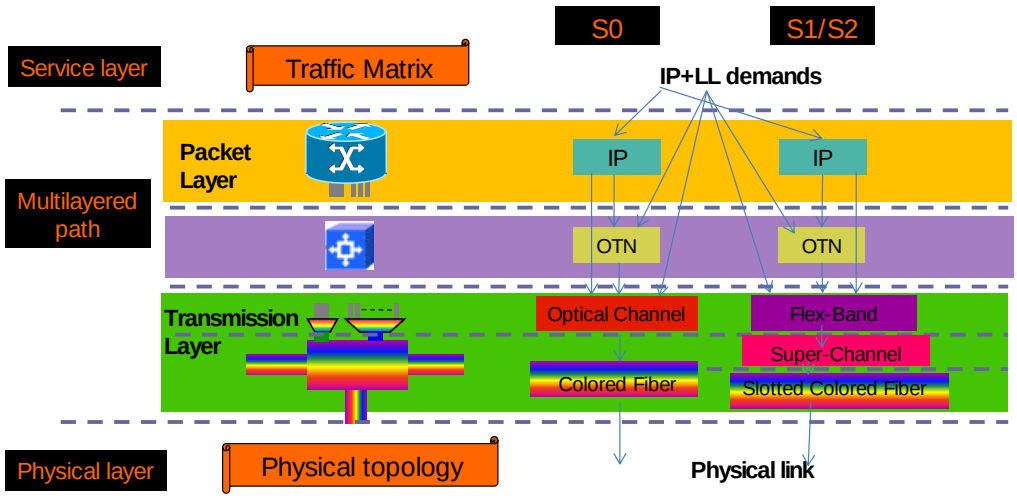

Figure 5.2 – Model of the multi-layer transport network architecture

Figure 5.2 represents the three main macroscopic layers, two of which perform electrical aggregations. The upper-most layer is a packet-based layer and represents all IP flows carried on the network. It performs packet aggregation as done in IP routers. The layer just below corresponds to the OTN switching layer, that will be studied as an option in our three scenarios. This layer allows the aggregation, in a circuit way, of both IP flows and TDM traffic demands. Hence, an OTN container may perform a new aggregation stage in the electrical domain before transporting the signal to the transmission layer. Lastly, the lower-most layer is the optical transmission layer which multiplexes all

demands and transports optical channels along the optical fibre. It typically represents the flexible optical layer deeply studied up to this chapter.

If the right hand-side of this model represents above all a functional and generic view of the multi-layer transport network architecture, using the client/server relationships between various layers as standardized in [44], it also reveals an organic architecture given the fact that the IP layer corresponds to IP routers, OTN layer to OTN switch and the transmission layer to the ROADM equipment in scenarios S0 and S1 or the FOX-C node in scenario S2. Each layer is generic and performs Termination and Connection functions. As for the Adaptation functions, they are managed by the mapping rules (explained later).

In the scenario S0, the transmission layer is composed of two sub-layers: the “Optical Channel” sub-layer represents, as its name suggests, a WDM channel, while the “Colored Fibre” sub-layer stands for the multiplex of 80 WDM channels transmitted in the optical fibre. In the scenario S1 and S2, the transmission layer is decomposed in three different sub-layers called “Sub-band”, “Super-Channel” and “Slotted Colored Fibre”, respectively. They already reveal the three levels of optical switching reminded in the introduction (Figure 1.1). The first sub-layer performs the choice of the adequate modulation format and data rate that can be carried by a sub-band as a function of the transmission reach. As an example, for a given traffic demand, the transmission reach requested may vary depending on the physical path on the physical topology and the number of electrical regeneration points along this physical path. Different sub-bands coming from the “Sub-Band” sub-layer are then aggregated inside a super-channel container in the “Super-Channel” sub-layer.

In scenario S1, the super-channel entity is autonomous and transports the traffic in an end-to-end way, without undergoing any sub-band optical switching process. The super-channel is viewed as the solution available from now on to define a macro optical channel of higher capacity than those managed by the sub-band with a rather spectral efficiency manner. This becomes increasingly spectrally efficient as the number of sub-bands to aggregate increases. In this study, the number of sub-bands is limited to eight. It means that in S1 the super-channel contains only one demand coming from the client layer.

This is really the main difference with scenario S2, where two levels of optical switching are performed inside the FOX-C node. Actually, the super-channel is no longer an end-to-end entity since it may aggregate different sub-bands coming from different traffic demands. By doing that, one node may optically let some sub-bands of one super-channel pass through while extracting one or several sub-bands from the super-channel (or inversely add one or several sub-bands inside free spectrum portions within the spectrum initially allocated to the super-channel). The super-channel then becomes a real flexible optical container with variable capacity. However, in this study, the Flexible Super-Channel bandwidth has been dimensioned for a maximum of 16 slots (200GHz).

As done for scenario S0, in scenario S1 and S2, super-channels are multiplexed by the “colored slotted fibre” sub-layer. Contrary to S0, where the fibre is dimensioned with 80 slots of 50 GHz of spectrum each, for S1 and S2 the fibre supports 320 spectral slots of 12.5 GHz. In scenarios S1 and S2, a guard band of one slot is always inserted on both sides of any super-channel, or also on both sides of a single sub-band in S1.

As represented with arrows in Figure 5.2, the electrical OTN layer is handled as an option in our three scenarios. As an example, LL (for Leased Line) demands can be mapped directly on an optical channel or mapped through the OTN layer. In this case, one demand may be aggregated with other demands inside an adequate OTN container (ODUn) of higher data-rate before being transported over the optical channel. Results presenting the use of this option are identified as $S_i$bis scenario. We also analyze the case where all aggregation is performed on the electrical OTN layer before the signal is transported over the fibre. That scenario is identified by $S_i$bisOTN and represents the case where the OTN switching has been forced.

5.3 Transport Network use case

In this study we evaluate and compare the multi-layer transport network architecture variation through a real networking use case. To that end, we consider the proposed national reference network topology presented in subsection 4.2.1 and deeply described in subsection 2.1.1 of D2.1 [25]. It is representative of a typical transport backbone operated by a Tier-1 operator in Europe. For reminder, the topology is composed of 51 nodes connected together through 75 links. We make the assumption that each link contains a sufficient number of fibre pairs (one fibre per direction), whose exact number will be determined by the dimensioning resulting from the network optimization process.

Since we have to analyze the multi-layer transport network architecture variation in response to a global traffic volume increase, mainly triggered by the predominance of IP based traffic, we consider a relevant associated traffic matrix very close to the one presented in section 2.2.2 of D2.1 [25]. We consider 371 traffic demands, half of which correspond to IP-packet-based traffic and are terminated on the IP layer, and the other half, identified as LL demands, correspond to circuit-based traffic terminated directly on the client interfaces of the optical transmission layer of Figure 5.2 or the OTN layer when the latter is used.

Several traffic volumes V_i are considered through the study. The initial traffic volume V1 represents almost 7 Tbps of ingress traffic. Although the number of IP and LL demands is quite equivalent, the part of the global ingress traffic corresponding to the IP traffic volume is twice as important as that of the LL demands. Note also that, in this rather concrete use case, the traffic demands are not uniformly spread over the different nodes of the topology, where some nodes appear as pure transit nodes while other nodes sometimes have to manage and terminate a rather important traffic volume such as e.g. 1.5 Tbps for one node (with the same proportion between IP and LL demands).

To study sensitivity to traffic increase, we usually make the initial traffic matrix grow globally without diversifying the growth factor between IP and LL traffic demands, except when it is explicitly mentioned. The variation of the traffic load is generally based on a constant yearly growth ratio of 35%.

Table 5.1 – Data rate and modulation format for our three scenarios with the associated maximum transmission reach

Scenario	*Bitrate (Gbps)*	*Modulation format*	*Reach (Km)*
S0	100	QPSK	2000
S1	50	BPSK	4000
	100	QPSK	2000
	200	16-QAM	400
S2	12.5	BPSK	4000
	25	QPSK	2000
	33.3	8-QAM	750
	50	16-QAM	400

Table 5.1 shows the triplet linking the three following parameters together: modulation format, optical reach and data-rate supported, which is available at the sub-band termination function. As already said, the optical channel of scenario S0 occupies one spectral slot of 50 GHz. In S1, the sub-band occupies three spectral slots of 12.5 GHz, which means 37.5 GHz, thanks to the use of the Nyquist filtering. As for S2, the eOFDM sub-band occupies one spectral slot of 12.5 GHz.

Let us notice that half the traffic matrices are composed of IP flows and the other half are composed of TDM flows. However, the proportion in terms of data rate is different, with IP flows representing more or less two thirds of the global traffic load.

5.4 Multi-layer network architecture optimization issue

In complement to the routing and spectrum allocation on the flexible optical layer studied in chapter 4 by means of simulations, here we study the positioning of the different network atomic functions from both a horizontal and a vertical point of view thanks to a specific multi-layer optimization tool (MULOT tool) conceived and developed internally in Orange-Labs and presented in section 1.4 of D2.1 [25]. The tool is based on a simulated annealing meta-heuristic to find, after an important number of tested combinations, the adequate combination of multi-layer paths that gives the best global network cost. Obviously, we are never sure to obtain the theoretical optimum but are rather confident to yield a nearly optimal solution. Throughout the different iterations, the tool tests a lot of combinations changing either the physical path or the behaviour inside at least one node on a given physical path. Changing the behaviour inside a node consists of changing the way to relay the information on one node (changing of layer for example).

Based on the generic G.805 model, the MULOT platform may be adapted to many network case studies to a given extent. For the purpose of the FOX-C project, it has been configured to be able to insert and manage the electrical OTN switching option in our three scenarios.

Throughout the optimization process, the global network cost is inferred from the addition of the individual cost of the different items constituting the multi-layer node.

5.5 Multi-layer network node cost model

Table 5.2 summarizes the relative cost items used in this study for the most essential components constituting the transport function required for the different layers. This cost model has been elaborated from an average of real costs coming from different transmission equipment suppliers, some of which have sometimes been negotiated through several steps. Note that the cost difference between the client interfaces in the three layers is due to the use of mean costs that reflect devices that may come from different suppliers, whose developments are often managed in different business divisions and with sometimes important functional differences.

Table 5.2 – Costs for the main elements of the multi-layer transport node

Item	*Cost*
IP Router parameters	
Router (shelf and switch fabric)	1.62
10GE interface card	5.08
100GE interface card	8.42
OTN switch parameters	
Shelf size 1 (0,8Tbps, 16 slots)	10.15
Shelf size 2 (1,6Tbps, 16 slots)	12.77
Shelf size 3 (1,6Tbps, 32 slots)	17.47
Shelf size 4 (3,2Tbps, 32 slots)	20.91
Colored Line Interface (100Gbps)	9.59
10 x 10G client interface card (10 XFP included)	2.65
1 x 100G client interface card	5.56
WDM ROADM parameters	
ROADM degree 1 (shelf and switch fabric)	2
ROADM degree 2	12.36
ROADM degree 3	17.87
ROADM degree 4	23.77
Additional degree	34
10GE interface	0.04
100GE interface	4.17
100Gbps Wavelength (for scenario S0)	8.33
Slot (for scenario S1 and S2)	2.08
HSR optical filter (for scenario S2)	2.82

In Table 5.2 we find again the organic view of a multi-layer node that may be composed of an IP routing function, an OTN switching function and an Optical switching function. For each layer, we

distinguish the item corresponding to the relay or connection of information (typically the ROADM function for the transmission layer) from items managing the client or line interfaces.

For the OTN switch, in order to optimize the cost related to the use of this layer, we considered several sizes of OTN chassis varying according to either the number of tributary/line interfaces or the capacity of switching. The choice of the most adequate configuration is automatically made by the optimization tool.

In this study, the optimization process is driven by the global objective to maximize the filling of the fibre in terms of data rate while minimizing the number of occupied spectral slots of 50 GHz or 12.5 GHz for scenarios S0 and S1/S2, respectively. Thus, we need to establish the cost of one slot (12.5 GHz). For that, we take as a reference the price of the flexible coherent WDM interface working at 100 Gbps and implementing the SD-FEC functionalities, which corresponds to the termination of an optical channel in scenario S0. Since this 100 Gbps transponder occupies 4 slots of 12.5 GHz, we roughly estimated the cost of one slot (for scenarios S1 and S2) as being a quarter of the 100 Gbps transponder cost.

During the optimization process, when the maximum capacity of the fibre is reached (80 slots for S0, 320 slots for S1/S2), a new degree is automatically added to the flexible ROADM node.

In scenario S2, we introduce the HSR processor, corresponding to the optical filter developed in the project, to add or drop narrow sub-bands to/from a super-channel. Since the addition/extraction of sub-bands is managed at the add/drop stage of the ROADM, we introduce this element at the termination of each sub-band occupying less than 4 slots. Indeed, for sub-bands of higher spectrum occupancy than 4 slots, we consider that the add/drop stage of the ROADM does not require any other specific component than the standard WSS already considered and quoted in the different elements constituting the ROADM. Said in other words, the add/drop of sub-bands larger than 50GHz is performed through standard WSS constituting the ROADM whereas the add/drop of narrow (and ultra-narrow) sub-bands occupying less than 50GHz is performed via the use of the additional HSR processor component.

Since we are in a multi-layer node context, in complement to this cost model, we also need to specify some dimensioning rules in order to map a client layer over a server layer. First of all, the mapping of IP demands over either the OTN or the optical layer is performed through the use of 10-GE and/or 100-GE interfaces. LL demands are managed either directly by the optical layer (typically the Add/Drop stage of the ROADM) or through the OTN switch using also 10-GE and/or 100-GE client interfaces. The threshold to choose a 100-GE interface rather than N-fold 10-GE interfaces is fixed to 70- and 100-Gbps for IP and LL demands respectively. For instance, if an IP path requires a bandwidth of 80-Gbps, a 100-GE interface is set in the IP router whereas for an LL path requiring the same bandwidth, eight 10-GE interfaces will be set. This threshold has been determined from cost differentials existing between the different types of interfaces on the IP, OTN or ROADM equipment.

5.6 Global multi-layer network cost results

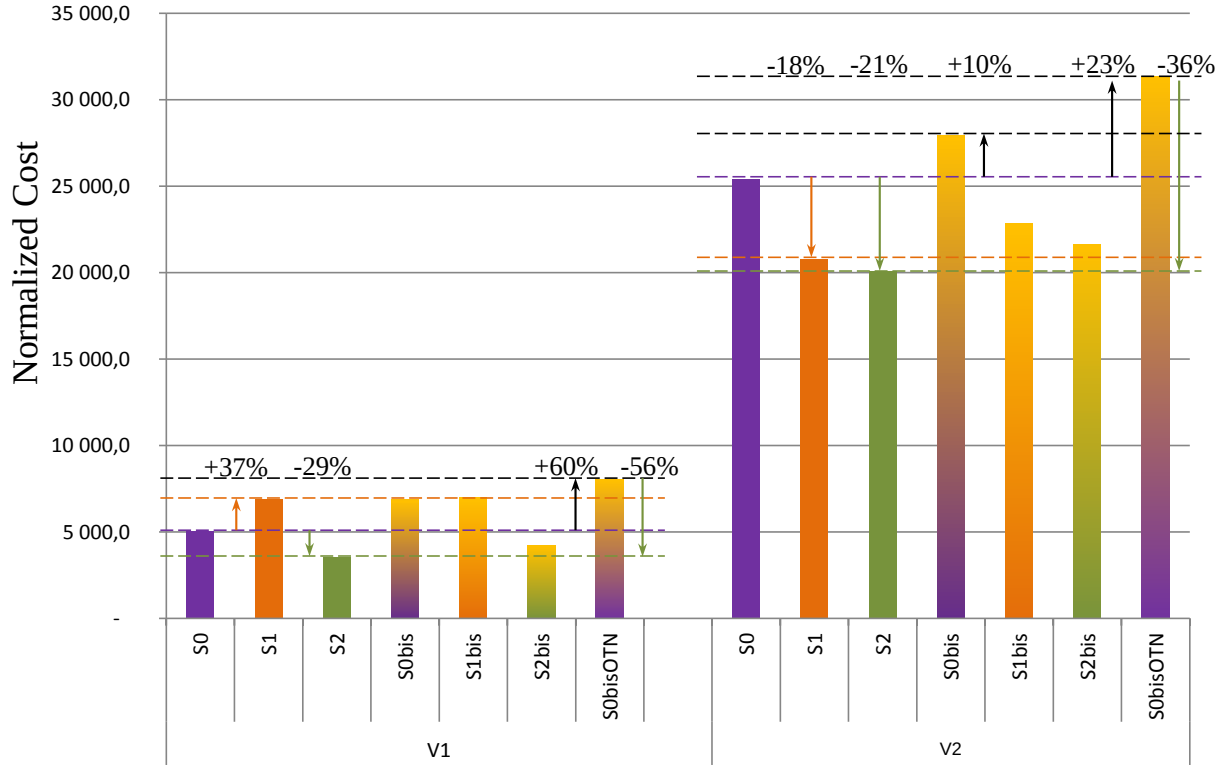

Figure 5.3 – Global multi-layer transport network cost comparison, for traffic volume V1 and V2

Figure 5.3 presents the CAPEX results of the global Techno-Economics analysis for our three scenarios S0, S1, S2 on the case study described previously. It takes into account two different traffic volumes: V1, which is the initial traffic volume, and V2, which corresponds to a traffic increase projection spanning roughly eight years with a constant per-year traffic growth of 35%. We perform a multi-layer optimization and dimensioning using our MULOT optimization tool for each of these three scenarios and their extensions using an OTN electrical aggregation layer.

First of all, in view of the results shown in Figure 5.3, the FOX-C scenario (S2) is always the best from a CAPEX point of view whatever the traffic matrix is. For the initial traffic volume V1, scenario S2 (which is the FOX-C solution using super-channel of MB-OFDM sub-bands) is 29% less expensive than S0 whereas scenario S1 (which combines Nyquist-WDM super-channel and mixed 37.5/50-GHz spectral grid) is 37% more expensive than our reference S0. When we increase the initial traffic matrix by a factor of 8.17, we observe an important gain for scenario S1 at traffic volume V2 that roughly concurs with the results of scenario S2. Indeed, our two flexible scenarios (S1 and S2) are better than our reference, with a CAPEX gain of around 20%. However, scenario S2 remains more interesting with a cost reduced by 3% compared to S1. These results clearly prove the economic interest of the FOX-C MB-OFDM based concept for these traffic volumes. Even though we have penalized scenario S2 with the introduction of the HSR processor that is increasingly used as the number of optical channels of small capacity increases (i.e. at V1), we see that, globally, it remains economically more interesting.

We can also notice in view of the results for scenario S1, the beneficial effect of introducing super-channels when the average traffic volume per demand increases thanks to its efficient way to provide optical channels of high capacity.

In consequence, with our cost model, the migration from S0 to S2 appears justified in the short term and reinforces the development of the ultra-narrow and ultra-selective optical filters.

Since the OTN layer offers an additional aggregation capability by mapping IP and LL demands over the optical layer, we analyze the effect on the network of using this additional layer in order to favor the

filling of the sub-bands between the Packet layer and the transmission one. We evaluate again the impact in term of global network costs for our three scenarios. Scenarios S0bis, S1bis and S2bis in Figure 5.3, respectively, highlight CAPEX results when we use the OTN layer possibility. Overall, for traffic volume V1, there is no real economic interest to use the OTN aggregation on our network case study. It reveals a cost increase of 37% for S0bis and S1bis and a substantial gain of 16% for S2bis when compared to S0. These results may be explained by the fact that the OTN usage requires an additional shelf. Nevertheless, we were expecting that this over-cost could be counterbalanced on the optical layer by the benefits of the aggregation. Unfortunately, this is not the case in this case study. With regard to these results, the bottom line is that S2 still remains the most cost effective scenario. These results are more or less the same for traffic volume V3, except that scenarios S1bis and S2bis become cheaper than our reference scenario S0.

These results compare different solutions that are not totally equivalent from a functional point of view given the fact that, as an example, the FOX-C solution brings a high level of flexibility and aggregation capability to the optical layer. This is the reason why we introduced the S0bisOTN scenario, which corresponds to a scenario where we force the use of the OTN aggregation layer for all demands. As a consequence, direct mapping of IP or LL demands over the optical layer is no longer allowed. This solution is presented as a short-term solution to optimize the optical channel usage, in order to minimize the optical layer dimensioning. However, Figure 5.3 reflects that S0bisOTN is always more expensive than the current scenario S0, with an over-cost of 60% or 23% for traffic volumes V1 and V2, respectively. Now from a global transport function point of view, scenario S0bisOTN and S2 are similar. They represent two different solutions to manage the same issue, one performing aggregation in the electrical domain, the other directly in the optical layer. As represented in Figure 5.3, the optical-based solution offers a rather important gain of 56% or 36% for V1 and V2, respectively, with respect to the electrical one.

5.7 FOX-C node cost model refinement for MB-eOFDM transmission

One difficulty to perform such prospective global techno-economic study is the elaboration of a relevant cost model for a technology which is deeply experimented and demonstrated in research laboratory, but not commercial yet. The cost of an end product item of telecommunication equipment depends on many aspects, and notably integrates part of research and development costs. Moreover, since this is a very fluctuating value, it is often necessary to perform a number of sensitivity studies to grasp the level of confidence of the obtained results.

In the previous section 5.6, we presented results obtained with a rather coarse estimation of the sub-band cost elaborated from an average of real costs provided by different transmission equipment suppliers. As we have no real cost values coming from the industry regarding scenario S2, we now focus on the refinement of the cost assumptions summarized in Table 5.2. To that end, we relied on the transceiver and OXC designs elaborated in chapter 3 from discrete components to develop the new cost model presented in Table 5.3, where only the cost of components constituting the optical layer (for all scenarios) has been modified.

In this section, we therefore re-use the transceiver and node designs presented in chapter 3 and adapt them for low symbol-rate eOFDM signal transmission through directionless R&S nodes bearing in mind that they need to be as generic as possible and sufficiently compliant with our internal multi-layer optimization platform. Here, we do not pursue very accurate designs. Instead, we just need a global cost for the equipment item that is quite representative of what could be the reality.

5.7.1 Flexible sub-band transponder for low symbol-rate signal transmission

To estimate the CAPEX cost of an optical channel (in S0) or a sub-band (in S1/S2) termination, we reuse the design elaborated for a single carrier transceiver as represented in Figure 3.1. Whether it is for the generation of a single-carrier transceiver with SD-FEC for S0 or the generation of a sub-band with SD-FEC and Nyquist filtering in S1, we find the same number of discrete components. We can also

consider this design for the generation of a sub-band in scenario S2 in the case where there is no photonic integration yet.

Regarding the cost of this item, we re-use the different components and their associated costs presented in Table 3.1. However, since in our optimization platform we consider more a sub-band transponder device than a transceiver one, we add a new “OTN framer and mapper” component that we have estimated to cost $8.15k. Thus, as explained above, we obviously obtain the same cost for both the “transponder without Client interface” used in S0 and S1 and for the “Sub-band of at least 3 slots” used in S2 as it appears in Table 5.3. Moreover, in order to take into account the specificity of the eOFDM technology, in which flexible transponders generate optical channels of rather small capacity with spectrum occupancy typically in the region of one slot or two slots, we introduce a new cost assumption. The previous design considers cost of electronic components for the generation of a sub-band of 3 slots width. Such components, usually running at 32 Gbaud, are more expensive than components running at lower symbol rate. Thus, we consider in our new cost model that we could have dedicated hardware generating sub-bands of one slot whose cost is one third of the initial 3-slot sub-band cost and, similarly, dedicated hardware generating sub-bands of two slots whose cost is, this time, two thirds of the initial one.

5.7.2 Flexible FOX-C node cost model adapted to MULOT

Since it is not possible to implement in our optimization platform an automatic ROADM dimensioning taking into account several different parameters (typically the number of degrees *D* and the number of HSR processors *N* defined for the optical cross connect in 0), we have been forced to adapt the FOX-C optical cross connect to our environment. Figure 5.4 depicts our flexible ROADM model, which has the advantage (for the optimization purpose) of simply evolving linearly when we add a new degree. It represents the future flexible optical node that operators expect to deploy in the rather short term due to its colorless and directionless functionalities. Our Flexible FOX-C node design is exclusively based on the use of WSS in order to be totally directionless, which comes at the expense of adding extra WSSs. In our refined cost model we have not designed a specific super-channel transponder model since it can be intrinsically included or managed by the WSS constituting either the different degrees or the add/drop stage thanks to the one-slot guard band we keep between super-channels.

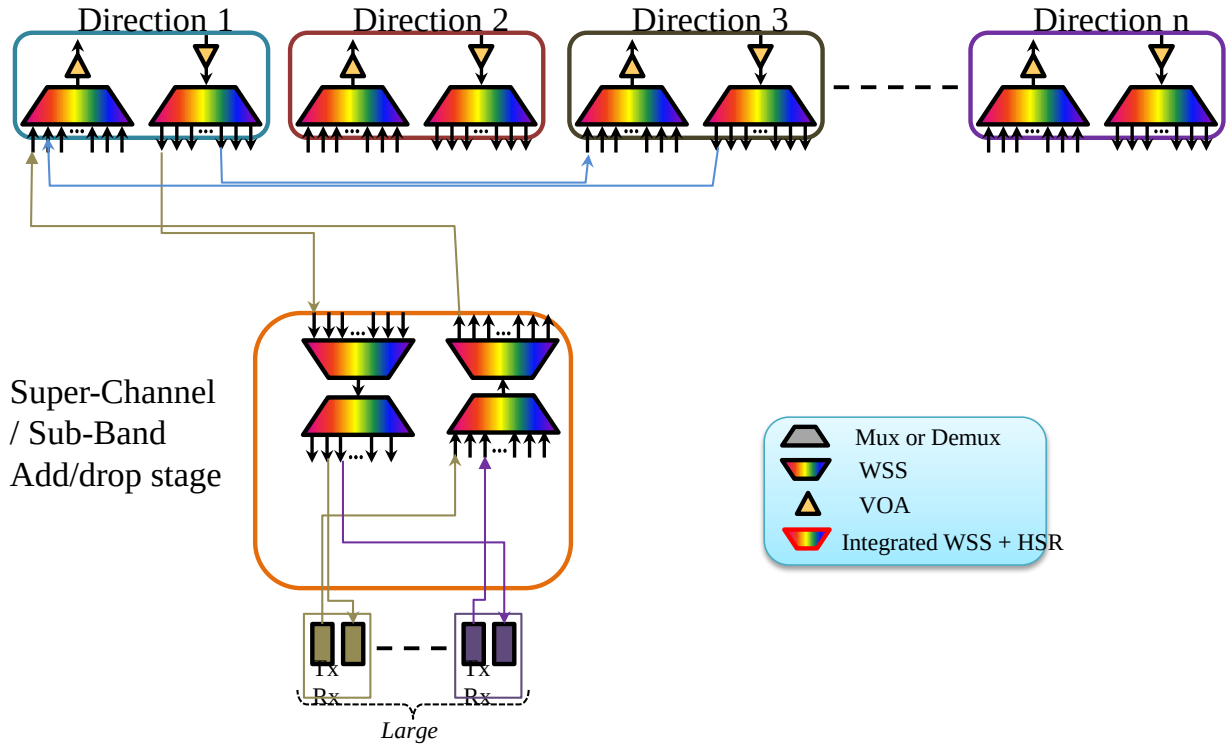

(a)

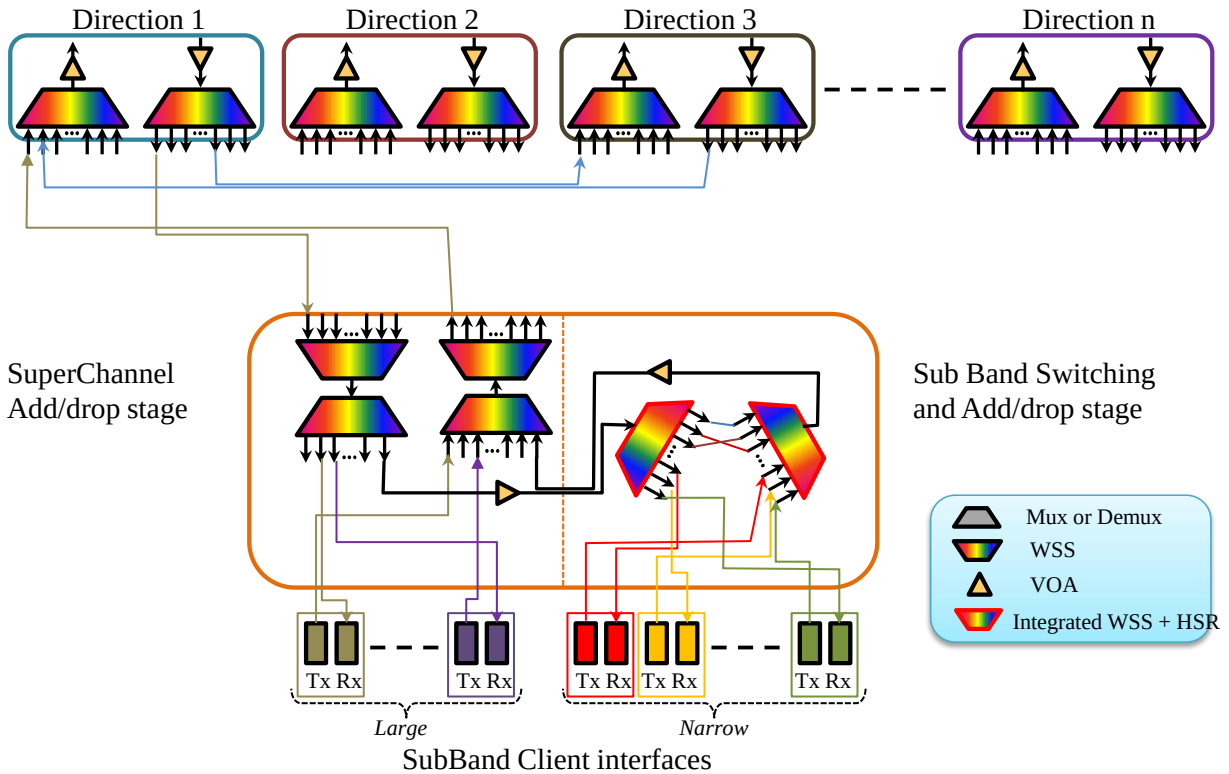

(b)

Figure 5.4 – a) Flexible ROADM colorless, directionless used for scenario S0 and S1. b) Flexible FOX-C ROADM with ultra-selective sub-band switching used for scenario S2

Table 5.3 – New cost model elaborated from discrete components

	Relative Costs		
	S0	S1	S2
IP Router cost items			
Router Fabric and Matrix	1,62	1,62	1,62
Cost a 12 x 10GE ports (max 100GB) interface card	5,08	5,08	5,08
Cost of 1 x 100GE port interface card (IMM - 1-PT 100GE - CFP - with Base Lic.)	8,42	8,42	8,42
	-	-	-
OTN Switch cost items	-	-	-
Shelf size 1 (0,8Tbps, 16 slots)	10,15	10,15	10,15
Shelf size 2 (1,6Tbps, 16 slots)	12,77	12,77	12,77
Shelf size 3 (1,6Tbps, 32 slots)	17,47	17,47	17,47
Shelf size 4 (3,2Tbps, 32 slots)	20,91	20,91	20,91
	-	-	-
Colored Line Interface (100Gbps)	9,59	9,59	9,59
	-	-	-
10 x 10G client interface card (10 XFP included)	2,65	2,65	2,65
1 x 100G client interface card	5,56	5,56	5,56
	-	-	-
Flexible ROADM cost items	-	-	-
Cost of the base optical matrix (degree 1)- ROADM (Colorless, Directionless)	9,79	9,79	9,79
Cost of the base optical matrix (degree 2)- ROADM (Colorless, Directionless)	13,70	13,70	13,70
Cost of an additional degree- ROADM (Colorless, Directionless)	4,58	4,58	4,58
Cost of the Ultra Selective A/D stage			10,31
	-	-	-
Cost Int10GClient (SFP)	0,04	0,04	0,04
Cost Int100GClient (CFP)	4,17	4,17	4,17
Cost of the "Transponder" without Client Interface	6,86	6,86	-
Cost items specifics to Scenario S2			
Cost of the Sub-Band of at least 3 slots			6,86
Cost of the Sub-Band of 2 slots			5,28
Cost of the Sub-Band of 1 slot			3,71

As seen in Figure 5.4, the flexible ROADM is composed of:

- A given number of tributary elements (100Gbps transponder in S0, flexible Sub-band transponder in S1/S2)
- A given number of line direction or degree
- A specific Add/Drop stage for super-channel and / or sub-band
- For scenario S2, a specific ultra-selective sub-band Add/Drop/switching stage made of “integrated WSS-HSR” components

Regarding the ROADM dimensioning, it can be noticed that the ultra-selective sub-band stage of Figure 5.4(b) is only used, and consequently quoted, in a node when a super-channel is terminated and some of the sub-bands it is composed of need to be dropped, added or switched (which also includes the case where the sub-band is simply transmitted in pass-through).

As for the flexible sub-band transponder for the ROADM, we adapted the cost model presented in 0. We introduced the new component developed by Finisar and HUJI in the FOX-C project: the integrated WSS including the HSR optical filter that allows ultra-selective sub-band switching. Its cost has been estimated to be $24k. We also reduced the WSS component cost by 40% in order to reflect the reality when an operator deploys a rather large-scale optical network.

5.7.3 New Global network cost results

Figure 5.5 presents new CAPEX results for the same two traffic volumes considered in the previous section, and for our three scenarios S0, S1, S2, including the use of the OTN for scenario S0.

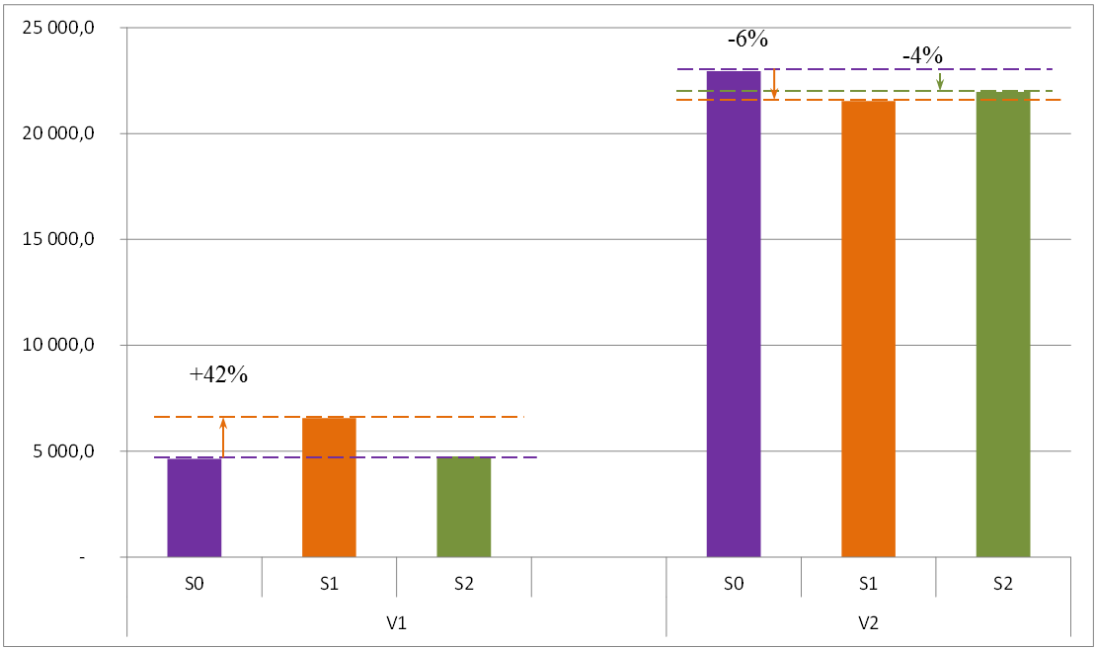

Figure 5.5 – Global multi-layer transport network cost comparison, for traffic volume V1 and V2, with new cost model

For the initial traffic volume V1, the reference scenario (S0) remains naturally very close to the previous results. The over-cost of scenario S1 becomes slightly more pronounced (+5 points) with this new ROADM design and cost model. With this assumptions, the FOX-C scenario (S2) becomes, from a CAPEX point of view, equivalent to our reference.

Let us remember that by comparing S0 and S2 we are in fact comparing different solutions that are not totally equivalent from a functional point of view given the fact that the FOX-C solution brings a much higher level of flexibility and aggregation capability on to the optical layer. However, we see that the over-cost, directly linked here to the implementation of the ultra-selective optical switching, may be totally counter-balanced as the traffic volume increases. At traffic volume V2, both S1 and S2 bring a slight CAPEX benefit of about 5%.

5.7.4 Sensitivity to Flexible transponder cost and traffic increase

When we analyse deeply the different elements constituting the multi-layer transport node, we see that, globally, two thirds of the flexible ROADM cost concerns the tributary stage, and particularly the flexible sub-band transponder part. This means that the tributary stage item represents the optical equipment part where we should expect the biggest gains. As a result, we have analyzed the effect of a reduction of this item on the global network cost. Figure 5.6 presents global multi-layer network cost evolution in the long term, when the traffic volume increases by a very high factor. We extrapolated the initial traffic matrix for traffic volume V1 to traffic volumes V2, V3 and V4, corresponding to a traffic load factor of respectively 1, 8.17, 13.33 and 26.66, which represents an average data rate per connection of respectively 18.76, 153.27, 250 and 500Gbps.

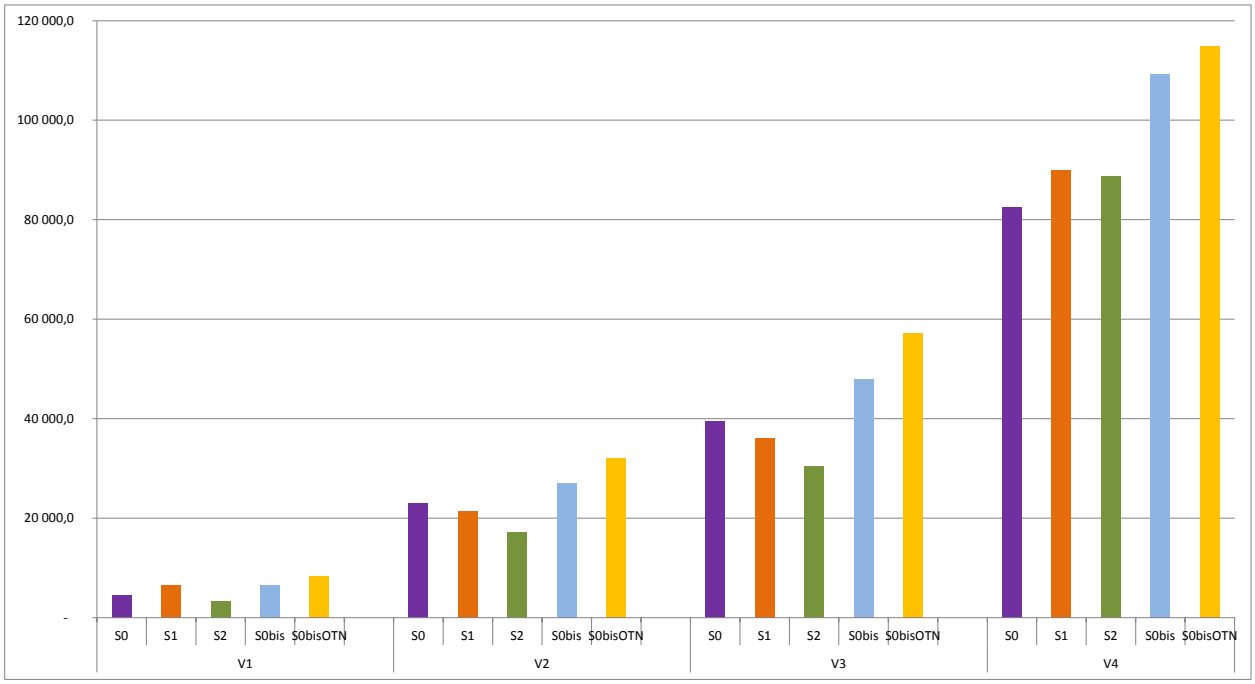

Figure 5.6 – Global multi-layer transport network cost comparison, with traffic increase sensitivity and a flexible sub-band transponder cost sensitivity (for S2)

We observe that the CAPEX benefit of scenario S2 is more pronounced when the traffic volume is rather low. Indeed, with our traffic increase method, we lose all traffic demands of low capacity as we increase the average data rate per connection. For traffic volume V1, S2 is once again cheaper with a cost saving of about 30%, and about 23% at traffic volume V3. But on the other hand, S2 presents an over cost of 7% with regards to S0 at traffic volume V4.

When we dig deeper in the details of our multi-layer optimization results, we observe the appearance of a side effect for high traffic volume (here, V4), which is rather amazing and particularly unexpected because these are precisely the conditions that make the super-channel concept being relevant. It might be possible that the very high average data load for data requests makes the 100 Gbps data rate of scenario S0 becoming a relatively fine enough granularity, which could make scenario S0 becoming economically the most interesting. Another explanation could be that, at V4, we have reached the limit of our optimization platform, which probably requires some configuration modifications adapted to the case of ultra-high data rate in order to obtain a better optimum.

At first sight, it seems that the optimization favors the ultra-high data rate modulation format that offers the highest capacity (here, the 16-QAM) to the detriment of other less dense modulation formats, such as the DP-QPSK, for example. By doing that, the optical reach of the sub-bands generated with 16-QAM is limited in our study to 400km. As a result, this systematic choice entails a detrimental effect on the global multi-layer architecture because it increases the electrical regeneration in the IP router, which is exacerbated with high volumes of traffic load. The proportion of the IP traffic in the cost becomes more and more predominant, which has an impact on the client interfaces of all the considered under-lying layers, in particular in terms of transponders for the optical layer.

6 Conclusions

This document reported on the results arising from the techno-economic studies carried out on a FOX-C enabled network based on the transmitter-receiver designs analysed in T3.2 and T3.3 and the switching node implementations investigated in T4.1 and T4.2. Two all-optical (AO-OFDM and N-WDM) and three electrical multiplexing schemes (eOFDM, eFOFDM and N-FDM) with up to 16QAM modulation format were taken into consideration.

At the nodes, two switching levels are considered in the FOX-C project. At the fibre link level, a WSS selects a super-channel that contains the channels to be dropped locally. At the super-channel level, a filtering technology with ultra-fine granularity is used to separate the closely spaced (or even overlapping) channels. Two filter models have been proposed in WP4 at the super-channel level: a high resolution (HSR) filter for non-overlapping channels such as those generated by N-FDM transceivers and an all-optical interferometric (TIDE) filter for overlapping channels such as those generated by AO-OFDM transceivers. The filtering effects of the HSR-based FOX-C nodes have been investigated for (q)N-WDM transmission through simulations with VPI and Matlab and a model to estimate the OSNR penalty at the nodes has been introduced. We have observed that the OSNR penalty increases with the input OSNR at the node. This model has been used, together with a QoT tool developed in Matlab, to estimate the maximum reach for all the multiplexing schemes investigated in the FOX-C project. This tool has been thought out to be fed into the network operator planning tool.

In a super-channel transmission environment, such as the one being investigated in the FOX-C project, it is important to determine what the optimum spectral slot size is at both the super-channel and sub-channel levels in order to minimise the guard bands and, therefore, maximise the spectral efficiency. Driven by the development of the HSR filters in WP4, we have analysed the optimum granularity at the sub-channel level in a qN-WDM super-channel transmission system and demonstrated that moving to a gridless scenario, despite showing the best performance in terms of blocking probability when combined with very fine resolution filters, may only be justified if the additional investment in the required technology can be offset by a significant turnover increase. Other than that, the results made a case for allocating the sub-channels on the 3.125-GHz grid provided that filters with resolutions finer than 1.2 GHz are employed.

Regarding the FOX-C networking studies, two scenarios have been considered: a network based on just the optical transmission layer (referred to as “single-layer”) and a multi-layer network. In both cases, a reference cost and power consumption model has been developed for the techno-economic evaluation of networks based on the different transponders and optical cross-connects investigated in the FOX-C project. In the single-layer optical network study, the full FOX-C solution (Add & Drop) was compared to the conventional and quasi-FOX-C (Drop & Continue) solutions. The reported results over two reference networks (a large national-scale Orange group network with 51 nodes and the continental GÉANT2 Pan-European network with 34 nodes) showed that the full FOX-C solution outperforms all conventional solutions in the range of study when it comes to spectrum utilization and overall cost of transceivers. However, for all-optical sub-channel add/drop, expensive filtering elements are needed at the network intermediate nodes, which results in an overall ROADM cost penalty. Finally, by using the cost of the “dark” 12.5-GHz spectrum slot to monetise the spectrum resource saving, the total cost of ownership was estimated and compared for all cases under study. The full FOX-C solution showed ~20% total cost benefits compared to the second best solution on both topologies.

The multi-layer system modelling studies were carried out on a powerful and accurate tool (MULOT) for the overall system performance evaluation, aiming at the identification of the operating limits and benefits of the FOX-C network (as an all-optical traffic grooming capable solution) compared with the

legacy OTN-based traffic grooming scenario in terms of cost saving. The results, with up to 29% global cost reduction when compared with a multi-layer network based on current 100G DP-QPSK transmission, justify the migration to the FOX-C solution in the short term and reinforce the development of the ultra-narrow and ultra-selective optical filters.

References

[1] *Cisco White Paper, "Cisco Visual Networking Index: Forecast and Methodology, 2013-2018".*

[2] *I. Tomkos, S. Azodolmolky, J. Solé-Pareta, D. Careglio, E. Palkopoulou, "A tutorial on the flexible optical networking paradigm: state-of-the-art, trends, and research challenges," (invited paper), Proc. of the IEEE, vol. 102, pp. 1317-1337, September 2014.*

[3] *Carena, A.; Curri, V.; Bosco, G.; Poggiolini, P.; Forghieri, F.; , "Modeling of the Impact of Nonlinear Propagation Effects in Uncompensated Optical Coherent Transmission Links," Lightwave Technology, Journal of , vol.30, no.10, pp.1524-1539, May15, 2012*

[4] *Gao, G.; Chen, X.; Shieh, W.; , "Analytical Expressions for Nonlinear Transmission Performance of Coherent Optical OFDM Systems With Frequency Guard Band," Lightwave Technology, Journal of , vol.30, no.15, pp.2447-2454, Aug.1, 2012*

[5] *Poggiolini, P.; , "The GN Model of Non-Linear Propagation in Uncompensated Coherent Optical Systems," Lightwave Technology, Journal of , vol.30, no.24, pp.3857-3879, Dec.15, 2012.*

[6] *P. Poggiolini, A. Carena, V. Curri, G. Bosco, and F. Forghieri"Analytical Modeling of Nonlinear Propagation in Uncompensated Optical Transmission Links" IEEE Photonics Technology Letters, v. 23, n. 11, June 1, 2011*

[7] *Francesco Vacondio, Olivier Rival, Christian Simonneau, Edouard Grellier, Alberto Bononi, Laurence Lorcy, Jean-Christophe Antona, and Sébastien Bigo, "On nonlinear distortions of highly dispersive optical coherent systems," Opt. Express 20, 1022-1032 (2012)*

[8] *G. P. Agrawal, "Fibre-Optic Communication Systems", Third Edition, Wiley-interscience, 2002*

[9] *Freude, W. et al., "Quality metrics for optical signals: Eye diagram, Q-factor, OSNR, EVM and BER," Transparent Optical Networks (ICTON), 2012 14th International Conference on, vol., no., pp.1-4, 2-5 July 2012*

[10] *X. Chen and W. Shieh, "Closed-form expressions for nonlinear transmission performance of densely spaced coherent optical OFDM systems", Optics Express, vol. 18, no. 18, August 2010*

[11] *D. Klonidis, S. Sygletos, D.M. Marom, S. Fabbri, A. Ellis, E. Pincemin, C. Betoule, G. Thouenon, D. Hillerkuss, B. Baeuerle, A. Josten, J. Leuthold, J. Zhao, S. Ben-Ezra, J.F. Ferran, M. Angelou, G. Papastergiou, P. Zakynthinos, and I. Tomkos, "Enabling Transparent Technologies for the Development of Highly Granular Flexible Optical Cross-Connects", paper We.D1.5, ICTON 2014.*

[12] *Carena, V. Curri, G. Bosco, P. Poggiolini, and F. Forghieri, "Modeling of the Impact of Nonlinear Propagation Effects in Uncompensated Optical Coherent Transmission Links", J. Lightwave Technol. 30, 1524-1539 (2012).*

[13] *R. Rudnick, et. al, "Sub-banded / single-sub-carrier drop-demux and flexible spectral shaping with a fine resolution photonic processor," Proc. ECOC 2014, paper PD.4.1.*

[14] *S. J. Savory, "Digital filters for coherent optical receivers", Opt. Express 16, 804-817 (2008)*

[15] *Riichi Kudo, Takayuki Kobayashi, Koichi Ishihara, Yasushi Takatori, Akihide Sano, and Yutaka Miyamoto, "Coherent Optical Single Carrier Transmission Using Overlap Frequency Domain Equalization for Long-Haul Optical Systems", J. Lightwave Technol. 27, 3721-3728 (2009).*

[16] *Satoshi Tsukamoto, Kazuhiro Katoh, and Kazuro Kikuchi, "Coherent Demodulation of Optical Multilevel Phase-Shift-Keying Signals Using Homodyne Detection and Digital Signal Processing",, IEEE Photon. Technol. Lett. 18, 1131-1133 (2006).*

[17] *Rene Schmogrow, Bernd Nebendahl, Marcus Winter, Arne Josten, David Hillerkuss, Swen Koenig, Joachim Meyer, Michael Dreschmann, Michael Huebner, Christian Koos, Juergen Becker, Wolfgang Freude, and Juerg Leuthold, "Error Vector Magnitude as a Performance Measure for Advanced Modulation Formats", IEEE Photon. Technol. Lett. 24, 61-63 (2012).*

[18] F. Heismann, "System requirements for WSS filter shape in cascaded ROADM networks", Proc. OFC 2010, OThR1 (2010).

[19] G. Bosco, A. Carena, A. Curri, P. Poggiolini, F. Forghieri, "Performance Limits of Nyquist-WDM and CO-OFDM in High-Speed PM-QPSK Systems", Photon. Technol. Lett. 22, 1129 – 1131, 2010.

[20] H. Zang, J. P. Jue, and B. Mukherjee, "A Review of Routing and Wavelength Assignment Approaches forWavelength-Routed Optical WDM Networks, " Optical Networks Magazine, vol. 1, pp. 47-60, 2000.

[21] K. Christodoulopoulos, I. Tomkos and E. A. Varvarigos, "Elastic Bandwidth Allocation in Flexible OFDM- based Optical Networks," Journal of Lightwave Technology, vol. 29, no. 9, pp. 1354 -1366, 2011.

[22] Pouria Sayyad Khodashenas, J. Comellas, J. Perelló, and S. Spadaro, "Correlation Between Traffic Granularity and Defragmentation Periodicity in Elastic Optical Networks," Transactions on Emerging Telecommunications Technologies, Article first published online: 27 January 2014, DOI: 10.1002/ett.2795.

[23] Pouria Sayyad Khodashenas, J. Comellas, S. Spadaro, J. Perelló and G. Junyent, "Using Spectrum Fragmentation to Better Allocate Time-Varying Connections in Elastic Optical Networks," Journal of Optical Communications and Networking, vol. 6, no. 5, pp. 433-440, 2014.

[24] Pouria Sayyad Khodashenas, J. Comellas, S. Spadaro and J. Perelló, "Dynamic source aggregation of subwavelength connections in elastic optical networks," Journal of Photonic Network Communications, vol. 26, no. 2-3, pp. 131-139, 2013.

[25] FP7 Call 8 FOX-C project, deliverable D2.1, 2013.

[26] CHRON Project : "D.2.1: Specification of the network scenario and service requirements", Version 2.0, December 28, 2011.

[27] A. Nag, M. Tornatore, "Impact of channel spacing on the design of a mixed-line-rate optical network," in Proc. ANTS, New Dehli, India, Dec. 2009.

[28] J. D. Reis, D. M. Neves, A. L. Teixeira, "Density and Guard Band in Migration Scenarios to Coherent Ultra-Dense WDM," in Proc. Globecom, Houston, United States, vol. 54, pp. 1-5, Dec. 2011.

[29] M. Jinno, B. Kozicki, H. Takara, A. Watanabe, Y. Sone, T. Tanaka, A. Hirano, "Distance-adaptive spectrum resource allocation in spectrum-sliced elastic optical path network," IEEE Commun. Mag., vol. 48 , no. 8, pp. 138-145, Oct. 2010.

[30] A. V. Oppenheim, R. W. Schafer, "Digital Signal Processing," Prentice-Hall, 1975.

[31] X. Zhou, L. E. Nelson,"400G WDM Transmission on the 50 GHz Grid for Future Optical Networks," J. Lightw. Technol., vol. 30, no. 24, pp. 3779 - 3792, Dec. 2012.

[32] F. Heismann, "System requirements for WSS filter shape in cascaded ROADM networks," in Proc. OFC, March 2010, OThR1.

[33] S. Poole, S. Frisken, M. Roelens, C. Cameron, "Bandwidth-flexible ROADMs as network elements," in Proc. OFC, March 2011, OTuE1.

[34] M. Xia, R. Proietti, S. Dahlfort, and S. J. B. Yoo, "Split spectrum: a multi-channel approach to elastic optical networking," Optics Express, Vol. 20, Issue 28, pp. 29143-29148, 2012.

[35] A. Rosa, C. Cavdar, S. Carvalho, J. Costa, and L. Wosinska, "Spectrum allocation policy modeling for elastic optical networks," in Proc. HONET, 2012, pp. 242–246.

[36] Xi Wang, et. al, "Blocking performance in dynamic flexible grid optical networks - What is the ideal spectrum granularity?," Proc. ECOC 2011, paper Mo.2.K.6.

[37] P. C. Schindler, R. Schmogrow, S. Wolf, B. Baeuerle, B. Nebendahl, C. Koos, W. Freude, and J. Leuthold, "Full flex-grid asynchronous multiplexing demonstrated with Nyquist pulse-shaping," Opt. Express 22 (9), 10923-10937, 2014.

[38] P. Torres-Ferrera, J. M. Rivas-Moscoso, Dimitrios Klonidis, Dan M. Marom, R. Gutiérrez-Castrejón, and I. Tomkos,"Filtering effects of cascaded flex-grid ROADMs with high spectral resolution filters on the transmission of Nyquist and quasi-Nyquist WDM super-channels, " Proc. ICOCN 2014, paper M12.6.

[39] CHRON Project : "D.2.4: Cognitive Heterogeneous Reconfigurable Optical Network", Version 1.0, January 2, 2013.

[40] C. Mas Machuca, "Expenditure study for network operators," Nottingham, UK, June 2006. International Conference on Transparent Optical Networks.

[41] E. Palkopoulou, M. Angelou, D. Klonidis, K. Christodoulopoulos, A. Klekamp, F. Buchali, E. Varvarigos and I. Tomkos, "Quantifying Spectrum, Cost, and Energy Efficiency in Fixed-grid and Flex-grid Networks," Journal of Optical Communications and Networking, vol. 4, no. 11, pp. B1-B10, 2012.

[42] K. Christodoulopoulos, M. Angelou, D. Klonidis, P. Zakynthinos, E. Varvarigos and I. Tomkos, "Value Analysis Methodology for Flexible Optical Networks," Proc. ECOC 2011, paper We.10.P1.89.

[43] E. Pincemin, et. Al, "Multi-Band OFDM Transmission at 100Gbps with Sub-Band Optical Switching", J. Lightwave Technol. vol. 32, pp. 2202-2219, 2014.

[44] ITU-T G.805 Recommandation, "Generic functional architecture of transport networks", 2000.